INFORMATION TO USERS

This manuscript has been reproduced from the microfilm master. UMI films the text directly from the original or copy submitted. Thus, some thesis and dissertation copies are in typewriter face, while others may be from any type of computer printer.

The quality of this reproduction is dependent upon the quality of the copy submitted. Broken or indistinct print, colored or poor quality illustrations and photographs, print bleedthrough, substandard margins, and improper alignment can adversely affect reproduction.

In the unlikely event that the author did not send UMI a complete manuscript and there are missing pages, these will be noted. Also, if unauthorized copyright material had to be removed, a note will indicate the deletion.

Oversize materials (e.g., maps, drawings, charts) are reproduced by sectioning the original, beginning at the upper left-hand corner and continuing from left to right in equal sections with small overlaps.

Photographs included in the original manuscript have been reproduced xerographically in this copy. Higher quality 6" x 9" black and white photographic prints are available for any photographs or illustrations appearing in this copy for an additional charge. Contact UMI directly to order.

ProQuest Information and Learning
300 North Zeeb Road, Ann Arbor, MI 48106-1346 USA
800-521-0600

Reproduced with permission of the copyright owner. Further reproduction prohibited without permission.

Reproduced with permission of the copyright owner. Further reproduction prohibited without permission.

NOTE TO USERS

This reproduction is the best copy available.

UMI

Reproduced with permission of the copyright owner. Further reproduction prohibited without permission.

Reproduced with permission of the copyright owner. Further reproduction prohibited without permission.

Investigating the Role of Interstitial Fluid Flow in Bone Adaptation and Metabolism

by

Liyun Wang

A dissertation submitted to the Graduate Faculty in Engineering in partial fulfillment of the requirements for the degree of Doctor of Philosophy, The City University of New York.

2002

Reproduced with permission of the copyright owner. Further reproduction prohibited without permission.

UMI Number: 3037452

Copyright 2002 by
Wang, Liyun

All rights reserved.

UMI Microform 3037452
Copyright 2002 by ProQuest Information and Learning Company.
All rights reserved. This microform edition is protected against
unauthorized copying under Title 17, United States Code.

ProQuest Information and Learning Company
300 North Zeeb Road
P.O. Box 1346
Ann Arbor, MI 48106-1346

Reproduced with permission of the copyright owner. Further reproduction prohibited without permission.

© 2002

Liyun Wang

All Rights Reserved

Reproduced with permission of the copyright owner. Further reproduction prohibited without permission.

This manuscript has been read and accepted for the Graduate Faculty in Engineering in satisfaction of the dissertation requirement for the degree of Doctor of Philosophy.

1/22/02
Date

Professor Susannah P. Fritton
Chair of Examining Committee

1-22-2002
Date

Professor Mumtaz Kassir
Executive Officer

1/22/02
Date

Professor Sheldon Weinbaum

Date

Professor Stephen C. Cowin

1/24/02
Date

Dr. Stephen B. Doty

Supervisory Committee

The City University of New York

Reproduced with permission of the copyright owner. Further reproduction prohibited without permission.

Abstract

Investigating the Role of Interstitial Fluid Flow in Bone Adaptation and Metabolism

By

Liyun Wang

Advisor: Professor Susannah P. Fritton

Musculoskeletal disorders affect hundreds of millions of people around the world today and remain a major threat especially to women and the elderly. It is clinically important to understand how the musculoskeletal system adapts to its physiological environments and remains healthy. This thesis includes four studies that investigate the role of bone interstitial fluid flow in bone adaptation and metabolism. The first study investigated how the different sized bone pores affect interstitial fluid flow in mechanically loaded bone. I developed a theoretical model and predicted the non-linear cusp-like fluid pressure profiles around the osteonal canals, which had been found experimentally but previously unexplained. The second study addressed the paradox that net solute transport occurs in cyclically loaded bone when the net fluid transport is zero. A lacunar-mixing process was proposed that for the first time outlined a detailed mechanism of convective mass transport from the blood supply to the osteocytes. The convective transport was found to increase with increasing loading amplitude and decrease with increasing loading frequency. The third study involved in vivo tracer experiments to quantify the tracer movement in the absence of mechanical loading and to delineate the bone interstitial fluid pathway. Four tracers of various sizes (reactive red, microperoxidase (MP), horseradish peroxidase (HRP), and ferritin with a molecular

Reproduced with permission of the copyright owner. Further reproduction prohibited without permission.

diameter of approximately 1, 2, 6, and 10 nm, respectively) were injected into the rat circulation. The number of the osteocytes labeled with these tracers was found to decrease with increasing molecular size. Results from this study suggest that the pore size of the interstitial fluid pathway is between 6-10 nm, because reactive red, MP, and HRP appeared in osteocytic lacunae while ferritin was found only in vascular pores. Finally, in the fourth study the osteogenesis of the blood pressure induced interstitial fluid flow were examined under the condition of venous stasis. The model showed that the shear stress on osteocytic membrane due to blood flow is too small to account for the periosteal bone growth associated with venous stasis. I postulated that the elevated pressure on the periosteum might trigger the periosteal response in venous stasis.

Reproduced with permission of the copyright owner. Further reproduction prohibited without permission.

Acknowledgments

I am indebted to Professors Susannah P. Fritton, Sheldon Weinbaum, and Stephen C. Cowin for their wonderful advice, guidance, and financial support for the past five and half years. Special thanks go to Dr. Stephen B. Doty at the Hospital for Special Surgery who has kindly trained me to perform the in vivo experiments in his laboratory. Their mentoring and training are highly appreciated.

Many people have helped me and inspired me along my way. They are Chris Fritton, Orla O'Shea, Janane N. Diouri, Anthony Labissiere, and Dr. Betsy Myers at the Hospital for Special Surgery; and Drs. Mitchell B. Schaffler, Karl Jepsen, and Bob Majeska at Mount Sinai School of Medicine. Thank you all!

I am blessed to have been a lucky member of the big family consisting of the faculty, staff, and all the students at the New York Center for Biomedical Engineering. I thank Dr. Laurent Mars, Ms. Carol Bamberger, Stewart Russell, Nerine Green, Ji Song, Guoyu Yang, Xiaping Hu, Mia Mia Thi, Lidan You, Li Yuan Mi, Peng Guo, Thoma Beno, Young June Yoon, Cesare Ciani, and many others. Knowing these wonderful individuals was the fun part of my PhD studies.

It would have been impossible for me to get my PhD without the support of my family. My daughter, Grace, always lifted my heart whenever I failed in an experiment and felt depressed. My husband, Peixiang, postponed his own PhD studies and worked very hard so that I could focus on my studies. My parents and parents-in-law came from China and helped us to take care of Grace. This dissertation, therefore, should be dedicated to my beloved family.

Reproduced with permission of the copyright owner. Further reproduction prohibited without permission.

Table of Contents

Reproduced with permission of the copyright owner. Further reproduction prohibited without permission.

Reproduced with permission of the copyright owner. Further reproduction prohibited without permission.

Reproduced with permission of the copyright owner. Further reproduction prohibited without permission.

List of Tables

Reproduced with permission of the copyright owner. Further reproduction prohibited without permission.

List of Illustrations, Charts, Diagrams

Reproduced with permission of the copyright owner. Further reproduction prohibited without permission.

Reproduced with permission of the copyright owner. Further reproduction prohibited without permission.

Chapter 1 Introduction

The new millennium witnessed the launching of a widely endorsed international campaign, the Bone and Joint Decade (2000-2010), at the headquarters of the World Health Organization in Geneva, Switzerland in January 2000. This campaign calls for public attention and research efforts on the musculoskeletal system and its disorders. The musculoskeletal system supports the weight of the trunk, protects the internal organs, confers the power of locomotion, and serves as the mineral reservoir to maintain proper metabolism. Musculoskeletal disorders, such as joint diseases, osteoporosis, osteoarthritis, rheumatoid arthritis, low back pain, spinal disorders, severe trauma to the extremities, and disabling conditions in children, affect hundreds of millions of people around the world today and remain a major threat especially to women and the elderly. Because the population is aging rapidly, the number of people older than 50 is predicted to double by 2020 (World Health Report, 1998, www.boneandjointdecade.org). Therefore, more efforts are needed to address the clinical problems associated with the musculoskeletal system.

The goal of this dissertation is to better understand how physiological forces and blood circulation influence bone growth, adaptation, and metabolism. This line of research provides important insights into bone physiology and helps us to better understand and to develop methods to combat many of the musculoskeletal disorders mentioned above.

Reproduced with permission of the copyright owner. Further reproduction prohibited without permission.

Bone Tissue and Bone Cells

There are two types of bone in mammalian skeleton: cortical (or compact) bone and trabecular (or cancellous or spongy) bone. Cortical bone is very dense and forms the outer shells of all bones and the diaphyses of long bones, while trabecular bone consists of small interconnected plates and rods called trabeculae and forms the ends of long bones. Both cortical and trabecular bone have a layered (lamellar) structure. Cortical bone consists of layers of lamellae in either a parallel or concentric arrangement, and the concentric cylinders are called osteons. The central lumens of the osteons, also called osteonal canals, house blood vessels and nerve fibers (Fig.1-1). The typical size of an osteon is in the range of 100-300 microns in diameter and its central canal is usually in the range of 20-50 microns. A trabecula usually consists of several parallel lamellae and has a typical thickness of 200 microns with no blood vessels inside (Cooper et al., 1966; Black et al., 1974).

There are four types of bone cells: osteoblasts, bone lining cells, osteocytes, and osteoclasts. Osteoblasts cover bone surfaces and are able to deposit extracellular matrix. Bone lining cells are resting cells that cover inactive bone surfaces and do not produce extracellular matrix. As the deposition front moves, some osteoblasts are left behind in the newly formed matrix and become osteocytes. Osteocytes, the most abundant bone cells, are housed in small ellipsoidal spaces called lacunae within the calcified matrix. The long axis of a lacuna is ~10 microns. Osteocytes encased in the lacunae maintain contacts with each other and with osteoblasts located on the bone surfaces via a system of cell processes located in the canalicular channels with a radius of 50 to 200 nm (Fig. 1-1).

Reproduced with permission of the copyright owner. Further reproduction prohibited without permission.

Osteoclasts are multi-nucleated cells recruited from the blood stream to the resorption sites and are responsible for destroying bone matrix.

The intercellular network formed by osteocytes and osteoblasts is believed to play an important role not only in sensing external loading and communicating signals between cells (Cowin et al., 1991; Moss, 1997; Zhang et al., 1997; Burger and Klein-Nulend, 1999) but also in bone metabolism (e.g., Cooper et al., 1966; Piekarski and Munro, 1977). The lacunar-canalicular pores housing the osteocytic processes are connected to the vascular pores (i.e., osteonal canals and the transverse Volkmann's canals) that contain blood vessels (Fig. 1-1). Therefore, the lacunar-canaliculi porosity provides a continuous fluid pathway for the osteocytes to obtain nutrients from the blood vessels and to dispose of wastes to the blood vessels (Cooper et al., 1966). In addition to the vascular porosity and the lacunar-canalicular porosity, collagen-hydroxyapatite porosity is proposed to exist between the crystallites of the mineral hydroxyapatite (Cowin, 1999). Although there is no doubt that the vascular pores and the lacunar-canalicular pores form a continuous interstitial fluid pathway, whether the collagen-hydroxyapatite porosity is a part of the fluid pathway is still debated. Some investigators believe that this microporosity is unlikely to be a continuous pathway for fluid flow because most water in this porosity is bound by interaction with the ionic crystal (Neuman and Neuman, 1958, Weinbaum et al., 1994), while others think that it may be permeable to interstitial fluid (e.g., Salzstein et al., 1987; Mak et al., 2000).

Reproduced with permission of the copyright owner. Further reproduction prohibited without permission.

Bone Adaptation

Despite its inert appearance as a calcified tissue, bone is a living and continuously self-renewing tissue. Bone is capable of adapting its mass and structure to its environmental mechanical, hormonal, and metabolic changes. For example, exercise increases bone mass while reduced loading such as long time bedrest or space flight results in bone loss. This responsive behavior of bone, often termed bone adaptation or bone remodeling, remains intriguing since Wolff observed more than a century ago that the organization of bone structural components appeared to coincide with the axes of principal stress when the bone was subjected to mechanical loading. In addition to mechanical stimuli, bone also responds to hormonal and vascular factors, as shown in post-menopausal osteoporosis and venous stasis induced periosteal bone growth (Kiaer. 1994).

Although it is well accepted that mechanical stimuli are critical for bone maintenance and bone growth, it still remains unclear which aspect(s) of mechanical loading is the stimulation signal to osteocytes. Strain magnitude (e.g., Lanyon et al., 1982; Rubin and Lanyon, 1987; Chambers et al., 1993; Torrance et al., 1994; Cullen et al., 2001), strain rate (e.g., O'Connor et al., 1982; Hart et al., 1984; Turner et al., 1995; Mosley and Lanyon, 1998; Qin et al., 1998), strain gradient (e.g., Gross et al., 1997; Judex et al., 1997), error strain (Judex and Zernicke, 2000); strain energy (Carter et al., 1987; Huiskes et al., 1987; Brown et al., 1990; Levenston and Carter, 1998) have been proposed to be the mechanical stimulation, and phenomenological studies (e.g., Cowin, 1976; 1983; Hart et al., 1984; Siffert et al., 1996; Fernandes et al., 1999; Adachi et al., 2001; Ramtani and

Reproduced with permission of the copyright owner. Further reproduction prohibited without permission.

Zidi, 2001) have been performed to explore theoretically how the change of certain aspects of mechanical loading induces the bone adaptation response.

Bone's Mechanosensory System

One of the fundamental mysteries in bone adaptation is the mechanotransduction mechanism by which osteocytes sense their external mechanical stimuli and initiate the deposition or resorption of bone tissue. It is generally believed that osteocytes, the most abundant cells that are buried in the mineralized matrix, are the sensory cells in bone's mechanosensory system, due to the fact that the osteocytes form an interconnected cellular network with each other and also with osteoblasts. This cellular network is believed to communicate cellular signals to osteoblasts to initiate bone deposition as well as to recruit osteoclasts to take away existing bone matrix (Cowin et al., 1991; Burger et al., 1995).

Shear stresses resulting from load-induced interstitial fluid flow have been suggested to be involved in the signal transduction from the mechanical loading to the bone cell population (Weinbaum et al., 1991; 1994; Turner et al., 1994; Cowin et al., 1995); and the sensitivity of bone cell populations to fluid shear stress has been demonstrated with biochemical responses (i.e., releasing nitric oxide, prostaglandin, and calcium, etc.) in cell cultures within flow chambers (Reich et al., 1990; Burger et al., 1991; Williams et al., 1994; Hung et al., 1995; Klein-Nulend et al., 1995; Johnson et al., 1996; Smalt et al., 1997; Jacobs et al., 1998; Chiquet, 1999; Chen et al., 2000; Cheng et al., 2001; Donahue et al., 2001; Ogasawara et al., 2001).

Reproduced with permission of the copyright owner. Further reproduction prohibited without permission.

An alternative candidate mechanism is that bone cells respond directly to deformation (mechanical strain). In vitro experiments have shown that bone cell substrate deformation can influence DNA and protein synthesis, cyclic AMP production, and release of PGE2 (Duncan and Misler, 1989; Buckley et al., 1990; Duncan and Turner, 1995; Rawlinson et al., 1996; Toma et al., 1997; Ziambaras et al., 1998; Mikuni-Takagaki, 1999; Walker et al., 2000; Kurata et al., 2001). However, the strain applied to in vitro cell cultures in those studies (up to 10%) is generally much higher than the recorded peak strains in human and animal bone (~ 0.2% up to ~ 0.5%, Burr et al., 1996; Yoshikawa et al., 1994; Milgrom et al., 2000; Fritton and Rubin, 2001). Recently theoretical models have been proposed to explore the amplification mechanism of mechanical strain from the tissue level to the cellular level due to the fluid flow-induced drag force on the pericellular transverse fibers in mechanically loaded bone (Cowin and Weinbaum, 1998; You et al., 2001).

Other secondary effects of mechanical loading have also been proposed to be the stimuli for bone remodeling. Microcracks (or microdamage) in the bone matrix has been proposed to provide a stimulus for bone repair and remodeling (Carter and Hayes, 1977; Burr et al., 1985; Martin, 1992; Burr, 1993; Mori and Burr, 1993; Taylor and Prendergast, 1997; Bentolila et al., 1998; Verborgt et al., 2000). Experimental studies have found that accumulation of microcracks or microdamage is associated with the decline of osteocytic lacunar density (Vashishth et al., 2000). Rat bone has been found to undergo intracortical remodeling in response to high levels of cyclic strain, and intracortical resorption is associated both with bone microdamage and with regions of altered osteocyte integrity (Bentolila et al., 1998).

Reproduced with permission of the copyright owner. Further reproduction prohibited without permission.

Interstitial Fluid Flow and Streaming Potentials

Because of its potential role in bone's mechanosensory system, interstitial fluid flow has been investigated in mechanically loaded bone. Interstitial fluid flow is produced in the lacunar-canalicular porosity as the porous bone matrix is deformed and spatial pressure gradients are produced. As the fluid passes the negatively charged bone matrix, an electric current is created and electrical potentials, also called streaming potentials or strain-generated potentials, can be recorded in bone (Eriksson, 1974). Because electrokinetic analyses have shown that streaming potentials are proportional to the fluid pore pressure in bone (Salzstein et al., 1987; Cowin, 1999), streaming potentials have been used as an indirect measure of interstitial fluid.flow in mechanically loaded bone (Eriksson, 1974; Starkebaum et al., 1979; Gross and Williams, 1982; Pienkowski and Pollack, 1983; Scott and Korostoff, 1990; Otter et al., 1994; MacGinitie et al., 1997). In addition, streaming potentials due to the hydraulic pulsatile blood pressure have been recorded in bone, suggesting that blood pressure can also drive interstitial fluid flow (Otter et al., 1990).

Theoretical models have been established to enhance our understanding of bone fluid behavior due to mechanical loading. Pollack and coworkers developed a mathematical model that predicted the phase and frequency of streaming potentials (i.e., fluid flow) consistent with experimental data if a continuous microporosity was assumed to exist in the matrix (Salzstein et al., 1987). Weinbaum, Cowin, and coworkers have argued that the lacunar-canalicular porosity is the anatomical site of the streaming potentials and a pericellular fiber matrix fills the fluid annular space surrounding the

Reproduced with permission of the copyright owner. Further reproduction prohibited without permission.

osteocytic cell process (see Fig. 1-2) (Cowin et al., 1991; Weinbaum et al., 1994; Zeng et al., 1994; Cowin et al., 1995; Cowin and Weinbaum, 1998; You et al., 2002). They predicted that a stimulating shear stress (8-30 dyn/cm^2) is induced on the osteocytic cell membrane under physiological strains (Weinbaum et al., 1994) and a good agreement with experimental streaming potential data can be achieved (Cowin et al., 1995). One of their recent studies also shows that the drag force induced by the bone fluid flow on the fibers in the pericellular matrix can produce a 1% to 10% hoop (circumference) strain on the osteocytic cell process membrane (You et al., 2001).

However, there are two remarkable experimental findings that are not consistent with these theoretical models. As an indirect measure of bone fluid flow, the detailed streaming potentials were recorded using electrodes across neighboring osteons of a stressed bone specimen in four-point bending in the pioneering experiment of Starkebaum et al. (1979). The measurement was performed when the specimen was mechanically loaded at 1 Hz, which led to the remarkable observation that the local spatial gradients in voltage near the osteonal canals were 10 to 30 times greater than the spatial gradients across the whole bone specimen. A second, more recent, paradox is the observation of Otter et al. (1994) that the relaxation time for the bone fluid pressure or the strain generated-potentials does not appear to depend on the thickness of the cortical bone specimen. This behavior is incompatible with the spatially homogeneous theory developed in Salzstein et al. (1987), Weinbaum et al. (1994), and Cowin et al. (1995), where the characteristic time for the relaxation of the bone fluid pressure is proportional to the square of the bone specimen thickness and the osteonal structure is not considered. The experiments of Starkebaum et al. (1979) and Otter et al. (1994) suggest that the

Reproduced with permission of the copyright owner. Further reproduction prohibited without permission.

heterogeneous microstructure of bone should be considered in models of fluid flow and the assumption that bone fluid relaxes across the bone specimen thickness via the continuous same-sized small pores may be incorrect. To address these two paradoxes, a large-scale heterogeneous osteonal bone model has been developed (Wang et al., 1999) and will be discussed in Chapter 2 of this dissertation.

Interstitial Fluid Flow and Bone Metabolism

In addition to the suggested role in bone's mechanosensory mechanism, load-induced interstitial fluid flow has been proposed to enhance mass transport in cortical bone to insure metabolic function of osteocytes (Piekarski and Munro, 1977; Knothe Tate et al., 1998a, b, and c; 2000). In living tissue, cells usually obtain nutrients and dispose of waste products by the process of diffusion between blood vessels and cells. However, since osteocytes are buried in the calcified matrix, nutrients and wastes must pass through the long and narrow canalicular channels before reaching their destinations. Although a small molecule such as procion red (300-400 Daltons) with a molecular diameter of less than 1 nm was found to perfuse the lacunar-canalicular porosity within 10 min of post-injection in the absence of mechanical loading (Knothe Tate et al., 1998b), diffusion alone may be insufficient to transport large molecules for cell metabolism. Knothe Tate and coworkers have injected procion red into the rat and sheep bone under mechanical loading and found that the number of pericellular lacunar spaces labeled with the fluorescent tracer is significantly higher in loaded bone than in unloaded bone KnotheTate et al., 1998a; Knothe Tate and Knothe, 2000; Knothe Tate et al., 2000).

Reproduced with permission of the copyright owner. Further reproduction prohibited without permission.

Although theoretical models have shown a significant greater interstitial fluid displacement in mechanically loaded bone (Piekarski and Munro, 1977; Kufahl and Saha, 1990; Knothe Tate et al., 1998c), there is no detailed mechanism of how the enhancement of solute transport is achieved regardless of the reversibility of the fluid movement. In cyclically loaded bone, there is no net fluid exchange during a whole cycle of loading between the central osteonal canal and the porous bone matrix for any periodic waveform. With no net fluid exchange, it seems unlikely that the osteocytes inside the bone matrix could gain any net nutrient supply from the convective fluid flow. A fundamental question is thus how can net mass transport occur in cyclically loaded bone? To address the question of irreversibility of solute transport, a lacunar mixing process was proposed, which produces a difference in tracer concentration between inward and outward flows and thus enhances the net tracer transport in cyclically loaded bone (Wang et al., 2000). The model will be presented in Chapter 3.

Exploring Bone Microstructure and Tracking Interstitial Fluid Flow Using Molecular Tracers

In order to understand the interstitial fluid pathway in bone, tracer techniques have been used to perfuse the different bone fluid compartments. A substance (also called tracer, marker, or dye) that can be detected by its radioactivity or fluorescence or histochemical reaction is usually injected into the blood circulation. After a certain time period, the amount or distribution of the tracer can be studied by examining the tracer's radioactivity or fluorescence or chemical reactions with certain reagents. Tracers of different molecular weights and sizes have been used to explore different fluid

Reproduced with permission of the copyright owner. Further reproduction prohibited without permission.

compartments such as the vascular space, the extravascular space, and the bone matrix pores. A summary of the tracers can be found in Knothe Tate et al. (1998b). Briefly, large tracers such as strontium-labeled red blood cells and microspheres with a diameter greater than 15 microns are usually used to measure the vascular space in bone. Smaller tracers such as ferritin (10 nm in diameter), albumin (7 nm in diameter), horseradish peroxidase (6 nm in diameter), microperoxidase (2 nm in diameter), and procion red (1 nm in diameter) have been used to explore vascular and lacunar-canalicular pores. To explore the collagen-hydroxyapatite porosity in the bone matrix, tracers of further smaller sizes such as sucrose and EDTA must be used.

The previous studies employing different tracers such as ferritin, horseradish peroxidase, microperoxidase, and procion red to explore the fluid pathways in bone have provided conflicting results. For example, ferritin was found to form halo-shaped labeling in the bone matrix surrounding the blood vessels in two-day-old chick bone (Dillaman, 1984) and in adult dog bone (Montgomery et al., 1988), while more recent studies showed incomplete rings of a ferritin front surrounding the blood vessels in the adult goat (Qin et al., 1999; Mak et al., 2000). For horseradish peroxidase, some studies found the tracer in almost all lacunae and not in the mineralized matrix (Doty and Schofield, 1972; Tanaka and Sakano, 1985) while others found the tracer labeling in the mineralized matrix of adult rat bone (Dillaman et al., 1991) or labeled lacunae in the inner third of the cortex (Knothe Tate et al., 1998b). For microperoxidase, Tanaka and Sakano (1985) found the tracer was present in the canaliculi but was excluded from the mineralized matrix, while a more recent study reported two discrete labeling bands in the mineralized matrix (Knothe Tate et al., 1998b). For procion red, one study reported that this tracer

Reproduced with permission of the copyright owner. Further reproduction prohibited without permission.

was excluded from the mineralized bone matrix 30 minutes post-injection in fresh sections of the rat tibia (Knothe Tate et al., 1998b), while a later study found the tracer in the matrix in PMMA sections of the rat tibia (Knothe Tate et al., 2001).

The inconsistency of tracer labeling patterns may be due to several factors, such as different species and age of experimental animals, varied circulation time (the time period between injection and the stop of circulation), and different histological processing methods used in each experiment. Due to the hardness of bone tissue, bone samples have to go through several necessary and time-consuming histological procedures before the final tracer labels can be visualized. The main artifact for tracer studies, therefore, is the re-displacement of the tracer particles during the long time period when the samples are immersed in aqueous solutions for fixation, decalcification, embedding, or staining processes. To address these conflicting results from previous tracer studies, and more importantly, to further explore the fluid pathway in bone, a well-controlled perfusion experiment has been performed, which will be presented in Chapter 4.

Blood-driven Fluid Flow and Periosteal Bone Growth in Venous Stasis

Besides mechanical loading as a primary stimulus for bone adaptation, the ability of blood flow to influence bone growth and remodeling has been recognized for a long time (Trueta, 1963; Kiaer, 1994). Altered circulation such as stasis in the venous system of an extremity caused by applying tourniquets or vein ligation has been shown to stimulate bone formation or increase bone mass in the young dog (Kelly and Bronk, 1990), the young goat (Welch et al., 1993), and in a disuse rat model (hindlimb suspended) (Bergula et al., 1999). There are many other studies demonstrating similar effects (e.g., Lilly and

Reproduced with permission of the copyright owner. Further reproduction prohibited without permission.

Kelly, 1970; Arnoldi et al., 1972; Green and Griffin, 1982; Liu and Ho, 1991). The blocking or compromised venous drainage in those experiments has been found to be associated with increased intramedullary pressure, decreased artery inflow, and decreased pulse of intramedullary pressure (Ficat and Arlet, 1980). The underlying mechanism of the periosteal bone growth induced by venous stasis, however, remains unclear. Several factors associated with bone vasculature have been proposed, including changes in oxygen tension, CO_2 tension, local pH (reviewed in Kiaer, 1994), increased interstitial fluid flow (shear stress or streaming potentials) (Kelly and Bronk, 1990; Hillsley and Frangos, 1994; Welch et al., 1993; Bergula et al., 1999), and increased transcapillary filtration (Kelly et al., 1990; Bronk et al., 1993).

To explore the role of interstitial fluid flow in the venous stasis induced periosteal bone growth, a theoretical model was developed to examine the osteogenic capacity of blood pressure-driven fluid flow in terms of fluid shearing stress on the osteocytic membrane. Unlike previous theoretical models of bone interstitial fluid flow that have been developed to explain the tracer distribution due to the centrifugal bulk fluid movement in porous bone matrix (Dillaman et al., 1991; Keanini et al., 1995), this new model links the interstitial fluid flow in the lacunar-canalicular porosity with the excitation of osteocytes and osteogenesis, which will be discussed in Chapter 5.

Organization of the Dissertation

This dissertation consists of six chapters. The present chapter serves as an introduction to the entire dissertation and the last chapter concludes the dissertation and offers suggestions for future work. The remaining four chapters focus on the questions

Reproduced with permission of the copyright owner. Further reproduction prohibited without permission.

that have been raised in this chapter, namely, the non-linear fluid flow behavior in heterogeneous porous bone matrix, lacunar-mixing in cyclically loaded bone, perfusion of porous bone matrix using tracers of various sizes, and the osteogenesis of blood-induced fluid flow. Each of the four chapters contains sections of Introduction, Methods, Results, and Discussion. Two chapters have been published in peer-reviewed journals and the other two will be submitted for publication. A brief synopsis of Chapters 2-6 follows:

Chapter 2 is entitled "Fluid Pressure Relaxation Depends Upon Osteonal Microstructure: Modeling an Oscillatory Bending Experiment," and was published in the *Journal of Biomechanics* 32 (1999): 663-672. A spatially heterogeneous large scale model was developed to explore the hypothesis that the primary relaxation of the excess bone fluid pressure in mechanically loaded osteonal bone occurs through the osteonal canals and not between the surfaces of the bone specimen as had been assumed until now. This new model considered two levels of bone's intrinsic porosities (osteonal canal and lacunar-canalicular pores) and corrected a fundamental error in previous models with a uniform pore size. Using this new model, two long-standing paradoxes were successfully solved about bone fluid relaxation, i.e., the non-linearity of streaming potentials in osteonal bone and the independence of fluid relaxation time with the thickness of bone.

Chapter 3 is entitled "Modeling Tracer Transport in an Osteon Under Cyclic Loading," and was published in the *Annals of Biomedical Engineering* 28 (2000): 1200-9. A novel lacunar mixing mechanism was proposed and simulated computationally to explain the fundamental conundrum as to how during cyclic mechanical loading there can be net solute transport in bone when there is no net fluid movement over a loading cycle.

Reproduced with permission of the copyright owner. Further reproduction prohibited without permission.

The lacunar mixing hypothesis is that the fluid space in an osteocytic lacuna facilitates a nearly instantaneous mixing process of bone fluid that creates a difference in tracer concentration between the inward and outward canalicular flow and thus ensures net tracer transport to the osteocytes during cyclic loading, as has been shown experimentally. The sequential spread of the tracer from the osteonal canal to the lacunae was investigated for an osteon experiencing a sinusoidal loading.

Chapter 4 is entitled "Delineating the Bone Interstitial Fluid Pathway in Vivo," and will be submitted to *Bone*. Four different sized tracers (reactive red, microperoxidase, horseradish peroxidase, and ferritin) were injected into the rat jugular vein and allowed to circulate for 5 minutes. The tracer labeling patterns showed that reactive red, microperoxidase, and horseradish peroxidase passed through the canaliculi into the osteocytic lacunae, while ferritin was excluded from the mineralized matrix and could not label the osteocytes. This result suggests that the fiber spacing of the pericellular matrix proposed by Weinbaum and Cowin (Weinbaum et al., 1994; Cowin et al., 1995) should be in the range of 6-10 nm. The tracer movement in the absence of mechanical loading was also quantified, with the results suggesting that microperoxidase and horseradish peroxidase, but not reactive red and ferritin, are suitable for tracking load-induced fluid flow.

Chapter 5 is entitled "Blood Pressure-Driven Interstitial Fluid Flow in Bone," and will be submitted to the *Journal of Biomechanics*. A theoretical model was developed to quantitatively investigate the relative osteogenic capacity of mechanical loading and blood pressure. This model was developed to test the hypothesis that the increased interstitial fluid flow is responsible for the periosteal bone growth in venous stasis. The

Reproduced with permission of the copyright owner. Further reproduction prohibited without permission.

much lower shear stress induced by blood pressure in venous stasis suggests that the hypothesis is invalid and other factors associated with venous stasis must account for the periosteal bone growth. I postulate that a higher pressure on the periosteum and/or a higher pressure gradient within the periosteum may be the stimulus.

Chapter 6 concludes this dissertation and suggests some future work.

Reproduced with permission of the copyright owner. Further reproduction prohibited without permission.

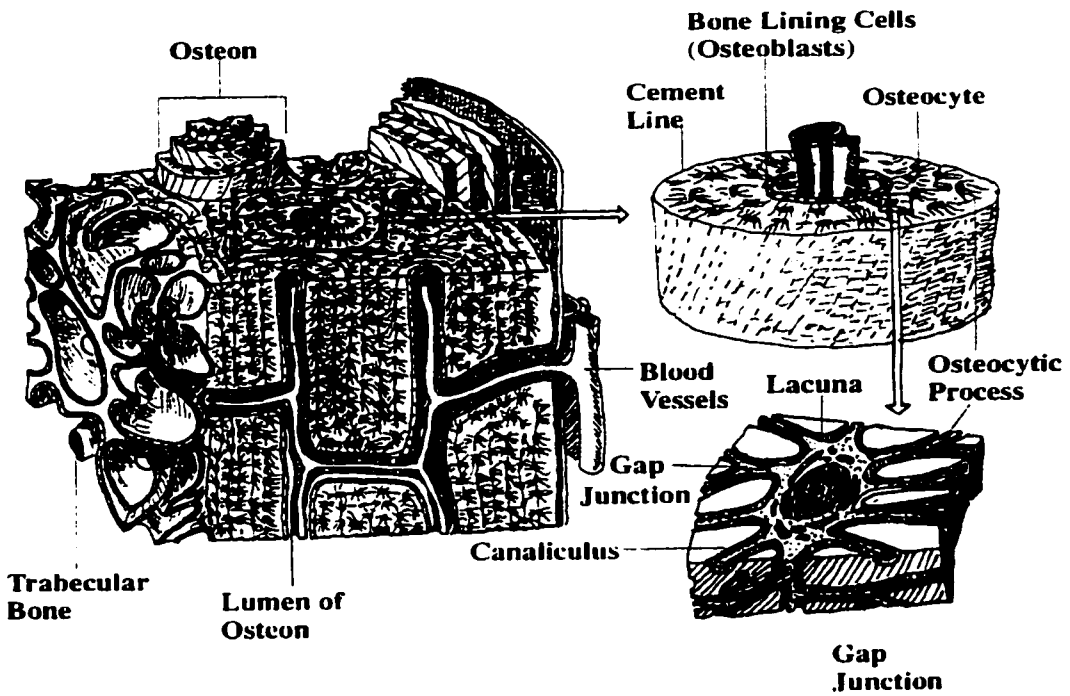

(A)

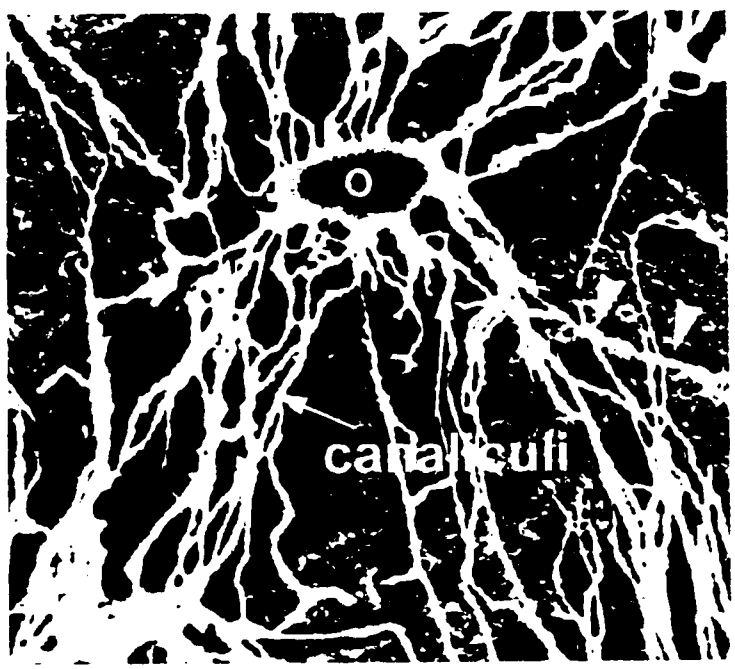

(B)

Fig. 1-1. (A) Bone structure (adapted from Zhang et al., 1997) (B) Osteocytic lacuna and canaliculi (from Curtis et al., 1985).

Reproduced with permission of the copyright owner. Further reproduction prohibited without permission.

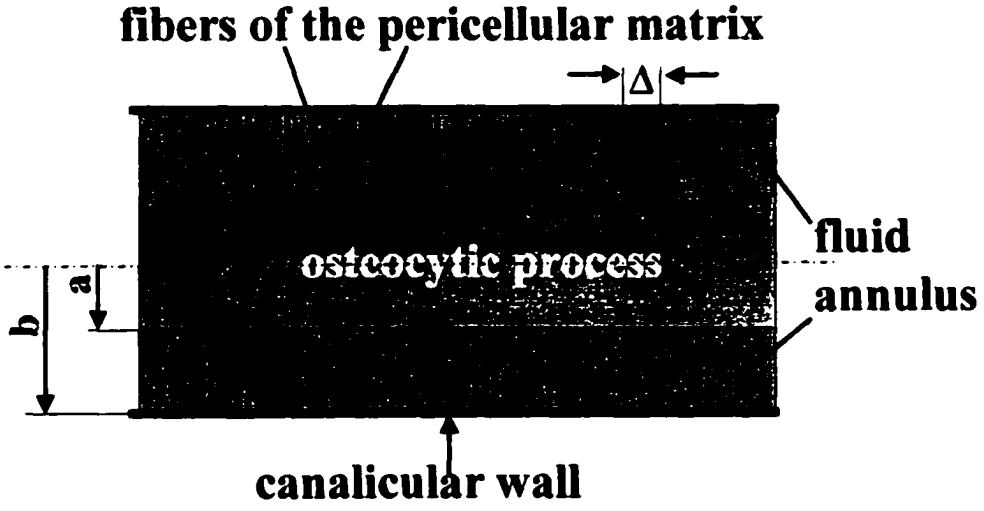

Fig. 1-2. A schematic model of longitudinal cross-section of a canaliculus. The osteocytic process is located in the center of the canaliculus. A pericellular fiber matrix fills the fluid annulus between the cell process (radius a) and the canalicular wall (radius b). The spacing between the fibers is Δ, which is believed to be 7 nm. Interstitial fluid flow in the canaliculus produces shearing stresses on the osteocytic cell process membrane and deforms the cytoskeleton due to the drag forces acting on the transverse fibers, which may help the cell to detect the external mechanical loading (adapted from Weinbaum et al., 1994).

Reproduced with permission of the copyright owner. Further reproduction prohibited without permission.

Chapter 2 Fluid Pressure Relaxation Depends Upon Osteonal Microstructure: Modeling an Oscillatory Bending Experiment*

Abstract

When bone is mechanically loaded, bone fluid flow induces shear stresses on bone cells that have been proposed to be involved in bone's mechanosensory system. To investigate bone fluid flow and strain-generated potentials, several theoretical models have been proposed to mimic oscillatory four-point bending experiments performed on thin bone specimens. While these previous models assume that the bone fluid relaxes across the specimen thickness, we hypothesize that the bone fluid relaxes primarily through the vascular porosity (osteonal canals) instead and develop a new poroelastic model that integrates the microstructural details of the lacunar-canalicular porosity, osteonal canals, and the osteonal cement lines. Local fluid pressure profiles are obtained from the model, and we find two different fluid relaxation behaviors in the bone specimen, depending on its microstructure: one associated with the connected osteonal canal system, through which bone fluid relaxes to the nearby osteonal canals; and one associated with the thickness of a homogeneous porous bone specimen (~ 1 mm in our model), through which bone fluid relaxes between the external surfaces of the bone specimen at relatively lower loading frequencies. Our results suggest that in osteonal bone specimens the fluid pressure response to cyclic loading is not sensitive to the permeability of the osteonal cement lines, while it is sensitive to the applied loading frequency. *Our results also reveal that the fluid pressure gradients near the osteonal

* Reprinted from *Journal of Biomechanics*, Vol 32, Wang et al., pp. 663-672, Copyright (1999), with permission from Elsevier Science.

Reproduced with permission of the copyright owner. Further reproduction prohibited without permission.

canals (and thus the fluid shear stresses acting on the nearby osteocytes) are significantly amplified at higher loading frequencies.

Introduction

Although it is well accepted that bone is able to adapt its structure to its mechanical environment, the mechanism by which bone cells sense their mechanical environment and initiate the deposition or resorption of bone tissue has not been ascertained. The shear stresses resulting from bone fluid flow when bone is stressed have been suggested to be involved in the signal transduction from the mechanical loading to the bone cell population (Weinbaum et al., 1994; Turner et al., 1994; Cowin et al., 1995), and the sensitivity of bone cell populations to fluid shear stress has been demonstrated in cell cultures within flow chambers (e.g., Reich et al., 1990; Williams et al., 1994; Hung et al., 1995; Klein-Nulend et al., 1995). Theoretical models have been established to enhance our understanding of bone fluid behavior in stressed bone either in homogeneous porous bone specimens (Salzstein et al., 1987; Weinbaum et al., 1994; Cowin et al., 1995) or in single osteons (Piekarski and Munro, 1977; Pollack et al., 1984; Petrov et al., 1989; Kufahl and Saha, 1990; Zeng et al., 1994); however, some experiments are still unexplained (Starkebaum et al., 1979; Otter et al., 1994).

The pioneering experiment of Starkebaum et al. (1979), in which the detailed strain-generated potentials (SGPs) were measured across neighboring osteons of a stressed bone specimen in four-point bending, led to the remarkable observation that the local spatial gradients in voltage near the osteonal canals were 10 to 30 times greater than the spatial gradients across the whole bone specimen. A second, more recent, paradox is the observation of Otter et al. (1994) that the relaxation time for the bone fluid pressure

Reproduced with permission of the copyright owner. Further reproduction prohibited without permission.

or the SGP does not appear to depend on the thickness of the cortical bone specimen. This behavior is incompatible with the spatially homogeneous theory developed in Salzstein et al. (1987), Weinbaum et al. (1994), and Cowin et al. (1995), where the characteristic time for the relaxation of the bone fluid pressure is proportional to the square of the bone specimen thickness and the osteonal structure is not considered. The experiments of Starkebaum et al. (1979) and Otter et al. (1994) suggest that the heterogeneous microstructure of bone should be considered in models of fluid flow and the assumption that bone fluid relaxes across the bone specimen thickness via the continuous same-sized small pores may be incorrect.

The new model developed in this paper explores the hypothesis that the primary relaxation of the excess bone fluid pressure in mechanically loaded osteonal bone occurs through the osteonal canals and not between the surfaces of the bone specimen as has been assumed until now. While such behavior might be anticipated for individual osteons that have an impermeable outer boundary (cement line) and are uncoupled (Pollack et al., 1984; Petrov et al., 1989; Kufahl and Saha, 1990; Zeng et al., 1994), we shall show, quite surprisingly, that this same behavior is obtained when there is osteonal coupling and bone fluid flow across the cement line. This new model examines both the effect of the osteonal canals and the leakage of bone fluid across the cement line due to the partial penetration of this osteonal boundary by canaliculi. The model combines the microstructural analysis of the lacunar-canalicular porosity developed in Weinbaum et al. (1994) and Cowin et al. (1995) in a spatially heterogeneous larger scale model for the osteonal array.

Reproduced with permission of the copyright owner. Further reproduction prohibited without permission.

Methods

Starkebaum et al. (1979) measured the local variation of SGPs across a 1-mm thick osteonal bone specimen under 1 Hz four-point bending (Fig. 2-1a). To mimic this experiment, we formulate an idealized model of an osteonal bone specimen that includes the microstructural details of the osteons such as the osteonal canals (the circles), the cement lines (the squares) and the lacunar-canalicular porosity that occupies the region between the osteonal canal and cement line in each osteon (Fig. 2-1b). The specimen thickness (2D) is 1.2 mm and there are six rows of osteons across this thickness. The boundary of each osteon (cement line) is simplified into a square with a length (d) of 200 μm, although anatomically it would tend to be circular. The diameter of the osteonal canals (d_c) ranges from 0 to 60 μm. The special case of zero canal size (d_c = 0 μm) is included in the model as a limiting case. The specimen is loaded sinusoidally with an overall linear stress distribution across the specimen thickness due to the applied bending moment M. Please note that physiological loading usually induces stresses that are aligned or parallel to the osteonal canals and that in our model the induced stresses are transverse to the osteonal canals to mimic the loading in Starkebaum et al. (1979).

Since the dimensions of the specimen in the x and z directions are much larger than that in the y-direction, we consider that pure bending is applied to the specimen according to the St. Venant approximation, and we only consider the fluid flow in the y-direction. Similar to the models in Weinbaum et al. (1994), Zeng et al. (1994) and Cowin et al. (1995), this model assumes that the fluid flows through the lacunar-canalicular porosity where we assume there is a gel-like matrix in the fluid annulus surrounding the osteocytic process in the canaliculi (see Fig. 1 of Cowin et al., 1995). Because tracer

Reproduced with permission of the copyright owner. Further reproduction prohibited without permission.

studies have shown that both the small tracer microperoxidase (2 nm) and the even smaller tracer procion red are blocked by the walls of canaliculi (Tanaka and Sakano, 1985; Ayasaka et al., 1992; Knothe-Tate et al., 1998) and because there is no evidence showing that the collagen-hydroxyapatite pores are continuous pathways for convective fluid flows, the contribution of such smaller pores to bone fluid relaxation is not considered in this model.

Weinbaum et al. (1994) solved the problem of fluid flowing through a gel-like matrix in the canalicular annulus surrounding the osteocytic process. In that paper, the Darcy permeability constant, k, was obtained by first determining the fluid flux in a single canaliculus and then multiplying this flux by the number of canaliculi per unit area n (n = 0.022 μm^{-2} from Zeng et al., 1994):

$$k = \frac{2\pi n a^4 q^3}{\gamma^3}\left\{A_1\left[I_1(\gamma/q) - qI_1(\gamma)\right] + B_1\left[qK_1(\gamma) - K_1(\gamma/q)\right] + \frac{\gamma(q^2-1)}{2q}\right\} \qquad (1)$$

where

$$A_1 = \frac{K_0(\gamma) - K_0(\gamma\ q)}{I_0(\gamma\ q)K_0(\gamma) - K_0(\gamma\ q)I_0(\gamma)} \text{ and } B_1 = \frac{I_0(\gamma\ q) - I_0(\gamma)}{I_0(\gamma\ q)K_0(\gamma) - K_0(\gamma\ q)I_0(\gamma)} \qquad (2)$$

In these equations a represents the radius of the osteocytic process (100 nm), b is the radius of the canaliculus (200 nm), q = b/a, $\gamma = b/\sqrt{k_p}$, where $\sqrt{k_p}$ is the thickness of the fiber interaction layer near the canalicular wall (~7 nm), and I_0, I_1, K_0 and K_1 are modified Bessel functions (Weinbaum et al., 1994). This Darcy permeability constant will appear in the diffusion constant, c, in the governing equation of the pore pressure (Eq. 3).

Poroelasticity (Biot) theory has previously been used to calculate the bone fluid pressure in the canaliculi produced by an external sinusoidal loading perpendicular to the

Reproduced with permission of the copyright owner. Further reproduction prohibited without permission.

long axis of an osteon (Zeng et al., 1994). The basic assumptions of Biot theory are (1) the porous material is an ideal elastic media following Hooke's law and (2) the fluid flows through the porous skeleton according to Darcy's law. The governing equation for the bone fluid pressure in a single osteon was derived from the balance laws and the constitutive equations (i.e., the isotropic stress-strain relations and the strain compatibility equations) in Zeng et al. (1994); in our model, we first transform the governing equation for the single osteon to Cartesian coordinates (Eq. 3). (For a comprehensive review of bone poroelasticity, please see Cowin (1999).)

$$\frac{\partial^2 p}{\partial x^2}+\frac{\partial^2 p}{\partial y^2}-\frac{1}{c}\frac{\partial p}{\partial t}=-\frac{\sigma\omega B}{3c}\cos\omega t\left[1-\frac{d_c^{\,2}(x^2-y^2)}{2(x^2+y^2)^2}\right] \tag{3}$$

In Eq. 3 the coordinate origin is the center of the osteonal canal, and the external oscillatory bending is $-\sigma \sin\omega t$. The Skempton constant B is a factor representing the coupling and relative compressibility of the solid and fluid phases in bone (B = 0.53), and the parameter c is a diffusion constant given by (k/μ)*(13.5 GPa) where the viscosity of bone fluid, μ, is assumed to be that of salt water and the Darcy permeability constant k has been given in Eq. 1 (Weinbaum et al., 1994).

Because pure bending is applied to the specimen in the oscillatory bending experiment, the resulting stress field is not uniform in the y-direction as in Zeng et al. (1994). The overall stress field according to beam theory is $\sigma(y, t) = (m\sin\omega t)y/I$, where $m\sin\omega t$ is the sinusoidal bending moment and I is the area moment of inertia. If six local coordinate systems $(x^{(n)}, y^{(n)})$ are defined at the center of each osteon (n = 1 to 6, see Fig. 2-2), the governing equation for the bone fluid pressure $(p^{(n)})$ within the nth osteon is given as:

Reproduced with permission of the copyright owner. Further reproduction prohibited without permission.

$$\frac{\partial^2 p^{(n)}}{\partial x^{(n)2}} + \frac{\partial^2 p^{(n)}}{\partial y^{(n)2}} - \frac{1}{c}\frac{\partial p^{(n)}}{\partial t} = -\frac{m(y_c^{(n)} + y^{(n)})\omega B}{3cI}\cos\omega t\left[1 - \frac{d_c^{\,2}(x^{(n)2} - y^{(n)2})}{2(x^{(n)2} + y^{(n)2})^2}\right] \quad (4)$$

where $y_c^{(n)}$ is the global coordinate for the center of the nth osteon. Eq. 4 is rendered dimensionless by the introduction of the following dimensionless variables:

$$X^{(n)} = \frac{x^{(n)}}{D},\ Y^{(n)} = \frac{y^{(n)}}{D},\ \tau = \frac{ct}{D^2},\ T = \frac{\omega D^2}{c},\ P = \frac{3pI}{mDBT} \quad (5)$$

thus

$$\frac{\partial^2 P^{(n)}}{\partial X^{(n)2}} + \frac{\partial^2 P^{(n)}}{\partial Y^{(n)2}} - \frac{\partial P^{(n)}}{\partial \tau} = -(Y_c^{(n)} + Y^{(n)})\cos T\tau\left[1 - \frac{D_c^{\,2}(X^{(n)2} - Y^{(n)2})}{2(X^{(n)2} + Y^{(n)2})^2}\right] \quad (6)$$

where D is the half thickness of the bone specimen (600 μm), $Y_c^{(n)} = \frac{y_c^{(n)}}{D}$ and $D_c = \frac{d_c}{D}$.

For our idealized bone specimen, the characteristic relaxation time of the fluid pressure, defined as $\tau_d = D^2/c$, is 1.08 s. For physiological loading (parallel to the osteonal canals), the governing equation for bone fluid pressure, which will not have an angular dependence, is given in Eq. 6 in the special case when $x = \pm y$.

The boundary conditions are assumed to be 'no flow' across the top and bottom external surfaces ($\partial p/\partial y = 0$ at $y = \pm D$) (Fig. 2-2), because the bone specimens were kept in a humid chamber during the bending experiments and the fluid surface tension will prevent bone fluid drainage at the fluid-air interfaces of wet bone for the lacunar-canalicular pores (Weinbaum et al., 1994; Cowin et al., 1995) but not for the osteonal canals. (One can readily show from Laplace's law for surface tension that osteonal canals of 25 μm radius will leak at pressures on the order of 0.05 atm, while the canaliculi of 0.2 μm radius at the free surfaces will not leak at pressures less than 7 atm). 'No flow'

Reproduced with permission of the copyright owner. Further reproduction prohibited without permission.

boundary conditions are also applied at the transverse periodic boundaries ($\partial p/\partial x = 0$ at $x = \pm d/2$) because of the structural symmetry of the osteonal arrays. As for the boundary conditions at the osteonal canals, Zhang et al. (1998) estimated that the fluid relaxation time in the osteonal canals (1.36 μs) is three orders of magnitude faster than that in the lacunar-canalicular pores (4.9 ms) under an impulsive step loading. Since the rise time of any physiological loading (typical impact loading is on the order of 10 ms) is much longer than the fluid relaxation time in the osteonal canals, a high pressure could not be sustained. In addition, in vivo fluid pressures in an osteonal canals cannot exceed the vascular pressure (~10^4 Pa, Wilkes and Visscher, 1975), or the blood vessels would collapse. Since the pressure in osteonal canal is much smaller than the pressure produced within the bone tissue when the bone is mechanically loaded (~10^6 Pa, Piekarski and Munro, 1977), a zero pressure is assumed for each osteonal canal.

It is generally believed that few canaliculi penetrate the cement lines, although Curtis et al. (1985) reported that some canaliculi could pass through the cement lines between first and second generation osteons in the cortices of long bones. Since the permeability at the cement lines between osteons has not been definitively determined, a variable parameter representing the osteonal coupling percentage has been applied at the cement lines ($y^{(n)} = \pm d/2$). The coupling percentage is varied from 0% to 100% to evaluate the effects of the osteonal coupling on the bone fluid relaxation. The 0% coupling represents 'no flow' ($\partial p^{(n)}/\partial y^{(n)} = 0$), while 100% coupling represents 'free flow' ($\partial p^{(n)}/\partial y^{(n)} = \partial p^{(n+1)}/\partial y^{(n+1)}$) across the cement lines. For the 100% coupling condition the permeability of the cement lines is the same as that of the surrounding bone. With partial coupling (10%, 20%, and 50%) between the osteons, only a portion of the

Reproduced with permission of the copyright owner. Further reproduction prohibited without permission.

central region of the cement lines is open to fluid flow, while the rest of the cement line is impermeable.

To mimic the experiment of Starkebaum et al. (1979), the magnitude of the sinusoidal loading m is chosen so that the outer fiber stress (mD/I) is 4 MPa, i.e., the outer fiber strain is approximately 200 με, and the peak fluid pressure (~ 5 atm) is about 12% of the maximum matrix stress (Zhang et al., 1998). Due to the complicated boundary conditions, we have solved the governing equations for the six osteons using an explicit finite difference method. Each osteon is mapped onto discrete mesh points (100 x 100). Similar to the bending experiments, the pressure is normalized to the outer fiber stress (mD/I). The dimensionless pressure (3Ip/(mDB), Eq. 5) is calculated at each mesh point as a function of time for the osteonal canal diameters of 0, 40, or 60 μm, and for osteonal coupling percentages of 0, 10%, 20%, 50% or 100%. These pressure calculations are made at frequencies ranging from 0.01 Hz to 500 Hz. The transcortical pressure difference (Δp), which is the average dimensionless pressure difference between the two external surfaces of the bone specimen, is also calculated for all of these conditions. The amplitude of the transcortical pressure difference (Δp) discussed in the Results section is the peak value of Δp when it reaches the steady state after the external sinusoidal loading is applied. The phase of Δp is the shift of the steady state response relative to the externally applied sinusoidal loading. The amplitude of Δp is calculated in the time domain while the phase of Δp is calculated using the FFT in the frequency domain.

Reproduced with permission of the copyright owner. Further reproduction prohibited without permission.

Results

Dimensionless pressure distributions across the bone specimen thickness show cusp-like shapes around the osteonal canals (where the pressure is 0) with a direction change from the compressive side of the bone specimen (where the pressure is positive) to the tensile side (where the pressure is negative) (Fig. 2-3). At a loading frequency of 1.5 Hz with an osteonal canal diameter of 40 μm, the local pressure gradients are steeper at the osteon centerline (x = 0) compared to those at the cement line (x = d/2) for both the100% and 0% osteonal coupling conditions (Figs. 2-3a and b). The only difference between the two coupling percentages is that there is a discontinuity at the cement lines for the 0% osteonal coupling condition where fluid cannot flow across the cement lines (Fig. 2-3c). The size of the osteonal canals and the loading frequency affect both the transcortical pressure difference and the local pressure gradients around the osteonal canals (Figs. 2-3d-e). With no osteonal canals (d_c = 0 μm), the bone specimen shows the largest transcortical pressure difference. For a specimen with osteonal canals (d_c = 40 or 60 μm), the transcortical pressure difference is greatly reduced, but larger local pressure gradients occur near the canals. When the loading frequency is raised from 1.5 Hz to 15 Hz, the local pressure gradients around the osteonal canals as well as the transcortical pressure difference increase three to four-fold (Fig. 2-3e).

Bone fluid relaxation behavior depends on the loading frequency as well as the microstructure of the specimen, i.e., the size of the osteonal canals and the osteonal coupling (Figs. 2-4 and 2-5). When the specimen does not include any osteonal canals and there are impermeable cement lines in the bone matrix, the bone fluid is confined and can only relax within each separate unit (200 μm x 200 μm). The space is so small that an

Reproduced with permission of the copyright owner. Further reproduction prohibited without permission.

equilibrium fluid pressure is achieved within each unit shortly after applying an external loading. For all loading frequencies, a positive fluid pressure is developed in the compressive side of the specimen and a negative pressure of the same magnitude in the tensile side; thus the amplitude of the established transcortical pressure difference (Δp) is relatively constant (Fig. 2-4a, $d_c = 0$ μm) and closely follows the temporal changes of the external bending moment (approximately zero phase, Fig. 2-5a, $d_c = 0$ μm). If we completely remove those impermeable barriers from the specimen by introducing 100% coupling between osteons, the fluid can relax from the compressive side to the tensile side of the specimen with a characteristic relaxation time of ~1 second. Therefore, for loading frequencies less than 0.1 Hz, the fluid pressure has enough time to relax across the entire specimen, which is illustrated by the low amplitude of Δp (Fig. 2-4b, $d_c = 0$ μm) and its high phase (~90°, Fig. 2-5b, $d_c = 0$ μm). As the loading frequency increases, the time interval available for the fluid to relax becomes shorter and shorter; therefore, Δp increases until it levels off at about 1 Hz (the characteristic frequency) (Fig. 2-4b, $d_c = 0$ μm), and the phase drops as Δp becomes more and more synchronized with the external loading (Fig. 2-5b, $d_c = 0$ μm). If we then add the osteons periodically into the specimen, the fluid can relax not only through the leakage at the cement lines (osteonal coupling) but also through drainage to the osteonal canals. In this case, the characteristic frequency has been shifted to ~20 Hz, compared to the characteristic frequency of ~1 Hz when the specimen contains no osteons (Figs. 2-4b and 2-5b).

Varying the percentage of osteonal coupling does not affect the amplitude of the transcortical pressure difference (Δp) in a bone specimen that contains osteons. When the coupling percentage of the cement lines is increased from 0% to 100% while keeping a

Reproduced with permission of the copyright owner. Further reproduction prohibited without permission.

constant canal size (d_c = 60 μm), the frequency response of Δp is the same for osteonal couplings of 0%, 10%, 20%, 50% and 100% (Fig. 2-6b). However, if the bone specimen does not include osteonal canals (d_c = 0 μm), the frequency response of Δp is sensitive to the osteonal coupling (Fig. 2-6a), because the only pathway for fluid relaxation out of each osteon occurs at the cement line.

Discussion

A model integrating two distinct bone porosities, the lacunar-canalicular porosity and the osteonal canals, is presented in this study. The effects of the osteonal canals and the osteonal coupling on the pressure relaxation of bone fluid flow are examined for the first time. The model demonstrates that the regularly arranged osteonal canals provide the primary space for bone fluid pressure to relax when the bone is mechanically loaded.

Electrokinetic analyses (Salzstein et al., 1987; Cowin, 1999) have shown that strain-generated potentials (SGPs) are proportional to the fluid pressure in bone, thus the two types of plots (pressure and voltage) can be compared. To date, the distribution of the SGPs at the osteonal level has only been reported for 1 Hz bending of bone specimens (Starkebaum et al., 1979). In our model, the pressure profiles have a cusp-like shape around the osteonal canals, with a change of cusp-like direction from the tensile side of the bone specimen (negative pressure) to the compressive side (positive pressure). The local pressure gradients along a line through the center of the osteonal canals are at least an order of magnitude greater than the transcortical pressure gradients at the cement line (Figs. 2-3a-b). Thus, by incorporating the osteonal canals into our model, we can explain the nonlinear voltage profiles and larger voltage fields within each osteon observed by

Reproduced with permission of the copyright owner. Further reproduction prohibited without permission.

Starkebaum et al. (1979). Mak et al. (1997) proposed a finite element model of three connected osteons and assumed that fluid was free to flow in the collagen-hydroxyapatite microporosity. They also found a similar pressure profile across the osteonal array in the case of external bending. However, their model included only four canalicular channels in each osteon, which is far fewer than the physiological number of canaliculi; our model provides a more realistic treatment of bone's microstructure.

The effect of the osteonal canal on the fluid pressure relaxation can be seen from the significant behavior changes or frequency shifts in both the magnitude and phase of Δp when the canal size is varied from 0 μm to 60 μm (Figs. 2-4 and 2-5). When the osteonal canals (40 μm or 60 μm in diameter) are periodically arranged across the bone specimen, the magnitude of Δp shows similar behavior, reaching a plateau at ~20 Hz, both when fluid can flow freely across the cement lines (100% coupling) or when fluid is confined in separate osteons (0% coupling). This suggests that in cortical bone the pore pressure relaxes mainly through the osteonal canals, which is further confirmed when the osteonal coupling is varied (Fig. 2-6b). This result can explain the paradox found by Otter et al. (1994) that the fluid (or SGP) relaxation time is not proportional to the square of the specimen thickness (D^2) as predicted by homogeneous models (Salzstein et al., 1987; Weinbaum et al., 1994; Cowin et al., 1995). While the D^2 dependence of the relaxation time is still valid in each osteon, our results show that the characteristic length scale for the fluid to relax is not the specimen thickness (1.2 mm), but instead the distance between the osteonal canals (200 μm). This would explain why the fluid relaxation time remained the same when the specimen thickness was reduced from 4 mm to 1 mm in Otter et al. (1994).

Reproduced with permission of the copyright owner. Further reproduction prohibited without permission.

Our results indicate that bone specimens with and without osteons exhibit different fluid relaxation behaviors. We have found that osteonal bone has a characteristic relaxation frequency of ~20 Hz whereas lamellar bone of 1.2 mm thickness has a characteristic relaxation frequency of ~ 1 Hz (Fig. 2-4b). However, normal cortical bone has a far more complicated structure than we have assumed in this model. The pore pressure relaxation is possibly achieved through both the osteonal canals and the surfaces of lamellar bone where there are no osteonal canals or the canal array is sparse. Even though we have no data on the coupling between these relaxation pathways at present, we have been able to predict the two limiting pressure relaxation behaviors through each pathway and we anticipate these limiting behaviors to be the upper and lower bounds for the frequency response of physiological cortical bone specimens. Not surprisingly, we find that the experimental data (Otter et al., 1994; Scott and Korostoff, 1990; Salzstein and Pollack, 1987) fall between these two limiting responses.

Other limitations of our model include: (1) adapting isotropic values for bone's mechanical properties and permeability while bone is an anisotropic material; (2) assuming the viscosity and bulk compressibility of the bone fluid to be the same as salt water; (3) using the theoretical permeability of the lacunar-canalicular porosity (Weinbaum et al., 1994); and (4) neglecting the inertia of the fluid and the displacement of the solid in the Biot theory formulation, which may introduce errors when a high frequency loading is applied to the porous media. In particular, our model is sensitive to the permeability of cortical bone associated with the lacunar-canalicular porosity. If this permeability were overestimated, the characteristic frequencies of the two limiting relaxation behaviors (i.e., 20 Hz and 1 Hz) would also be overestimated. We have no

Reproduced with permission of the copyright owner. Further reproduction prohibited without permission.

experimental permeability data at the lacunar-canalicular level; the measurements of permeability have been performed exclusively on the vascular porosity level (Li et al., 1987; Rouhana et al., 1981). From Eq. 1, the bone permeability on the level of the lacunar-canalicular porosity is estimated to range from 0.1×10^{-20} to 1.3×10^{-19} m^2 (the permeability value used in the above calculations is 1.7×10^{-20} m^2) for the following parameters: canalicular radius b = 200 nm, osteocytic process radius a = 100 nm, fiber spacing $\sqrt{k_p}$ ranging from 4 to 20 nm, canaliculi number ranging from $0.022/(\mu m)^2$ to $0.1/(\mu m)^2$, and fluid viscosity = 10^{-3} Pa s. The large range of the predicted permeability (2 orders of magnitude) induces a large variation of the predicted limiting relaxation frequencies. For the above permeability range, the upper limiting relaxation frequency range is approximately 2 - 150 Hz and the lower limiting relaxation frequency range is approximately 0.06 – 7.5 Hz.

Despite these limitations, our model sheds some light on a possible amplification mechanism in the transduction of the mechanical signal to the bone cells. Our study indicates that the local pressure gradients near the osteonal canals are significantly amplified at higher loading frequencies. For example, mechanical loading applied at 20 Hz may induce a transcortical pressure difference with an amplitude 10-fold higher than loading applied at 1 Hz (Fig. 2-6b), which in turn induces even greater local pressure gradients around the osteonal canals (Fig. 2-3e). These amplified pressure gradients would drive the bone fluid to flow over the osteocytic membranes at a higher velocity and thus induce larger shearing stresses acting on the osteocytes so that the osteocytes may detect the high-frequency mechanical stimuli with a higher sensitivity. This result may explain the experimental findings of greater bony ingrowth with mechanical loading

Reproduced with permission of the copyright owner. Further reproduction prohibited without permission.

applied at 20 Hz as compared to 1 Hz (Rubin and McLeod, 1994) as well as the studies showing low-magnitude 30 Hz mechanical loading can cause new bone formation (Rubin and McLeod, 1996).

Acknowledgments

This study was supported by grants from the Whitaker Foundation and the NIH (AR44211).

Reproduced with permission of the copyright owner. Further reproduction prohibited without permission.

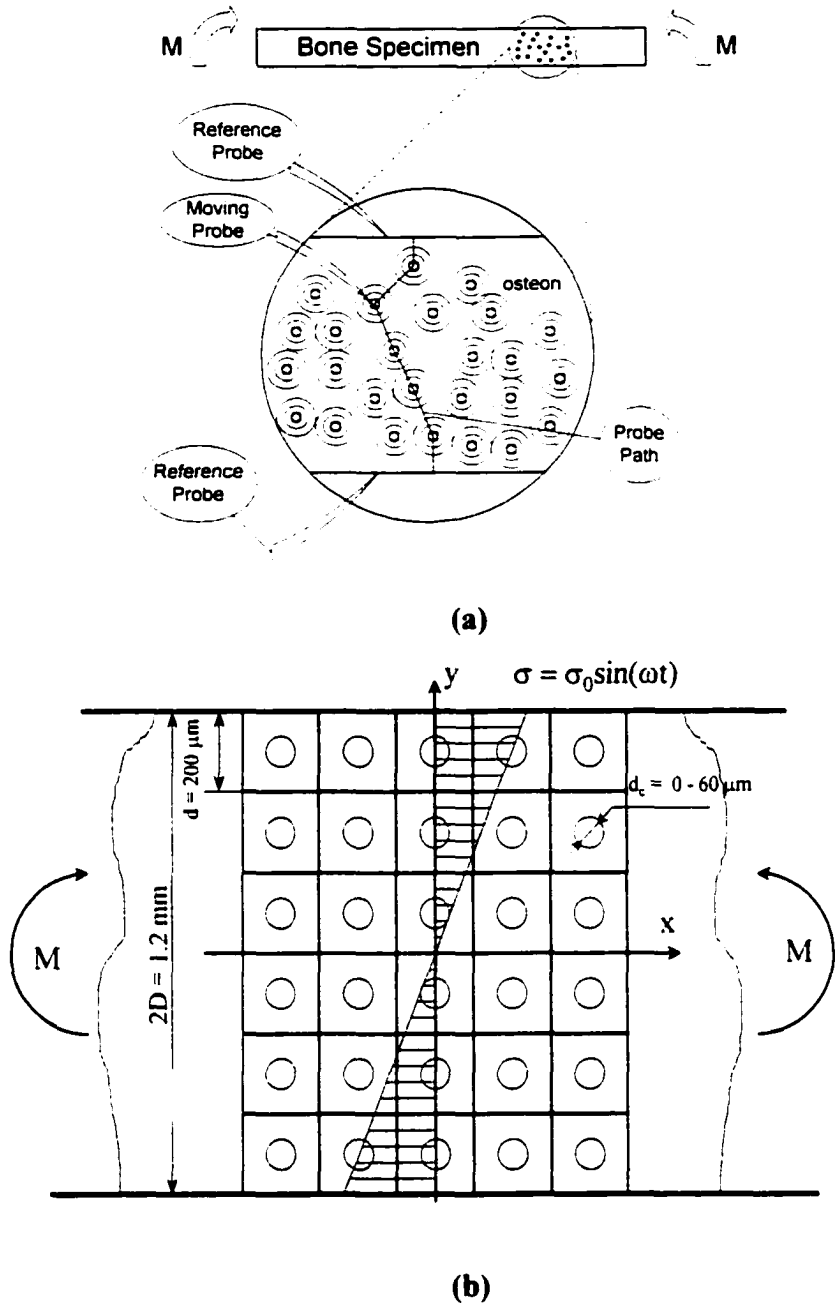

Fig. 2-1. (a) Measurement of microscopic SGPs across a bone specimen as performed in Starkebaum et al. (1979). The specimen size was approximately 30 mm x 10 mm x 1 mm. Two reference electrodes were placed on the two outer surfaces and the third electrode was moved across the specimen thickness along the probe path. Microscopic SGPs were recorded between the moving and reference electrodes when the specimen was under 1 Hz four-point bending. (b) A front view of the idealized model of a 1.2 mm-thick section of cortical bone similar in size to the specimens in the bending experiment shown in (a). Each repeated unit represents an osteon with an osteonal canal. A sinusoidal bending moment (M) is applied to the bone section, producing a linear stress (σ) distribution across the specimen.

Reproduced with permission of the copyright owner. Further reproduction prohibited without permission.

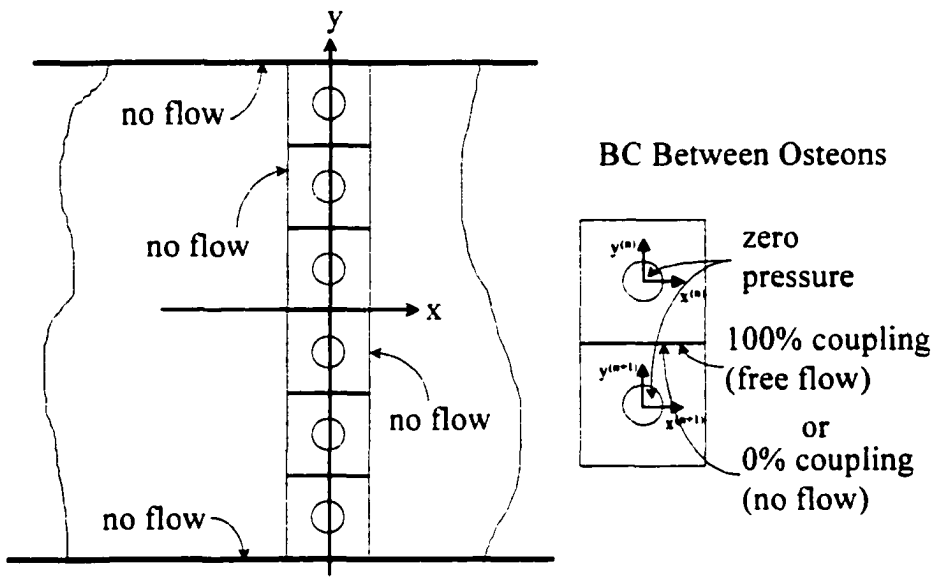

Fig. 2-2. Boundary conditions for the theoretical model. "No flow" conditions are applied to the outer surfaces and the transverse boundaries of the osteonal array, due to the fluid surface tension and the structural symmetry, respectively. A zero reference pressure is applied to the osteonal canals. Since the permeability of the cement lines is not known, a varied coupling percentage is applied: 0% coupling corresponds to "no flow" and 100% coupling corresponds to "free flow" across the cement line.

Reproduced with permission of the copyright owner. Further reproduction prohibited without permission.

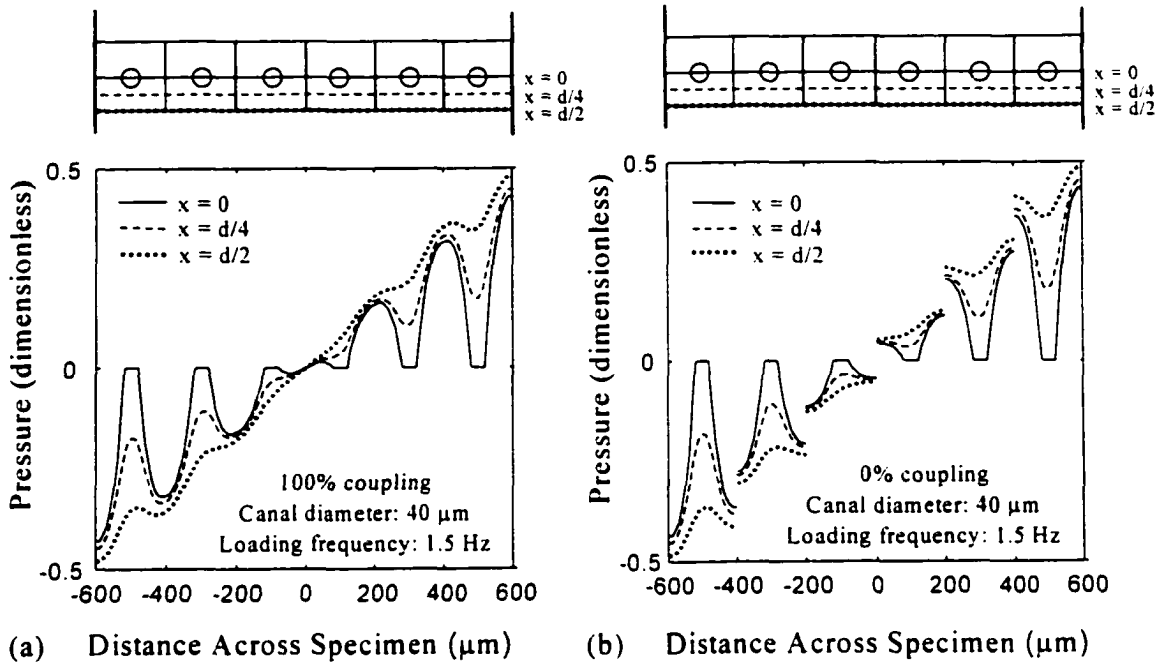

(a) Distance Across Specimen (μm) (b) Distance Across Specimen (μm)

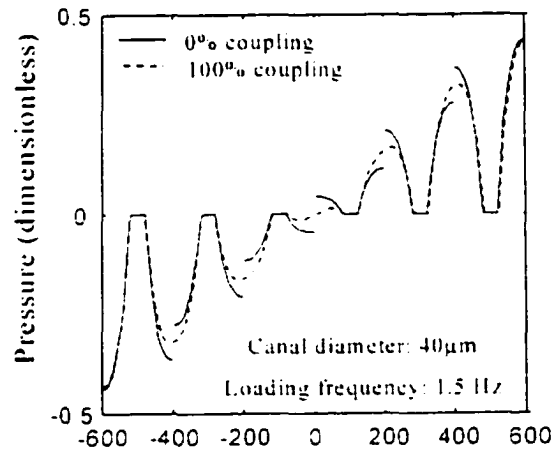

(c) Distance Across Specimen (μm)

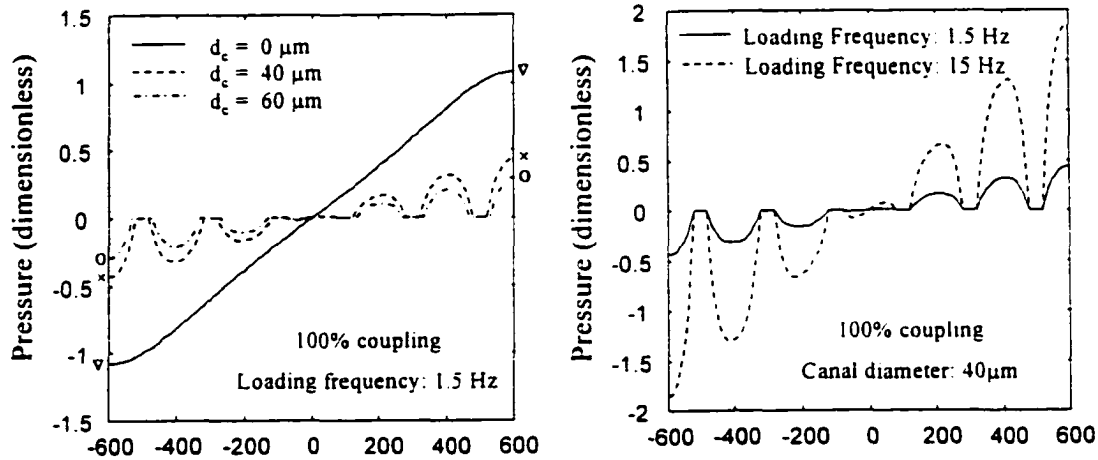

(d) Distance Across Specimen (μm) (e) Distance Across Specimen (μm)

Reproduced with permission of the copyright owner. Further reproduction prohibited without permission.

Fig. 2-3. Dimensionless pressure distributions from one surface of the bone specimen (y = -600 μm) to the other surface (y = 600 μm) for different conditions. (a) and (b) Pressure profiles for a specimen with 40 μm osteonal canals with the external loading applied at 1.5 Hz for 100% osteonal coupling (a) and for 0% osteonal coupling (b). x = 0: profile along a line passing through the canal centers; x = d/4: profile along a line halfway between the canal centers and the cement line; x = d/2: profile along a line passing through the cement lines. (c) Comparison of the local pressure gradients for 0% coupling and 100% coupling (x = 0). (d) Effects of the size of the osteonal canals (d_c = 0, 40, or 60 μm) on the pressure profiles and the transcortical pressure difference (Δp) for 100% osteonal coupling with the loading applied at 1.5 Hz. The transcortical pressure difference is the pressure difference between the points marked '∇', '×', or 'O' on the external surfaces. (e) Comparison of the local pressure gradients and transcortical pressure difference between loading applied at 1.5 Hz and 15 Hz.

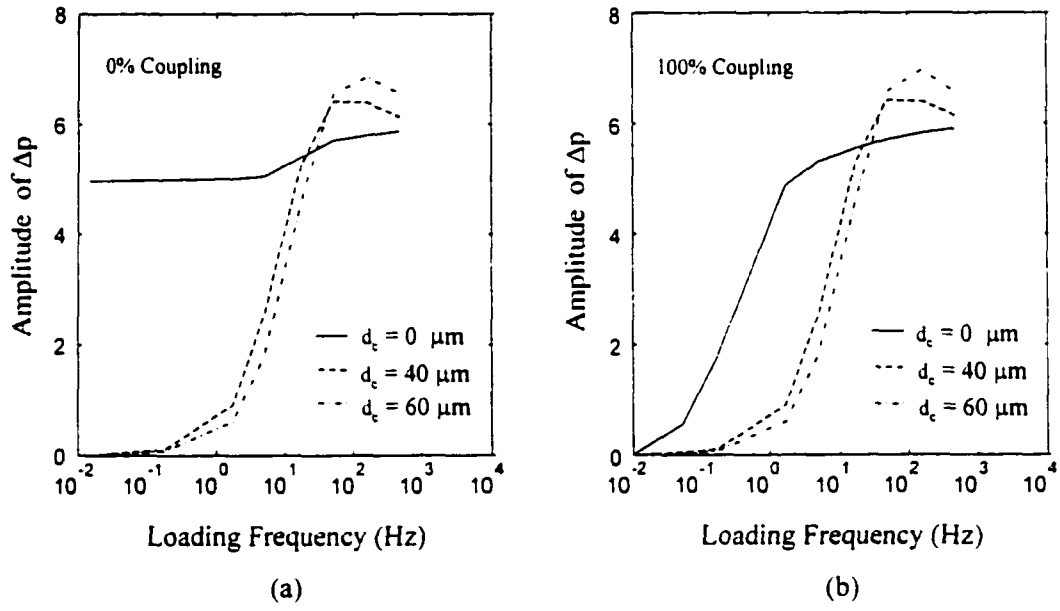

Fig. 2-4. The amplitude of the transcortical pressure difference (Δp) as a function of the loading frequency for a specimen with no osteonal canals (d_c = 0 μm) or with osteonal canals (d_c = 40 or 60 μm) for 0% osteonal coupling (a) and 100% osteonal coupling (b). The amplitude has different frequency responses when the canal size and the osteonal coupling are changed, revealing two different behaviors of fluid pressure relaxation when bone is mechanically loaded.

Reproduced with permission of the copyright owner. Further reproduction prohibited without permission.

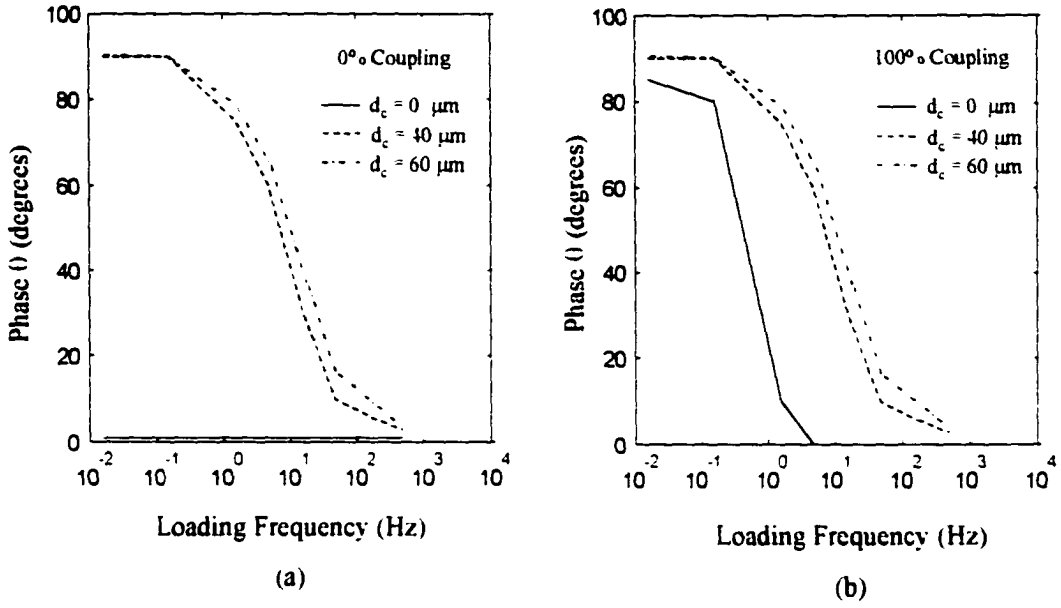

Fig. 2-5. The phase (θ) of the transcortical pressure difference (Δp) as a function of the loading frequency for a specimen with no osteonal canals (d_c = 0 μm) or with osteonal canals (d_c = 40 or 60 μm) for 0% osteonal coupling (a) and 100% osteonal coupling (b). Similar to the amplitude responses, the phase responses confirm the existence of the two different fluid pressure relaxation behaviors.

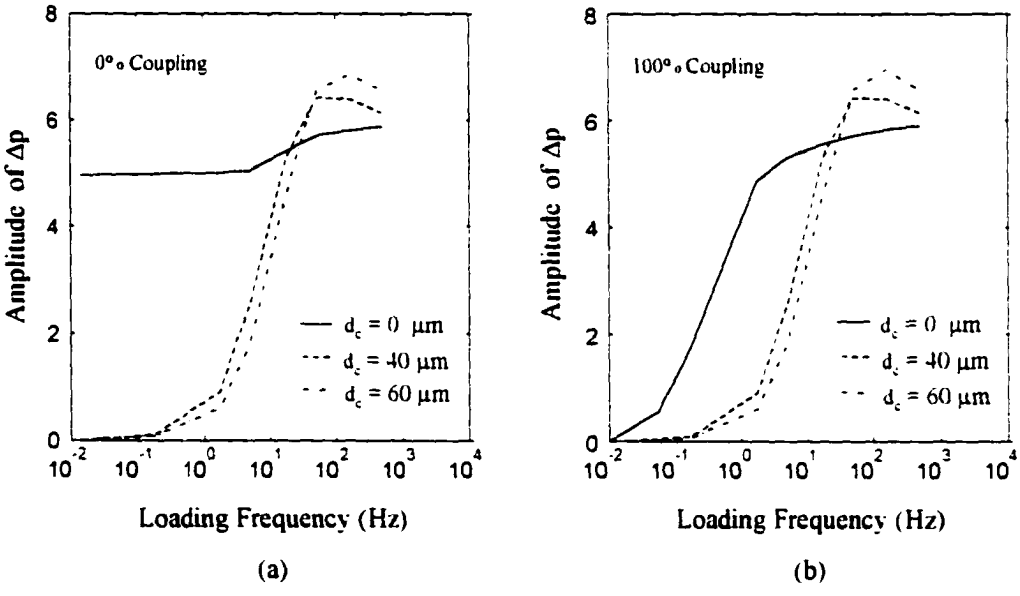

Fig. 2-6. The effects of osteonal coupling on the transcortical pressure difference, Δp. (a) When the bone specimen does not include the osteonal canals (d_c = 0 μm), the osteonal coupling affects the behavior of the pressure relaxation. (b) When the bone specimen includes the osteonal canals (d_c = 60 μm), the coupling percentage has no effect on the amplitude of the transcortical pressure difference, suggesting the fluid pressure relaxation is through the osteonal canals.

Reproduced with permission of the copyright owner. Further reproduction prohibited without permission.

Chapter 3 Modeling Tracer Transport in an Osteon Under Cyclic Loading*

Abstract

A mathematical model is developed to explain the fundamental conundrum as to how during cyclic mechanical loading there can be net *solute* (e.g., nutrient, tracer) transport in bone via the lacunar-canalicular porosity when there is no net *fluid* movement in the canaliculi over a loading cycle. Our hypothesis is that the fluid space in an osteocytic lacuna facilitates a nearly instantaneous mixing process of bone fluid that creates a difference in tracer concentration between the inward and outward canalicular flow and thus ensures net tracer transport to the osteocytes during cyclic loading, as has been shown experimentally. The sequential spread of the tracer from the osteonal canal to the lacunae is investigated for an osteon experiencing sinusoidal loading. The fluid pressure in the canaliculi is calculated using poroelasticity theory and the mixing process in the lacunae is then simulated computationally. The tracer concentration in lacunae extending radially from the osteonal canal to the cement line is calculated as a function of the loading frequency, loading magnitude, and number of loading cycles as well as the permeability of the lacunar-canalicular porosity. Our results show that net tracer transport to the lacunae does occur for cyclic loading. Tracer transport is found to increase with higher loading magnitude and higher permeability and to decrease with increasing loading frequency. This work will be helpful in designing experimental studies of tracer movement and bone fluid flow, which will enhance our understanding of bone metabolism as well as bone

---

* Reprinted with permission from Wang et al., Annals of Biomedical Engineering 28(10):1200-1209. Copyright 2000, Biomedical Engineering Society.

Reproduced with permission of the copyright owner. Further reproduction prohibited without permission.

adaptation.

Keywords: bone; bone fluid; mixing; lacunar-canalicular porosity; metabolism; mass transport; poroelasticity.

Introduction

How calcified bone tissue maintains adequate metabolism remains a puzzle. Molecular diffusion between cells and their nearby blood vessels, the mechanism by which cells usually obtain nutrients and dispose of waste products, may be insufficient to maintain bone metabolism since the bone cells (osteocytes) are buried in lacunae in the calcified matrix. Osteocyte signaling and nourishing materials such as ions, hormones, enzymes, cytokines, growth factors, and proteins can be readily perfused into the osteonal canal across the endothelial cells of the capillary wall by both flowing through the interendothelial clefts as well as through vesicles in the cytoplasm of the endothelial cells.[12,25] To obtain these nutrients, osteocytes need a continuous fluid pathway to the extracellular fluid in the osteonal canal, and the interconnected lacunar-canalicular network has been suggested to be this continuous pathway.[2,15-18,29] However, the fluid space in a canaliculus is between the plasma membrane of the cell process (radius 0.1 μm) and the mineralized canalicular wall (radius 0.2 μm), which is so narrow and long (the canalicular channel is several times longer than the diameter of an osteocyte body)[2] that molecular diffusion may be insufficient for cells far from the osteonal canals to maintain proper metabolic functions. Much smaller pores have been proposed to exist around the collagen-hydroxyapatite crystals, but no evidence shows that these pores

Reproduced with permission of the copyright owner. Further reproduction prohibited without permission.

provide a continuous pathway in mature bone because the fluid there may be bound to the matrix.[27] Knothe Tate *et al.*[17] experimentally demonstrated that procion red (MW 300-400; <1.0 nm in diameter) appeared in the lacunae of the mature rat bone only 10 minutes after being injected through the rat tail vein with no mechanical loading applied to the animal, while relatively little peroxidase reaction product was observed in the tissue when larger molecules such as microperoxidase (MW 1800-1900; 2 nm in diameter) and horseradish peroxidase (MW 40000; 6 nm in diameter) were injected and circulated for 2 hours. The relative difficulty in delivering the large molecules into bone tissue by diffusion implies that transport mechanisms besides diffusion may be necessary to maintain adequate bone metabolism.

Fluid flow resulting from dynamic mechanical stresses experienced by bone[7,31] has been proposed to be involved in transducing the external mechanical signals to bone cells[3,34,36] as well as to enhance cell metabolism in bone.[15,16,18,29] Piekarski and Munro[29] developed a theoretical model of an osteon comprised of interwoven concentric layers of liquid and porous bone where tubes of canaliculi connected two adjacent liquid layers. With axial cyclic loading applied to the osteon to mimic the axial loading of a long bone induced by walking, the local displacement of the fluid during half a walking cycle was calculated. This local solute displacement due to convection was found to be one to three orders of magnitude larger, depending on solute size, than the diffusive displacement during the same time period using a diffusion model where the osteon was devoid of any mechanical loading. The results of Piekarski and Munro[29] suggest that the load-induced flow significantly increases the efficiency of the transport mechanism operating between the blood supply and osteocytes. Kufahl and Saha[18] modeled an osteon that consisted of

Reproduced with permission of the copyright owner. Further reproduction prohibited without permission.

lacunae and canaliculi as well as a central osteonal canal. With a walking load applied to the osteon, the load-induced flow rates in the canalicular channels were evaluated as a function of time, location of the lacunae, and the canalicular diameters. When the canalicular diameter was 0.2 μm and the cell process as well as the pericellular matrix were assumed not to affect fluid flow, the load-induced flow during half a walking cycle was found to move a radial distance that covered four to five osteocytes from the capillary. In addition, Knothe Tate and Niederer[16] developed a finite element model of an osteon to study the relative contribution of convection and diffusion to mass transport and also found that the load-induced fluid flow enhanced tracer transport, which was also evident in their experimental study (Knothe Tate and Knothe[15]).

Although a significant load-induced fluid displacement has been demonstrated for a half loading cycle in the previous models,[16,18,29] no mechanism has been proposed to explain the irreversibility of the solute transport, but not the fluid transport, over the second half of the loading cycle. In a cyclically loaded bone (such as during walking sequences), the fluid sucked into the lacunar-canalicular porosity during a half cycle of loading would be squeezed out during the next half cycle of loading. This reversible flow of fluid would occur regardless of the waveform of the cyclic loading since the elastic restoring force of the solid bone matrix would imbibe new fluid as soon as the compression is relaxed. For any periodic loading the same amount of fluid enters and leaves the osteonal canal over a single cycle or a periodic steady-state could not exist. Therefore, there is no net fluid exchange during a whole cycle of loading between the central osteonal canal and the porous bone matrix for any periodic waveform. With no net fluid exchange, it seems unlikely that the osteocytes inside the bone matrix could gain

Reproduced with permission of the copyright owner. Further reproduction prohibited without permission.

any net nutrient supply from the convective fluid flow. We thus ask two fundamental questions: how can net mass transport occur in cyclically loaded bone and how is the transport increased by the mechanical loading as demonstrated in the experiments performed by Knothe Tate and Knothe?[15]

To address these questions, we hypothesize that the relatively large fluid space surrounding the osteocyte in a lacuna facilitates a nearly instantaneous mixing process of bone fluid that creates a tracer concentration difference between the inward and outward canalicular flow that is vital for net transport during cyclic loading. A tracer substance that mimics large nutrient molecules is readily leaked out of the capillary and initially is assumed to be present only in the osteonal canal. With a cyclic (e.g., sinusoidal) loading applied to the osteon, the sequential spread of the tracer from the canal to the lacunae encased in the mineralized matrix is investigated. Poroelasticity theory is adapted to predict the bone fluid pressure within the cyclically loaded osteon. The fluid flow in the canalicular channels is assumed to follow Darcy's law and its velocity and the fluid displacement are estimated. An iteration algorithm is proposed to mimic the nearly instantaneous mixing processes in the lacunae due to the cyclic loading, and the concentration of tracer in each lacuna is calculated as a function of loading frequency, loading magnitude, and number of loading cycles as well as the permeability of the lacunar-canalicular porosity of bone. This theoretical work will be a helpful tool in designing experimental studies of bone fluid flow, which will enhance our understanding of bone metabolism as well as bone adaptation.

Methods

Reproduced with permission of the copyright owner. Further reproduction prohibited without permission.

To model tracer transport in mechanically loaded bone, an idealized osteon is constructed similar to that in Zeng *et al.*[36] (Fig. 3-1). The osteon has a circular outer boundary, the cement line, (radius r_0 = 150 μm) and consists of three concentric layers of osteocytes and their lacunae as well as a central osteonal canal (radius r_i = 30 μm) that houses one capillary. The osteocytes and lacunae are simplified as spheres and spherical cavities, respectively (Fig. 3-1), even though they tend to be flattened ellipsoids histologically;[20] their radii are assumed to be 5 and 4 μm, respectively, which are reasonable approximations of measured data, e.g., 50 μm^2 cross-sectional area and 130 μm^2 longitudinal-sectional area of the osteocytic lacunae in the human tibia.[20] Our preliminary histological results from the rat tibia show that the osteocyte-to-osteocyte distance is approximately 30 μm, which is close to other measured values, e.g., 1 lacuna per 1000-3000 μm^2 in the dog.[1] Therefore, in our model the three concentric layers of osteocytes and their lacunae are evenly distributed in the cortex between the osteonal canal surface and the cement line (Fig. 3-1). Since the canalicular density in human secondary osteons has been measured to be 5-14 per 100 μm^2,[21] 10 canalicular channels are assumed to enter or exit the lacunae along each hemispherical half surface. Since the cell-to-cell distance is 30 μm and the lacunar radius is 5 μm, these canaliculi are modeled as 20 μm long tubes housing the cell processes, simplified as straight lines in Fig. 3-1.

In our model, the fluid is assumed to flow through the annular space of the canalicular channels between the cell process (radius of 0.1 μm) and the canalicular wall (radius of 0.2 μm). As proposed in previous studies,[3,34,36] our model assumes that the annular fluid space of a canaliculus is filled with a pericellular gel-like proteoglycan fiber matrix that acts as

Reproduced with permission of the copyright owner. Further reproduction prohibited without permission.

a molecular sieve for albumin similar to the surface glycocalyx found on endothelial cells. Some experimental studies have found proteoglycan fibers near osteocytes in mature bone.[13,32,33] Because of this pericellular fiber matrix, the fluid flow in the canalicular channels assumes an almost uniform velocity profile and this "plug" flow can be approximated using Darcy's law.[3,34] Because of the small size of the lacunar-canalicular porosity and its coexistence with the much larger vascular pores, there is no experimental data for the permeability of the lacunar-canalicular porosity in bone. However, the fiber matrix model developed previously provides a theoretical tool to estimate the intrinsic permeability of the lacunar-canalicular porosity from the fiber spacing that determines the hydraulic resistance of the canaliculi.[3,34,36] Although the size of albumin, the most abundant protein in plasma, has been suggested to be the physiological value for the fiber spacing (7 nm),[3,34] we assume three values for the fiber spacing (3, 7, or 18 nm) in our model to evaluate the effect of bone permeability on mass transport. For each fiber spacing, the intrinsic permeability associated with one canaliculus (k_p) is readily obtained (k_p has been estimated as a function of the fiber spacing in Cowin *et al.*[3]). Since we have assumed Darcy flow in the fiber-filled canalicular channels where the boundary effect has been neglected, the Darcy permeability (k) at the tissue level is calculated from the k_p of one canaliculus, along with the canalicular density (n_c, number of canaliculi per unit area of bone) and the cross-sectional area of the fluid space in one canaliculus (A): $k = n_c A k_p$. The estimated values of k and k_p for the three assumed fiber spacings will be utilized to calculate the fluid pressure and fluid velocity in the lacunar-canalicular porosity. It is assumed that the 10 canaliculi emanating from each lacuna receive equal flow.

To mimic the physiological cyclic loading of a long bone, e.g., during walking, the

Reproduced with permission of the copyright owner. Further reproduction prohibited without permission.

osteon in our model is sinusoidally loaded along its long axis ($\sigma = -\sigma_0 sin\omega t$) and the fluid pressures in the lacunar-canalicular porosity are then calculated using poroelasticity theory (reviewed in Cowin[4]). The fluid pressure in the osteonal canal is assumed to be zero, since the pressure in the canal cannot exceed the vascular pressure (~10^4 Pa, Wilkes and Visscher[35]) for an extended period of time, which is almost two orders of magnitude lower than the pressure induced by mechanical loading within the bone matrix (~10^6 Pa, Piekarski and Munro[29]). In addition, the fluid pressure relaxation time of the vascular porosity has been shown to be three orders of magnitude shorter than that of the lacunar-canalicular porosity and it seems unlikely that a high pressure is produced in the osteonal canal for physiological mechanical loading.[37] Since the cement line is believed to be impermeable for fluid flow, a non-leakage boundary condition is assumed at the cement line, i.e., the fluid pressure gradient vanishes there. The theoretical formula for the fluid pressure (p) in an axially sinusoidally loaded osteon derived in Zeng *et al.*[36] is:

$$P(R,\tau) = -\frac{1}{T}(\sin T\tau)\,\mathrm{Re}\left\{\frac{J(R,T)}{J(R_i,T)}\right\} + \frac{1}{T}(\sin T\tau) \qquad (1)$$

where R is the dimensionless cylindrical coordinate, R_i is the dimensionless radius of the osteonal canal, P is dimensionless pressure, τ is dimensionless time, T is dimensionless frequency, and $J(R,T) = I_0(\sqrt{iT}R)K_1(\sqrt{iT}) + I_1(\sqrt{iT})K_0(\sqrt{iT}R)$, where I_0, K_0, I_1, and K_1 are modified Bessel functions of the first and second kind. The dimensionless parameters are defined as follows:

$$R = \frac{r}{r_0},\ R_i = \frac{r_i}{r_0},\ \tau = \frac{t}{\tau_r},\ T = \omega\tau_r,\ P = \frac{3p}{\sigma_0 BT} \qquad (2)$$

where r is the radial coordinate; r_i and r_0 are radii of the osteonal canal and the outer

Reproduced with permission of the copyright owner. Further reproduction prohibited without permission.

boundary of the osteon, respectively; t is time; ω is the angular frequency of the sinusoidal loading applied to the osteon; p is the fluid pressure; σ_0 is the magnitude of the applied stress; B is a poroelastic parameter representing the relative compressibility of the fluid and solid phases of the porous bone tissue (B has been estimated to be 0.53 in Cowin *et al.*[3]); and τ_r (relaxation time) is the time constant for load-induced fluid pressure to decay in the lacunar-canalicular porosity. The relaxation time is proportional to the square of the outer radius of the osteon and inversely proportional to the Darcy permeability k at the tissue level,[3,34,36] and for the three fiber spacings used in our model (3, 7, or 18 nm), the relaxation time τ_r is estimated to be 1.3, 0.13, or 0.013 sec, respectively. Using Eqs. 1 and 2, the induced fluid pressure p in each lacuna of the osteon is calculated when the sinusoidal loading magnitude σ_0 is 20 or 40 MPa with an induced peak strain of 1000 or 2000 microstrain ($\mu\varepsilon$) (the axial Young's modulus is assumed to be 20 GPa) for a loading frequency f ($\omega = 2\pi f$) ranging from 0.5 to 100 Hz and for the three values of the fluid relaxation time τ_r corresponding to the fiber spacings of 3, 7, and 18 nm.

To obtain the fluid displacement in the canalicular channels, the fluid velocity in the canaliculi is calculated from the fluid pressure using Darcy's law:

$$u(t) = -\frac{k_p}{\mu}\frac{\partial p}{\partial r} \tag{3}$$

where p is the fluid pressure, u is the velocity of the fluid flow within one canalicular channel, μ is the viscosity of bone fluid which is assumed to be that of salt water, and k_p is the intrinsic permeability associated with one canaliculus, which has been estimated to be 1.109, 11.09, and 110.9 nm^2 for the fiber spacings of 3, 7, and 18 nm, respectively.[3] The

Reproduced with permission of the copyright owner. Further reproduction prohibited without permission.

pressure gradient ($\partial p/\partial r$) for each set of canaliculi is approximated by the ratio of the pressure difference at the two ends of the canalicular channels over the canalicular length ($\Delta p/\Delta r$). Using Eq. 3, the fluid velocity in each set of canaliculi (C1, C2, C3, and C4 in Fig. 3-1) is obtained as a function of time. Then we integrate this fluid velocity over a time period of half a loading cycle ($t_0 = 0.5/f$), and thus obtain the fluid displacement in each set of canaliculi (D_1, D_2, D_3, and D_4):

$$D_i = \int_0^{t_0} u(t)dt \,,\ i = 1\text{-}4 \tag{4}$$

To mimic nutrient transport in the load-induced canalicular flow, a tracer substance is initially assumed to fill the osteonal canal. Because the fluid volume in the osteonal canal is very large compared to that in the lacunae and canaliculi (Table 3-1), the canal is assumed to act as a reservoir for nutrient supply, and the tracer concentration remains 100% in the canal. Once the sinusoidal loading is applied to the osteon, for the first half loading cycle, the fluid with 100% tracer concentration from the osteonal canal is sucked towards lacuna 1. If the fluid displacement is greater than the canalicular length (20 μm), some fluid will enter the lacuna and mix there, raising the local tracer concentration. During the next half loading cycle, the same amount of fluid is squeezed back into the canal but with a lower tracer concentration compared to that of influx due to the dilution from mixing. Therefore, while there is no net fluid exchange over one cycle, the result is net tracer transport to the lacuna 1. The same transport mechanism of lacunar mixing moves the tracer outwards radially from lacuna 1 to lacuna 2, and so on. We assume that the tracer molecules are relatively large (> 2 nm) and move at the same velocity as the fluid in the canaliculi because the diffusive displacement for the tracer in the canaliculi is

Reproduced with permission of the copyright owner. Further reproduction prohibited without permission.

much less than its convective displacement as will be discussed later. The length of the canaliculi (l_0) is the mixing threshold for net tracer transport because only the fluid that passes this threshold length carries the tracer into the lacunae from the osteonal canal and from one lacuna to the next.

An iterative algorithm is developed to mimic the mixing process that occurs in the lacunae (Fig. 3-2). This lacunar mixing is very rapid since the jet flow enters the lacunar reservoir at very low Reynolds number, and thus the tracer spreads in all directions and fills the lacunar fluid space by diffusion. The tracer concentration in each lacuna (C_{Li}, i = 1-3) and canaliculus (C_{Ci}, i = 1-4) is initially zero and that in the osteonal canal (C_{SOURCE}) remains 100% all the time. The fluid volume Q_i that is exchanged between two adjacent compartments during half a cycle of loading (i.e., Q_1 between the osteonal canal and lacuna 1, Q_2 between lacuna 1 and lacuna 2, and Q_3 between lacuna 2 and lacuna 3) is the product of the number of the connecting canaliculi (n = 10 in our model), the cross-sectional area of the annular fluid space in a canaliculus (A), and the local fluid displacement (D_i), i.e., $Q_i = nAD_i$, i = 1-3. To simplify the explanation of the algorithm, all three lacunae are assumed to undergo a mixing process (i.e., the fluid displacement is greater than the mixing threshold (the length of the canaliculi), $D_i > l_0$). For the first half loading cycle, the influx flow for the first lacuna includes the fluid that was in the canaliculi (volume: V_C; concentration: C_{C1}) with the rest coming from the osteonal canal (volume: $Q_1 - V_C$; concentration: C_{SOURCE} = 100%); at the same time the outflow from lacuna 1 is pushed to the downstream canaliculi and lacuna 2 (volume: Q_2; concentration: C_{L1}). In the following iteration equations, an iterative step stands for half a loading cycle and the superscript ($n-1$, n, or $n+1$) of a tracer concentration indicates the tracer concentration

Reproduced with permission of the copyright owner. Further reproduction prohibited without permission.

value in the previous, current, or next iteration, respectively. After adding the amount of tracer brought in with the influx and subtracting that taken out with the outflow, the current concentration in the lacuna becomes:

$$C_{L1}^{n} = C_{L1}^{n-1} + \frac{V_C C_{C1}^{n-1} + (Q_1 - V_C) C_{SOURCE} - Q_2 C_{L1}^{n-1}}{V_L + Q_1 - Q_2} \tag{5}$$

and the concentration in the upstream (C_{C1}) and downstream (C_{C2}) canaliculi is also updated to be that of its upstream compartment, the osteonal canal and the first lacuna in this case, respectively:

$$C_{C1}^{n} = C_{SOURCE}; C_{C2}^{n} = C_{L1}^{n-1} \tag{6}$$

The calculation for the next two lacunae is similar except that the C_{SOURCE} in Eqs. 5 and 6 have to be replaced with the concentration of the upstream lacuna:

$$C_{Li}^{n} = C_{Li}^{n-1} + \frac{V_C C_{Ci}^{n-1} + (Q_i - V_C) C_{L(i-1)}^{n-1} - Q_{(i+1)} C_{Li}^{n-1}}{V_L + Q_i - Q_{(i+1)}}, \; i = 2, 3 \tag{7}$$

$$C_{Ci}^{n} = C_{L(i-1)}^{n-1}; C_{C(i+1)}^{n} = C_{Li}^{n-1}, \; i = 2, 3 \tag{8}$$

For the next half loading cycle, the fluid reverses its direction and undergoes the same displacement as it does during the previous half loading cycle. Since there is assumed to be no fluid flow across the cement line, lacuna 3 cannot gain or lose any tracer through the canaliculi set *C4*; therefore, the concentration in this lacuna remains the same as that at the previous half loading cycle:

$$C_{L3}^{n+1} = C_{L3}^{n} \tag{9}$$

However, the concentration of the downstream canaliculi *C3* is updated to be that of lacuna 3:

Reproduced with permission of the copyright owner. Further reproduction prohibited without permission.

$$C_{C3}^{n+1} = C_{L3}^{n} \tag{10}$$

For the downstream lacunae ($i = 2, 1$), both influx (Q_{i-1}) and outflow (Q_i) should be considered and the concentration for the downstream canaliculi should be updated accordingly.

$$C_{Li}^{n+1} = C_{Li}^{n} + \frac{V_C C_{C(i+1)}^{n} + (Q_{(i+1)} - V_C) C_{L(i+1)}^{n-1} - Q_i C_{Li}^{n-1}}{V_L + Q_i - Q_{(i+1)}}, \; i = 2, 1 \tag{11}$$

$$C_{Ci}^{n+1} = C_{Li}^{n}, \; i = 2, 1 \tag{12}$$

The program is run iteratively from the first loading cycle to the second loading cycle until finishing the predefined number of loading cycles. Preliminary calculations showed that the tracer concentrations in the lacunae reach plateaus after 250 loading cycles; thus, the tracer concentration in each lacuna is calculated as a function of the number of loading cycles (1-250 cycles), the loading magnitude (1000 με, 2000 με), and loading frequency (0.5-100 Hz), as well as the fiber spacing of the matrix in the canaliculi (3, 7, or 18 nm).

Results

In an axially cyclically loaded osteon, the fluid displacement in the canaliculi during half a loading cycle increases when the canalicular channels are closer to the source of fluid (osteonal canal) ($D_1 > D_2 > D_3$), decreases with increasing loading frequency (0.5-100 Hz), and increases as the bone matrix is made more permeable (Fig. 3-3). As shown in Eqs. 1-4, the fluid displacement is proportional to the magnitude of the mechanical loading. For the parameters examined in Figure 3, the largest fluid displacement occurs

Reproduced with permission of the copyright owner. Further reproduction prohibited without permission.

near the osteonal canal at 0.5 Hz loading (2000 με, 18 nm fiber spacing) while the smallest displacement occurs near the cement line at 100 Hz (2000 με, 3 nm fiber spacing). In the case of the densest fiber spacing of 3 nm, the fluid can cross the mixing threshold of 20 μm and reach the first lacuna for only lower loading frequencies (0.5-5 Hz) (Fig. 3-3a). However, if the bone matrix is more permeable with a larger fiber spacing of 7 nm, the fluid can reach both the first and second lacunae for the lower loading frequencies of 0.5-8 Hz; but only the first lacuna can be reached when the loading frequency is 20 Hz (Fig. 3-3b). If the fiber matrix is further increased to 18 nm, the fluid can reach the first two lacunae for a wide range of loading frequencies (0.5-80 Hz) (Fig. 3-3c).

The tracer concentration in the lacunae increases monotonically as the number of loading cycles increases and levels off after a certain number of loading cycles (Fig. 3-4). The speed and distance that the tracer is transported to a lacuna (osteocyte) are found to be closely related to the fluid displacement in each connecting canaliculi set (Fig. 3-4). When the loading is applied at 1 Hz and 2000 με (corresponding to locomotion) with a fiber spacing of 7 nm, the tracer concentration in the first two lacunae reaches 80% after 10 and 75 loading cycles, respectively (Fig. 3-4a). If we reduce the loading magnitude from 2000 με to 1000 με while other parameters remain the same (1 Hz, 7 nm fiber spacing), the tracer reaches the first lacuna only and it fills this lacuna at one-quarter the rate of the higher loading magnitude since the tracer concentration in the first lacuna increases to 80% after 40 loading cycles (Fig. 3-4b) compared to 10 loading cycles for a loading magnitude of 2000 με (Fig. 3-4a). If we increase the loading frequency from 1 Hz to 20 Hz (corresponding to foot strike after ground contact[14]) while other parameters

Reproduced with permission of the copyright owner. Further reproduction prohibited without permission.

remain the same (2000 με, 7 nm fiber spacing), the tracer penetrates the first lacuna only, and the tracer concentration reaches 80% after 88 loading cycles (Fig. 3-4c). As the fiber spacing is then increased from 7 to 18 nm (increasing the Darcy permeability by approximately one order of magnitude) while other parameters remain the same (2000 με, 20 Hz), tracer transport is enhanced as the tracer moves a greater distance at a higher speed (Fig. 3-4d), compared to the case of a 7-nm fiber spacing (Fig. 3-4c).

Discussion

Our model shows that the convective efficiency of transporting large-sized tracers (>2 nm) from the source (capillary in the osteonal canal) through canaliculi to an individual lacuna by load-induced fluid flow depends approximately on the ratio of the influx volume over that of the lacunar fluid space. Because the influx volume is proportional to the fluid displacement in the canaliculi during a half loading cycle, it is not surprising to find that mechanical loading with a higher magnitude increases the transport efficiency by spreading the tracer from the capillary to the surrounding lacunae at a faster rate and across a larger distance (Figs. 4a and 4b). It is also not surprising that a larger amount of tracer would be transported to the lacunae when bone is more permeable (Figs. 4c and 4d) because the fluid displacement (thus the volume of fluid exchange) increases with increasing permeability of the lacunar-canalicular porosity (Fig. 3-3). We have varied the permeability over a range of two orders of magnitude by assuming three values (3, 7, or 18 nm) for the fiber spacing of the pericellular matrix that is assumed to fill in the canalicular fluid space. This range of values has been selected since there is no experimental data in the literature for the permeability of the lacunar-canalicular porosity

Reproduced with permission of the copyright owner. Further reproduction prohibited without permission.

of bone. All existing measurements of hydraulic permeability of cortical bone have been performed exclusively on the vascular porosity level.[19,30] The lower limit for the fiber spacing (3 nm) could explain the restrictive transport of microperoxidase observed in Knothe Tate *et al.*[17]; the middle value (7 nm) would restrict albumin, while the upper limit (18 nm) would allow most proteins to be transported.

The results from the model also demonstrate that high-frequency loading is less effective at enhancing metabolite concentration per cycle of loading as suggested by Fyhrie and Kimura.[8] The loading frequency is found to have two opposing effects on the fluid exchange during a half cycle: an increased loading frequency results in higher load-induced fluid pressures in bone and thus higher fluid velocities in the canalicular channels, whereas the time period that the fluid is allowed to flow is reduced. Though these two effects partially cancel one another, there is still a net decrease of the fluid displacement (and thus less volume of fluid exchange) for higher loading frequencies, especially in the canaliculi that are further away from the osteonal canal (Fig. 3-3). Therefore, the efficiency of the mass transport is reduced for higher loading frequencies, which is demonstrated in the shorter distance that the tracer spreads from the osteonal canal and more cycles required to reach the same tracer concentration compared to the lower loading frequencies (Figs. 4a and 4c).

Less significant enhancement of mass transport has been found not only for loading at relatively higher frequencies but also for cells further from the osteonal canal (Fig. 3-4). In our model, the fluid never reaches the lacuna that is closest to the cement line (lacuna 3), because the cement line is idealized to be impermeable and the pressure gradient there vanishes. Although the canaliculi of the majority of the outermost lacunae

Reproduced with permission of the copyright owner. Further reproduction prohibited without permission.

in osteons radiate inward toward the osteonal canal, some canaliculi do penetrate the cement lines between adjacent osteons as well as between osteons and interstitial regions histologically.[5,10] This partial opening of the cement line may result in load-induced fluid influx into the outermost lacunae and thus may increase mass transfer into that area by convection. However, we do not expect the enhancement of mass transport by the load-induced fluid flow to be spatially uniform; instead, the enhancement would decay gradually as the lacuna distance from the capillary increases. Due to the spatial limit of mass transport of both convection and diffusion, osteocytes may have to be within a certain distance from the vessels for survival as has been previously suggested.[9,22] Lack of mechanical enhancement of nourishment may be the reason for the experimental finding that the percentage of dead or degenerated osteocytes increases as the distance from the osteonal canals increases in human ear ossicles.[22]

Our calculations also confirm that the load-induced fluid flow in the canalicular channels could greatly enhance diffusive mass transport between the capillary and the bone cells as suggested in previous studies.[15-18,29] In bone, the diffusion coefficient of glucose is on the order of 10^{-6} cm^2s^{-1}.[23] However, for larger molecules such as horseradish peroxidase, the diffusion coefficient D would be at least two orders of magnitude lower, i.e., 10^{-8} cm^2s^{-1}.[29] In an osteon loaded at 2000 με and a frequency (f) of 1 Hz, the average velocity during a half cycle ($U = 2fD_t$) is approximately 60 μm s^{-1} for the flow in the canaliculi connecting the first and second lacunae (*C2* in Fig. 3-1) when the fiber spacing is 7 nm. In this case, the Peclet number ($Pe = Ul_0D^{-1}$, the ratio of convection transfer *vs.* diffusion transfer) for horseradish peroxidase (6 nm in diameter) in a canaliculus (length l_0 = 20 μm) is estimated to be as high as (20 μm x 60 μm s^{-1})/(10^{-8} cm^2s^{-1}) = 1200, which

Reproduced with permission of the copyright owner. Further reproduction prohibited without permission.

means that the mass transport of large molecules is dominated by convective canalicular flow in the loaded osteon.

The most fundamental feature of the present model is that it draws a sharp distinction between transport processes in the canaliculi and the lacunae. In the canaliculi, the tracer transport can be convection- or diffusion-dominated depending on tracer size, whereas in the lacunae transport is nearly entirely due to diffusion because of the rapid decay of the jet velocity from the canalicular exits. The diffusive spreading of a tracer front over one cycle is given by the characteristic diffusion distance $\sqrt{D/f}$, where D is the diffusion coefficient for the tracer and f is the loading frequency. At 1 Hz of loading this distance is 1 μm for larger tracers (e.g., horseradish peroxidase) when $D = 10^{-8}$ cm^2s^{-1},[29] and for smaller tracers (e.g., glucose) this distance is increased to 10 μm when $D = 10^{-6}$ cm^2s^{-1}.[23] It is clear by comparing this characteristic length with the length of the canaliculus (20 μm) that convective fronts are sharply defined for larger tracers ($D < 10^{-8}$ cm^2s^{-1}), whereas the canaliculus will be diffusion-dominated for smaller tracers (e.g., small ions, $D > 10^{-6}$ cm^2s^{-1}). The present model, thus, does not apply to small ions.

In our model, the pathway for mass transport between the capillary and bone cells is assumed to be through the lacunar-canalicular channels via small openings in the osteonal canal wall. Although the layer of osteoblasts and lining cells covering the inner surface of the osteonal canal has been proposed to be a cellular barrier to bone fluid flow into or out of the canalicular channels,[24,28] tracer experiments have shown that larger marker molecules such as horseradish peroxidase and ferritin can pass the bone lining cell layer and perfuse into the bone matrix.[17,26] In addition, the measured permeability of the osteoblast monolayer has been found to be similar in magnitude to that of the endothelial

Reproduced with permission of the copyright owner. Further reproduction prohibited without permission.

monolayer *in vitro* ($\sim 10^{-17}$ m^2, Hillsley and Frangos[11]), which is almost three orders of magnitude greater than that of the canaliculi ($\sim 10^{-20}$ m^2, Zhang *et al.*[37]). Therefore, the osteoblast lining layer is unlikely to be a barrier for the canalicular fluid to reach the osteonal canal via the openings in the canal wall.

Although we have only presented results for tracer transport through the lacunar-canalicular porosity from a capillary to the lacunae within a cyclically loaded osteon, the idea and method used here can be adapted to solve other related problems. For example, the disposal of wastes from the lacunae to the osteonal canal can also be investigated in the cyclically loaded osteon using the same methods described above. The waste transport shows the same patterns as the nutrient transport except it operates in the opposite direction. We can also apply similar analyses to bones that do not have secondary osteons as modeled here. For example, rat bone has only primary osteons, which have no cement lines but have a capillary at their center with osteocytes surrounding the vessel. If one applies a symmetry boundary condition to the evenly distributed primary osteons in loaded rat bone, one obtains the same boundary value problem as in our model. In cancellous bone where the rod or plate-like trabeculae consist of several layers of osteocytes with the vasculature usually on the outer surfaces of the trabeculae, nutrients are transported inward from the bone-marrow interface toward cells in the middle region of the trabecula, similar to nutrients being transported from the osteonal canal outward toward the outermost cells in our model. Despite the different appearance of these bone tissues, similar analyses of the lacunar-canalicular fluid flow can be applied to investigate the mass transport in these tissues under mechanical loading. In both cases, the results from our model are applicable qualitatively, i.e., the load-induced fluid flow as an

Reproduced with permission of the copyright owner. Further reproduction prohibited without permission.

enhancement for mass transport and its limitations to loading frequency and spatial location are also valid for the primary osteons and the trabeculae, although the degree of the enhancement and its frequency and spatial limitations may differ from the numerical predictions of the current model.

Careful considerations should also be taken when we try to correlate these results from the microstructural model with the findings from tracer studies performed at the whole-bone level because of the inhomogeneous bone structure consisting of different osteonal, interstitial, and lamellar regions as well as the complex blood vascularization in bone. The assumptions in our model are very simplified and far from the real situation of the experimental setting. For example, the osteonal canal is assumed to be a tracer reservoir in our model, which may be accurate enough to represent the continuous nutrient supply from the blood vessel. However, in experiments where tracers were injected in a bolus not all the microvessels have been shown to be perfused with the tracers,[26] and the tracer (ferritin) that filled the extravascular space in the vascular canals was eventually washed out within 60 minutes due to bulk interstitial fluid flow and diffusion.[26] The drainage pathways for the interstitial fluid flow are not clear in bone where no lymphatic vessels have been detected, although prelymphatic channels have been proposed to exist.[26] The driving forces of this interstitial fluid flow, which is generally believed to be centrifugal in mature bone, are not well understood[26] and thus are not considered in our model.

There are several other limitations of our model. First, active transport via proteins in the cellular membrane is neglected. Also, the structure of the osteon is very idealized, as are the applied boundary conditions such as the zero reference pressure in the osteonal

Reproduced with permission of the copyright owner. Further reproduction prohibited without permission.

canal and the non-leakage boundary condition at the cement line. We have chosen a sinusoidal waveform for the applied mechanical stress, which is not very physiological. However, since an arbitrary waveform of cyclic loading can be constructed using a Fourier series superposition of sinusoidal signals, a sinusoidal waveform can be used as a simplification of more complex loading signals. Other limitations of our model include: (1) assuming only radial canalicular flow in the osteon; (2) adapting isotropic values for bone's mechanical properties and permeability while bone is an anisotropic material; (3) assuming the viscosity and bulk compressibility of the bone fluid to be the same as salt water; and (4) neglecting the inertia of the fluid and the displacement of the solid in the poroelasticity theory formulation, which may introduce errors when a high frequency loading is applied to the porous media.

Despite its simplicity and limitations, our model has successfully demonstrated that net mass transport does occur in a cyclically loaded osteon. Using this model, we have explored a novel concept that instantaneous mixing of bone fluid in the relatively large fluid space surrounding the osteocyte in a lacuna creates a concentration difference between inward and outward canalicular flow that is vital for net mass transport. The model has predicted that tracer transport within the cyclically loaded osteon increases with higher loading magnitude and higher permeability and decreases with increasing loading frequency. The method and results of this study can also be extended to other bone tissues including primary osteons and trabeculae. The theoretical predications of our model provide a helpful tool to design future experimental studies of tracer movement and bone fluid flow that will enhance our understanding of bone metabolism as well as bone adaptation.

Reproduced with permission of the copyright owner. Further reproduction prohibited without permission.

Acknowledgments

This study was supported by grants from the NIH (AR44211, AR46429), NSF (BES-9806202), and PSC-CUNY (669389, 61420).

Table 3-1. Extracellular Fluid Volume in Pores of Bone

Pores	Dimensions (μm)	Volume (μm^3)
osteonal canal* (hollow cylinder)	outer r = 30 inner r = 15 length = 500	1.1×10^6
lacuna† (spherical shell)	outer r = 5 inner r = 4	260
canaliculus‡ (hollow cylinder)	outer r = 0.2 inner r = 0.1 length = 20	2.0

Notes: *The annular fluid space is between the outer osteonal canal wall and the inner capillary wall in the osteonal canal.[2] †The fluid fills the spherical shell in a lacuna between the outer lacunar wall and the inner osteocyte.[20] ‡The fluid fills the annular space of a canaliculus between the outer canalicular wall and the inner cell process.[2]

Reproduced with permission of the copyright owner. Further reproduction prohibited without permission.

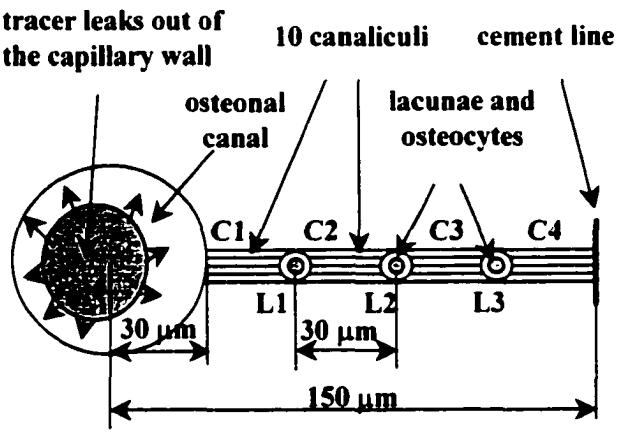

Fig. 3-1. A schematic drawing showing a part of an osteon. The osteon consists of three concentric layers of osteocytes (radii 4 μm) and lacunae (L1, L2, L3; radii 5 μm) that are evenly arranged in the cortex. The canalicular channels (20 μm long, i.e., the 30 μm cell-to-cell distance minus the 10 μm lacunar diameter) that join the adjacent osteocytes are believed to be the pathways for the tracer transport from the canal to the lacunae (C1, C2, C3 represent 10 canaliculi, respectively). A tracer, mimicking nutrients leaking from the capillary, is assumed to fill the fluid space of the osteonal canal with a concentration of 100%. The tracer is transported from the canal to the lacunae during mechanical loading.

Reproduced with permission of the copyright owner. Further reproduction prohibited without permission.

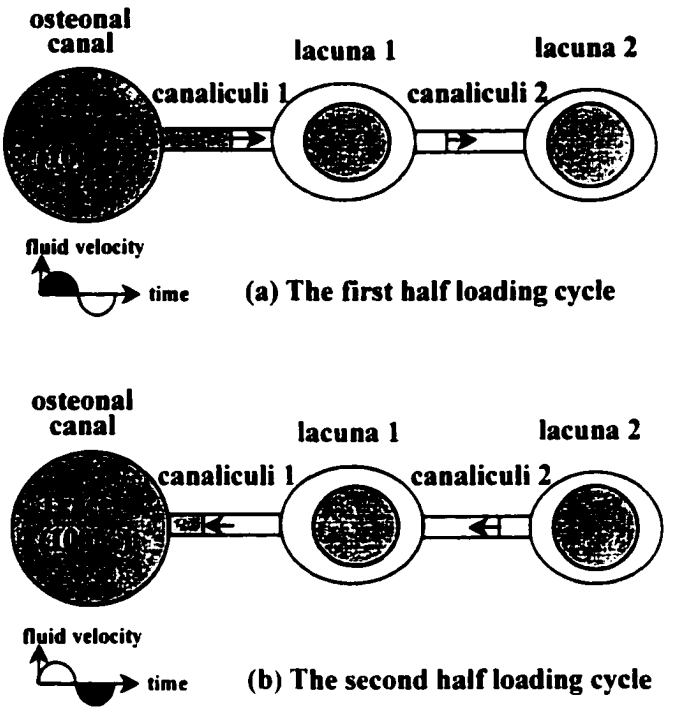

Fig. 3-2. A schematic drawing showing the lacunar mixing during a loading cycle. (a) For the first half loading cycle, the fluid with 100% tracer concentration from the osteonal canal is sucked towards lacuna 1. If the fluid displacement is greater than the canalicular length (20 μm), some fluid would enter the lacuna and mix there, raising the local tracer concentration. (b) For the next half loading cycle, the same amount of fluid is squeezed back into the canal but with a lower tracer concentration compared to that of influx due to the dilution from mixing. Therefore, while there is no net fluid exchange over one cycle, the result is net tracer transport to the lacuna 1. The same transport mechanism of lacunar mixing moves the tracer outwards radially from lacuna 1 to lacuna 2, and so on. In order to have tracer mixing in one lacuna, the local fluid displacement should be greater than the canalicular length. Therefore, the canalicular length is the threshold for the lacunar mixing. (The osteonal canal, the lacunae with osteocyte bodies, and the canalicular channels are not drawn to scale.)

Reproduced with permission of the copyright owner. Further reproduction prohibited without permission.

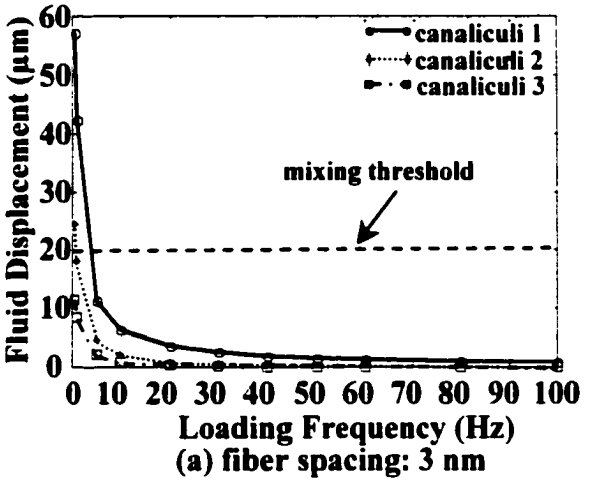

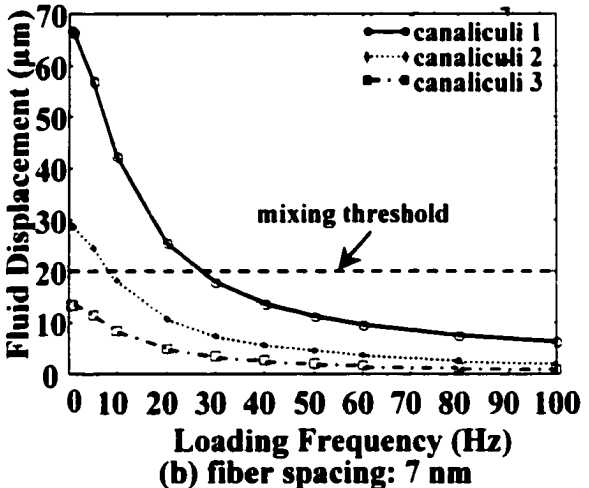

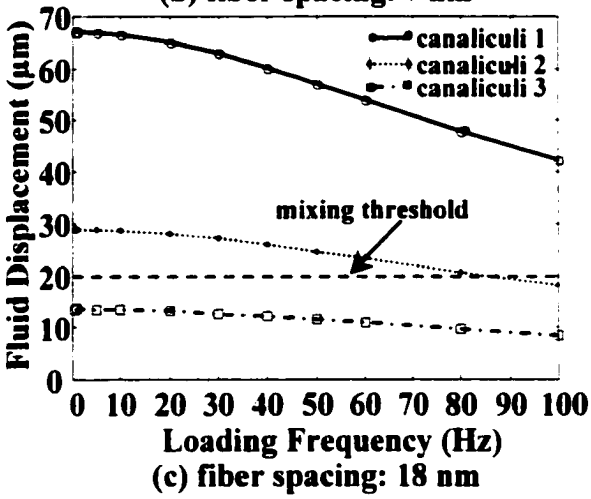

Fig. 3-3. The fluid displacement for the three canalicular sets (see Fig. 3-1) as a function of loading frequency for a loading magnitude of 2000 με and a canalicular annulus fiber spacing of (a) 3 nm, (b) 7 nm, and (c) 18 nm. The fluid displacement decreases as the canalicular set is further away from the osteonal canal and as the loading frequency is increased from 0.5 to 100 Hz. As the fiber spacing increases (increasing permeability of the lacunar-canalicular porosity), the fluid displacement is greater, particularly at higher frequencies. For tracer to reach each lacuna, the fluid displacement must be greater than the length of the canaliculi (20 μm), termed the mixing threshold.

Reproduced with permission of the copyright owner. Further reproduction prohibited without permission.

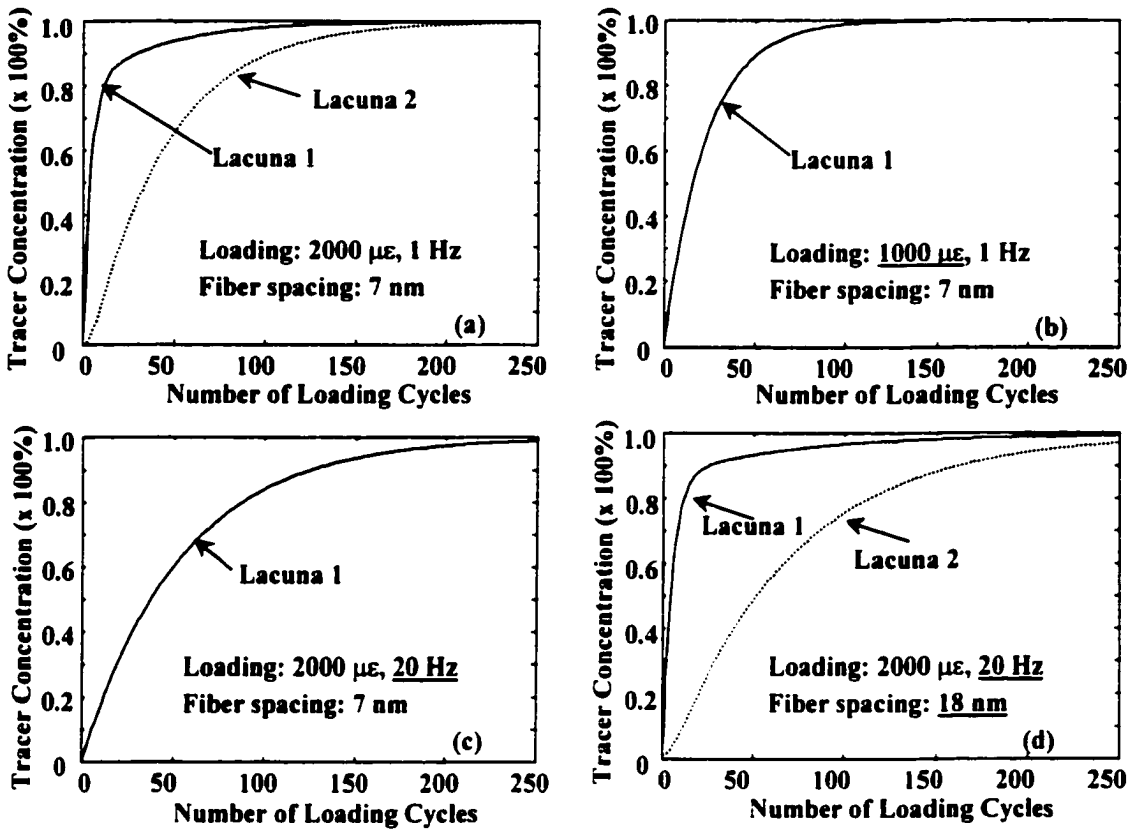

Fig. 3-4. The tracer concentration in the lacunae increases with increasing number of loading cycles and the efficiency of tracer transport (i.e., the speed and distance) depends on the loading magnitude, loading frequency, and bone permeability indicated by the fiber spacing of the fiber matrix in the canalicular channels. (a) The osteon is loaded at 2000 με and 1 Hz with a fiber spacing of 7 nm; (b) the osteon is loaded at a lower loading magnitude (1000 με) compared to (a); (c) the osteon is loaded at a higher loading frequency (20 Hz) compared to (a); (d) the osteon is loaded when the bone is more permeable (the fiber spacing is 18 nm) compared to (c). Mass transport is more efficient when the mechanical loading is of a lower frequency and a higher magnitude as well as when bone is more permeable at the lacunar-canalicular level.

Reproduced with permission of the copyright owner. Further reproduction prohibited without permission.

Chapter 4 Delineating The Bone Interstitial Fluid Pathway in Vivo

Abstract

Although interstitial fluid flow has been suggested to play a role in bone adaptation and metabolism, the constituents and ultrastructure of this interstitial fluid pathway are not well understood. The lacunar-canalicular porosity is generally believed to be a continuous fluid pathway through which the osteocytes obtain nutrients from the blood supply and dispose of wastes; however, whether the smaller collagen-hydroxyapatite porosity in adult bone is also part of the fluid pathway is still unclear. Previous studies injecting tracer molecules into bone vasculature provided conflicting results about the size of the interstitial fluid pathway. Electron microscopy studies have suggested that a fiber matrix surrounds the osteocytic cell processes and fills the pericellular fluid space. The fiber spacing (the pore size) of the pericellular matrix in the lacunar-canalicular porosity has not been determined experimentally. To delineate the interstitial fluid pathway four types of tracers with various sizes were injected into the rat: reactive red 120, microperoxidase (MP), horseradish peroxidase (HRP) and ferritin, with an approximate diameter of 1, 2, 6, and 10 nm, respectively. Five minutes after injection, all the tracers except ferritin were found in the osteocytic lacunae in the rat tibia and no tracer appeared to penetrate the mineralized matrix (the collagen hydroxyapatite porosity). The density of the labeled osteocytes or blood vessels (the number of the labeled osteocytes or blood vessels per mm^2) were measured at the anterior, posterior lateral, and posterior medial regions in the mid-diaphysial cross-sections. The pooled measurements showed that, compared to the control where all the osteocytes were stained with toluidine blue, the density of the osteocytes labeled with MP, HRP, and ferritin was significantly lower, while no significant difference was found between reactive red group vs the

Reproduced with permission of the copyright owner. Further reproduction prohibited without permission.

control ($P > 0.05$). However, the density of the blood vessels did not show any significant difference between the control, MP, and HRP groups ($P > 0.05$), while a significant difference was found between ferritin vs the control ($P < 0.05$). This study suggests that the pore size (fiber spacing) of the pericellular matrix in the lacunar-canalicular pores is between the size of HRP (6 nm) and ferritin (10 nm). (350 words)

Introduction

It is well established that living bone tissue is responsive to external mechanical signals by adapting its mass and structure; however, its cellular mechanosensory mechanisms are not yet well understood. Many investigators have tried to relate bone adaptation to different parameters of mechanical loading such as loading magnitude, loading rate (frequency), and loading regimen at the tissue level (e.g., Lanyon et al., 1982; Rubin and Lanyon, 1987; Jee et al., 1991; Turner et al., 1991; Chambers et al., 1993; Torrance et al., 1994; Mosley and Lanyon, 1998; Mosley, 2000; Rubin et al., 2001). Theoretical models have been developed to understand bone adaptation phenomenologically (Cowin, 1983; Hart et al., 1984; Carter et al., 1987; Huiskes et al., 1987; Prendergast and Taylor, 1994; Bagge, 2000; Huiskes, 2000; Adachi et al., 2001). Although mechanical stimuli have been shown to regulate bone cells' gene expression in vitro and in vivo (Raab-Cullen et al., 1994; Klein-Nulend et al., 1996; Jacobs et al., 1998; Miles et al., 1998; Chen et al., 2000; Moalli et al., 2000; You et al., 2001a), the mechanisms by which bone cells sense external mechanical stimuli remain unclear.

One candidate mechanism of bone's mechanotransduction is through load-induced bone interstitial fluid flow via shearing the osteocytic process membrane or deforming

Reproduced with permission of the copyright owner. Further reproduction prohibited without permission.

the cytoskeleton of the osteocytic process (Weinbaum et al., 1991; 1994; Hillsley and Frangos, 1994; Turner et al., 1994; Cowin et al., 1995; Burger and Klein-Nulend, 1999; Weinbaum et al., 2001; You et al., 2001b). Weinbaum, Cowin and coworkers have proposed a theoretical model of bone fluid flow where a pericellular fiber matrix similar to the surface glycocalyx of endothelial cells surrounds the osteocytes and fills the lacunar-canalicular fluid channels. The theory predicts that the interstitial fluid flow in the lacunar-canalicular channels yields a stimulating shear stress in the range of 5-30 dyn/cm^2 and a hoop strain of 1-10 percent in the cell process cytoskeleton under physiological mechanical loading (Weinbaum et al., 1994; You et al., 2001b). The fluid pressure predicted by the theory achieves a good agreement with strain-generated potentials measurements (Cowin et al., 1995; Wang et al., 1999). The key assumption leading to the above predictions is a fiber spacing (i.e., pore size) of the pericellular matrix, which is assumed to be 7 nm, the effective size of albumin, because the fiber matrix in the lacunar-canalicular porosity is believed to be the molecular sieve that prevents albumin, the most abundant protein in the serum, from leaking out of the vascular pores (Weinbaum et al., 1994; Cowin et al., 1995). Although electron microscopic studies have suggested the existence of such a fiber matrix in bone (Wassermann and Yaeger, 1965; Sauren et al., 1992; Shapiro et al., 1995; Aarden et al., 1996), the key assumption of the pore size of the fiber matrix remains to be confirmed experimentally.

Previous experimental studies injecting tracer molecules into bone provided conflicting results of which level of bone pores is continuous fluid pathway and the size of bone pores. The lacunar-canalicular porosity is generally believed to be a continuous

Reproduced with permission of the copyright owner. Further reproduction prohibited without permission.

fluid pathway through which the osteocytes obtain nutrients from blood supply and dispose of wastes (Cooper et al., 1966; Piekarski and Munro, 1977; Kufahl and Saha, 1990; Knothe Tate et al., 2000; Knothe Tate and Knothe, 2000; Wang et al., 2000); however, whether the smaller collagen-hydroxyapatite porosity within the mineralized matrix in adult bone is also part of the fluid pathway remains debated. In addition, there is no agreement on the size of the largest tracer molecules that can pass through the pores. For example, ferritin (~10 nm in diameter) was found to form halo-shaped labeling in the bone matrix surrounding the blood vessels in two-day-old chick bone (Dillaman, 1984), in adult dog bone (Montgomery et al., 1988), and in adult goat (Qin et al., 1999; Mak et al., 2000). These results suggest that the collagen hydroxyapatite porosity in the mineralized matrix is a continuous pathway for interstitial fluid flow and the size of this porosity is ~10 nm. Studies using horseradish peroxidase (HRP, ~6 nm in diameter) yielded conflicting results: some found the tracer in almost all the lacunae and did not penetrate into the mineral matrix (Doty and Schofield, 1972; Tanaka and Sakano, 1985), while others found strong labeling in the endosteal matrix of adult rat bone (Dillaman et al., 1991). Using microperoxidase (~2 nm in diameter), Tanaka and Sakano (1985) found the tracer was present in the canaliculi but was excluded from the mineralized matrix, while a more recent study reported two discrete labeling bands in the mineralized matrix (Knothe Tate et al., 1998b). Using procion red (<1 nm in diameter), one study reported that this tracer was excluded from the mineralized bone matrix 20 minutes post-injection in fresh sections of the rat tibia (Knothe Tate et al., 1998b), while a later study found the tracer in the matrix in PMMA-embedded sections of the rat tibia 9 seconds post-injection (Knothe Tate et al., 2001).

Reproduced with permission of the copyright owner. Further reproduction prohibited without permission.

To address the conflicting results from previous tracer studies and to delineate interstitial fluid pathway, we performed this study using four tracers: reactive red, MP, HRP and ferritin, ranging in size from approximately 1 to 10 nm. The goals of this study were (1) to begin to systematically to delineate the smallest pore size of the interstitial fluid pathway in vivo; (2) to determine whether the collagen hydroxyapatite porosity in the mineralized matrix of adult bone is continuous fluid pathway; (3) to quantify tracer movement and labeling patterns in absence of mechanical loading.

Methods

To explore the ultrastructure of interstitial fluid pathway, we injected into the rat blood system the following exogenous tracers: reactive red, a dye usually used as an affinity chromatography media; microperoxidase (MP) and horseradish peroxidase (HRP), enzyme proteins derived from equine heart cytochrome and horseradish, respectively; and ferritin, a colloidal ion. Their molecular weights, diameters, and dosages are listed in Table 4-1. We chose to use these tracers, because most of them have been safely used in previous tracer studies in vivo, and the molecular weights of the tracers span three orders of magnitude, from a thousand Daltons (reactive red) up to four hundred thousand Daltons (ferritin) (Table 4-1), which is a good representation of solute molecules in bone. The sizes of the tracers are in the range of 1 nm (reactive red) to 10 nm (ferritin), a range in which the most likely fiber spacing of the pericellular fiber matrix (7 nm) is thought to fall (Weinbaum et al., 1994; Cowin et al., 1995).

Animal preparation

Male Sprague-Dawley rats (body weight: 340 ± 50 g, n = 15) were divided into five groups (three animals per group) receiving reactive red, MP, HRP, ferritin, and saline

Reproduced with permission of the copyright owner. Further reproduction prohibited without permission.

(controls), respectively. Permission for this in vivo study was granted by the IACUC at the Hospital for Special Surgery. To optimize the consistency of tracer labeling and minimize diffusion artifacts, preliminary work was performed to test different injection locations, tracer dosages, circulation times (the time interval between tracer injection and the stopping of blood circulation), as well as the subsequent histological procedures. The experimental protocol was established as follows.

Tracer solutions were injected into rat jugular veins while the animals were under anaesthesia. Rats were anaesthetized via an intraperitoneal injection of a mixture of ketamine (80 mg/kg body weight) and xylazine (5 mg/kg body weight). Additional inhalation anaesthetic methoxyflurane was given if needed using a nose cone under a hood. The left jugular vein was exposed surgically and a 25G5/8 needle attached to a syringe was inserted into the vein to inject a bolus of tracer solution.

Tracer solutions were prepared from powder except for ferritin supplied as bottled liquid (concentration: 70 mg/ml). All tracers were purchased from Sigma, St. Louis, MO. The reactive red solution (concentration: 0.8%) was prepared by dissolving 1.4 g reactive red powder (purity: 60%) in 100 ml PBS and then filtering with a paper filter. The MP and HRP solutions were prepared by dissolving 25 mg MP or HRP in 1 ml PBS. All the tracer solutions as well as the saline used in control animals were administrated at 1 ml volume per 100 g body weight, giving a dosage of 8, 25, 25, and 70 mg per 100 g body weight for reactive red, MP, HRP, and ferritin, respectively. For a rat of 350 g body weight, the total fluid volume injected was approximately 3.5 ml, which was flushed into the jugular vein within 2 minutes.

Reproduced with permission of the copyright owner. Further reproduction prohibited without permission.

The tibia was chosen to be examined in this study because this long bone has been widely used in bone adaptation and tracer studies (e.g., Turner et al., 1991; Montgomery et al., 1991; Knothe Tate et al., 1998a,b; 2000; Mak et al., 2000). The tracer was allowed to circulate for 5 minutes post-injection, which we found to be long enough for the tracer to enter bone blood vessels throughout the tibiae. The rat was then sacrificed by carbon dioxide inhalation, which took ~2-5 minutes, and both tibiae were harvested and immersed into the fixatives immediately. Anatomical positions (anterior and posterior-lateral corners) were marked on the bone surfaces using colored markers to maintain orientation for later imaging and data analysis.

Histological processing of bone samples

To preserve the tracer distribution in its in vivo condition, the histological processing time was minimized in order to reduce the possible movement of tracer molecules after the blood circulation stopped. The histological processing for each tracer is as follows (Table 4-2):

Reactive red

The mid-diaphyses of the tibiae injected with reactive red were initially cut into 0.6 mm thick cross-sections using a diamond saw (Buehler, Lake Bluff, IL) and then fixed in 100% alcohol for 4 hrs. These calcified sections were ground down to 0.4 mm using polishing paper (Buehler, Lake Bluff, IL). The ground sections were put on glass slides and coverslipped with microscopy oil. To preserve the slides, nail polish was used to seal the edges of the coverslip and to prevent the oil leakage.

Microperoxidase and horseradish peroxidase

Reproduced with permission of the copyright owner. Further reproduction prohibited without permission.

The mid-diaphyses of the tibiae injected with MP and HRP were initially cut into 1.5-2.0 mm thick small blocks using the diamond saw and then fixed in 0.5% glutaraldehyde and 2% paraformaldehyde in 0.05 M cacodylatesodium buffer while being agitated in a shaker for 48 hrs. The small blocks were decalcified in 10% nitric acid while being agitated in a shaker for 48 hrs. Thin cross-sections (5-10 μm) were then cut from the blocks using a cryostat (Model OTF 5030, Bright Instrument Company, England) and air-dried for 12 hours.

Both MP and HRP in the thin cross-sections were visualized using 3,3'-diaminobenzidine tetrahydrochloride (DAB), a peroxidase substrate suitable for use in immunoblotting and immunohistological staining procedures. This substrate produces an insoluble end product that is brown in color to allow visualization of the tracers. Fresh DAB solution was prepared by dissolving 10 mg DAB tablet (Sigma, St. Louis, MO) in 15 ml PBS, which was then filtered. 12 μl hydrogen (H_2O_2) was added prior to use. Drops of DAB solution were applied to the thin sections for 1 hr at room temperature. After staining, the slides were rinsed in distilled water twice, air-dried, and coverslipped with mounting media.

Ferritin

The mid-diaphyses of the tibiae injected with ferritin were initially cut into 1.5-2.0 mm thick small blocks using the diamond saw and then fixed in 100% alcohol for 4 hrs. Since immersion into any acid interferes with staining of ferritin, the calcified blocks were stained *en bloc* for 1 hr in Perl's reagent, a freshly made 1:1 mixture of 4% potassium ferrocyanide and 4% hydrochloric acid. Ferritin is split by hydrochloric acid, allowing potassium ferrocyanide to combine with a ferric ion to form an end product

Reproduced with permission of the copyright owner. Further reproduction prohibited without permission.

called Prussian Blue, allowing visualization of the ferritin. The stained blocks were then decalcified in 10% nitric acid while being agitated in a shaker for 24 hrs. Thin cross-sections (5-10 μm) were cut from the blocks using the cryostat and air-dried for 2 hours. The thin cross-sections were then counterstained using 0.1% acid fuchsin for 5 seconds to achieve a pink background. After staining, the slides were rinsed in distilled water twice, air-dried, and coverslipped with mounting media.

Controls injected with saline

The mid-diaphyses of the tibiae injected with saline (controls) were processed identically as the MP and HRP-injected samples. The cryo thin sections were also stained with DAB as negative controls of the MP and HRP-injected sections. To show all the osteocytes and blood vessels in the mid-diaphysis of the rat tibia, the cryo thin sections from the controls were also stained with 0.1% toluidine blue O (molecular weight 305-383, Aldrich Chemical Co, Milwaukee, Wt) for 5 sec.

Microscopic imaging and data analysis

We examined the tracer distribution in three local regions, the anterior corner, the posterior lateral corner, and the posterior medial corner, in each tibial cross-section (Fig. 4-1), because the tracer was delivered through the blood vessels and the blood vessel distribution is heterogeneous across the tibia. To achieve consistency of sampling these regions, efforts were made to cut, collect, and image the sections in the same orientation for all animals. The fluorescent labeling of reactive red was examined using selective green light excitation, while the sections labeled with MP, HRP, and ferritin as well as the controls stained with DAB or toluidine blue were examined using routine light microscopy (Nikon Microphot-FXA). Digital images were taken from the three regions in

Reproduced with permission of the copyright owner. Further reproduction prohibited without permission.

each section using a 10x objective (~0.18 mm^2) using the Bioquant Nova image analysis system (R&M Biometrics, Nashville, TN) with a camera and an image intensifier (Optronics, Goleta, CA). Detailed tracer labeling was also examined and imaged using a 40x objective in some reactive red- and ferritin-stained sections.

Three parameters, the bone area (A_b), the number of the labeled blood vessels (N_v), and the labeled cells (N_c), were measured/counted from the 10x images of the thin cryo sections labeled with MP, HRP, ferritin, and toluidine blue using the Bioquant Nova imaging system. Two ratios were derived from these direct measurements: density of the labeled blood vessels, d_v (the number of blood vessels labeled per unit area (mm^2), $d_v = N_v/A_b$); and the density of labeled osteocytes, d_c (the number of osteocytes labeled per unit area (mm^2), $d_c = N_c/A_b$). The physiological interpretation of the two ratios are as follows: the density of labeled blood vessels (d_v) reflects how well the bone blood vessels are perfused with the injected tracer for the circulation time post-injection (5 minutes in this study) plus 2-5 min during sacrifice. The greater this density, the faster the tracer enters the bone vasculature. The labeled vessels are the sources of tracer that may subsequently leak out of the vessel wall and then penetrate the mineralized matrix if it can pass through the bone matrix pores. The density of labeled osteocytes (d_c) represents the amount of tracer that diffuses from the blood vessels into the osteocytic lacunae during the prescribed circulation time. The more cells that are labeled in an area, the more the tracer has diffused out of the vessels. Since the toluidine blue stains all the osteocytes and blood vessels, the two ratios calculated from these sections are the upper limits and serve as references for the sections injected with other tracers.

Reproduced with permission of the copyright owner. Further reproduction prohibited without permission.

For reactive red, only two measures and one ratio, the bone area (A_b), the number of the labeled cells (N_c), and the density of the labeled cells ($d_c = N_c/A_b$), were measured and calculated, because the bone samples injected with reactive red, unlike other groups, were calcified and thin sections (5-10 micron) were difficult to obtain due to technical limitations. In the relatively thick sections (~400 microns), the blood vessels were shown as a three-dimensional network and could not be counted as in the thin cross sections where the blood vessels were shown as oval or circles. To avoid overestimating the labeled cells, cells that were out of focus were not included in the measurement.

Measurement was performed at three regions (the anterior corner, the posterior lateral corner, and the posterior medial corner) per section, three sections per animal, and three animals per group. For each animal and each region, the mean values of the densities measured from the three sections were used for statistical analysis. An analysis of variance (ANOVA) was conducted to find whether the difference between the group means was significant using Excel. If yes, pairwise tests were performed to reveal which pairs of groups had significant difference using an online software (www.graphpad.com/calculators/posttest1.cfm). For all the statistical tests, a significant level of $P < 0.05$ was used.

Results

Five minutes post-injection, the four tracers showed a variety of labeling patterns (Fig. 4-2). The labeling of reactive red was extensive with dye found in most blood vessels and almost all the surrounding lacunae (Fig. 4-2 b). At higher magnification, the reactive red was found to fill the extracellular space of the lacunae and the fine

Reproduced with permission of the copyright owner. Further reproduction prohibited without permission.

canalicular channels as well, but it did not appear to penetrate the mineralized matrix (Fig. 4-3a). The labeling of MP and HRP was similar, with tracer found in blood vessels and the extracellular space of the osteocytic lacunae in the cortex, but not in the mineralized matrix (Fig. 4-2 c and d). The negative controls injected with saline confirmed that the DAB staining of MP and HRP were specific. Ferritin, the largest tracer used, was found in some blood vessels in the cortex with a blue halo usually seen around a labeled vessel, and no osteocytic lacunae were labeled (Fig. 4-2e). At higher magnification, the shade of the pink background staining between the vessel wall and the ferritin halo appeared to be different from that in the matrix (Fig. 4-3b), suggesting that the material in the gap is neither the mineralized matrix nor the blood vessel. The gap between the halo and the vessel wall was measured to be 2.2 ± 0.5 microns (from 25 measurements), suggesting that the halos lined the vascular canal walls without penetrating the mineralized matrix. The staining intensity was found to be varied from vessel to vessel (Fig. 4-4).

ANOVA analyses showed that the densities of the labeled osteocytes (d_c) and the labeled blood vessels (d_v) had significant difference among the five experimental groups receiving the four tracers and saline and no significant difference was found for the anterior (A), posterior lateral (L), and posterior medial (M) regions (Table 4-3 and Figs. 4-5 and 4-6). The pooled measurements from the three regions demonstrated a decrease of the density of the labeled osteocytes with increasing tracer size (Fig. 4-5). Compared to the controls where all the osteocytes were stained with toluidine blue (density: 1248 ± 70), the density of the osteocytes labeled with MP (838 ± 226), HRP (712 ± 247), and ferritin (0 ± 0) was significantly lower, while no significant difference was found between reactive red group (1101 ± 266) vs the control (Table 4-3). However, the density

Reproduced with permission of the copyright owner. Further reproduction prohibited without permission.

of the blood vessels did not show any significant difference among the control (115 ± 28), MP (90 ± 22), and HRP (101 ± 15) groups, while a significant difference was found between the ferritin (53 ± 20) and other groups (Table 4-3, Fig. 4-6).

Discussion

Although electron microscopy studies have suggested the existence of a pericellular structure in the canaliculi (Wassermann and Yaeger, 1965; Sauren et al., 1992; Shapiro et al., 1995; Aarden et al., 1996), there are no quantitative data on the fine structure of the pericellular matrix. The current study provides indirect evidence of the fiber spacing of the pericellular matrix in the lacunar-canalicular pores. Our results suggest that the pore size (fiber spacing) of the pericellular matrix in the lacunar-canaliculi falls in the range of 6-10 nm, because the reactive red (1 nm), microperoxidase (2 nm) and horseradish peroxidase (6 nm) could pass through the lacunar-canalicular pores and reach osteocytes away from the blood vessels, the source of the injected tracer, while the 10 nm ferritin was excluded from the mineralized matrix and is confined to the vascular canals. This range of the pore size contains the most likely fiber spacing (7 nm) proposed by Weinbaum and Cowin based on the proteoglycan fiber matrix that lines the surface of vascular endothelial cells and serves as a filter to prevent leakage of serum albumin (Weinbaum et al., 1994; Cowin et al., 1995).

None of the four tracers used in this study appeared to penetrate into the mineralized matrix within 5 min after injection, suggesting that either the assumed collagen hydroxyapatite porosity is not continuous fluid pathway or the size of this porosity is smaller than 1 nm (the size of reactive red, the smallest tracer used in this study). Smaller

Reproduced with permission of the copyright owner. Further reproduction prohibited without permission.

tracers or longer circulation time should be employed in future experiments to investigate the permeability of the mineralized matrix.

Previous tracer experiments performed to explore the fluid pathways in bone provided conflicting results. The tracer labeling is summarized for the previous studies and this present experiment (Table 4-4).

Reactive red

Our results indicate that this tracer of order 1 nm was excluded from the mineralized matrix following a short period (5 minutes) of perfusion (Figs. 4-2b and 4-3a), which is consistent with one experiment where procion red (molecular weight 300-400 Daltons, <1 nm in diameter) was not found in the mineralized matrix of adult rat bone 30 minutes post-injection (KnotheTate et al., 1998b). The same tracer was injected into mechanically loaded sheep bone (Knothe Tate and Knothe, 2000) and rat bone (Knothe Tate et al., 2000) for a varied circulation time ranging from several seconds to 18 minutes. The tracer was reported not to be present in the mineralized matrix. However, a recent study claims the procion red penetrates into the mineralized matrix in PMMA-embedded sections nine seconds post-injection (Knothe Tate et al., 2001). It usually takes many days to complete PMMA embedding, which usually involves immersing samples in many solvents and resins. In our preliminary experiments, reactive red was found to penetrate into the mineralized matrix in PMMA-embedded sections, while fresh-prepared sections of the same animals showed no labeling in the mineralized matrix. Further examination is needed to clarify this contradiction.

Reproduced with permission of the copyright owner. Further reproduction prohibited without permission.

Microperoxidase (MP)

Tanaka and Sakano (1985) demonstrated that MP passed through the unmineralized alveolar bone in the developing rat, but was excluded from the mineralized matrix 2 hours post-injection, while Knothe Tate et al. (1998b) found this tracer labeled the mineralized matrix of the rat tibia along two bands close to bone surfaces and was absent from the mid-cortex 2 hours after injection. Our study found that MP labeled both the blood vessels and the osteocytic lacunae across the whole rat tibia including the mid-cortex, and that MP did not penetrate into the mineralized matrix (Fig. 4-2c).

Horseradish peroxidase (HRP)

Doty and Schofield (1972) found quite uniform labeling of the blood vessels and the osteocytic lacunae in the rat femur within 30 minutes of injection. Similarly, Dillaman et al. (1991) found HRP labeling in blood vessels and osteocytic lacunae in rat femur 5 or 15 min after injection. They also reported stronger staining of endosteal canaliculi and osteocytic lacunae compared to the rest of cortex after 5 and 15 min post-injection and the endosteal staining started to be washed out 30 min after injection. Knothe Tate et al. (1998b) found that HRP labeling of blood vessels and osteocytic lacunae was present in the inner half of the cortex of the rat tibia where the bone was well-organized 2 hours post-injection. Our study found the HRP labeling of the blood vessels and osteocytic lacunae across the whole bone but no stronger staining near endosteum 5 min post-injection (Fig. 4-2d)

Ferritin

Previous studies reported halo-or partial halo-shaped ferritin labeling in the bone matrix in two-day old chick bone (Dillaman, 1984), adult dog bone (Montgomery et al., 1988), and adult goat bone (Qin et al., 1999; Mak et al., 2000) after the tracer was

Reproduced with permission of the copyright owner. Further reproduction prohibited without permission.

circulated for 10 to 30 minutes. Young bone may be more permeable than adult bone as suggested in permeability measurements (Li et al., 1987) and, therefore, ferritin of order 10 nm might penetrate the bone matrix in the two-day-old chick bone. However, unlike previous studies using adult bone, our study showed a totally different labeling pattern of ferritin in the rat. We found that the ferritin could label blood vessels but did not appear in the osteocytic lacunae and in the mineralized matrix (Figs. 4-2e and 4-3b). We also found the halo-shaped labeling near the labeled blood vessels with a small gap of ~2.2 microns, and the material in the gap did not appear to be the mineralized matrix (Fig. 4-4). Therefore, the halos we found appeared to outline the osteonal canal surfaces and did not enter the bony matrix. The discontinuous halo lines (Fig. 4-4) suggested that these halos could be from lining cells on the canal walls taking ferritin. To further confirm that the halos line the osteonal canal wall, it would be helpful to measure the gap between the halos and the labeled vessel walls in mechanically loaded rat bone. If the gap remains the same, the halos must be along the canal surface.

These different tracer labeling results suggest that the outcome of tracer labeling depends on many factors, such as the molecular weight of the tracer, circulation time, and the species and age of the experimental animals. All these important factors should be considered when interpreting the labeling results. This study also stressed the importance of adapting appropriate histological processing. When the blood circulation is stopped and the histological process begins, the movement of tracer molecules injected into the animal is not necessarily stopped. The tracer is probably still able to diffuse during the subsequent processing period, especially in aqueous solutions, because these tracers are not known to bind to cells or extracellular matrix. Due to the hardness of bone tissue,

Reproduced with permission of the copyright owner. Further reproduction prohibited without permission.

bone samples have to go through several necessary and time consuming histological procedures before the final tracer labels can be recorded. The main artifact for tracer studies, therefore, is the re-displacement of the tracer particles during the long time period of histological processes. For example, while bone is stained in the acid Perl's reagent, decalcified in acids, and then embedded in plastics, tracer molecules may be able to move into the matrix that was mineralized but now is decalcified. The re-displacement of the tracer may account for the fuzzy boundaries of the ferritin halos reported in Montgomery et al. (1988). Although Qin et al. (1999) and Mak et al. (2000) avoided using any decalcifying liquid, one should notice the acidity of the staining reagents and the resulted demineralization of the matrix. The low percentage of labeled osteonal canals (7%, compared to 45% in our study) suggests that the tracer might have been lost during the plastic embedding.

Therefore, in this study the histological processing protocol was optimized to reduce the processing time to avoid re-displacement of tracer via initially sectioning into smaller pieces, using strong agents to shorten decalcification time, and using cryosectioning instead of embedding the samples in plastics such as PMMA or MMA, a complicated process taking days to complete and involving long-time immersion of the samples in alcohols and plastic resins. The histological processing time for the four tracers in this study is much shorter than the time used in most of the previous studies (Table 4-4). For example, the tibiae injected with ferritin were processed within 2 days in this study, while the previous studies took much longer time (chick, ~2 days plus time for plastic embedding in Dillaman (1984); dog, ~2-4 weeks plus time for embedding in Montgomery et al. (1988); goat, 38 hrs plus MMA embedding time in Qin et al. (1999)

Reproduced with permission of the copyright owner. Further reproduction prohibited without permission.

and Mak et al. (2000)). However, even with this relatively short processing time, the ferritin staining might have been lost to some degree in this study, and, therefore, a significantly lower number of the labeled vessels was found for ferritin group compared to other groups.

The present study also provides quantitative data on tracer movement in the absence of mechanical loading. The data could be used to choose tracers for tracking bone fluid flow in mechanically loaded bone. There are two competing requirements of a suitable tracer: it should be small enough to pass through the bone pores where fluid flows and large enough to have limited diffusion. Our results show that, within 5 minutes, the percentage of the cells labeled with reactive red, MP, HRP, and ferritin decreases from 88%, 67%, 57%, to 0% (Table 4-2). Therefore, larger tracers (e.g., MP and HRP) are more likely to be able to show the convective transport besides the baseline transport (under no mechanical loading), because they have more unlabeled osteocytes compared to their smaller counterparts (e.g., reactive red). However, when the tracer is as large as ferritin, the tracer is most likely confined in the vascular pores and can not be used to track interstitial fluid flow.

Knothe Tate and coworkers have employed a very small tracer (procion red, molecular weight: 300-400 Daltons) in mechanically loaded bone (Knothe Tate et al., 1998a; 2000; 2001; Knothe Tate and Knothe, 2000). For the first time, they successfully demonstrated the existence of transport enhancement in loaded bone. However, the enhancement was only found at the early stages of loading and at higher loading frequencies greater than 2.0 Hz and no effect was found at the later stage of loading and at lower loading frequencies (Knothe Tate et al., 2000; Knothe Tate and Knothe, 2000).

Reproduced with permission of the copyright owner. Further reproduction prohibited without permission.

One explanation for this result is that the perfusion time in the conditions of lower loading frequencies and late stage of loading was sufficiently long so that the baseline tracer movement in the absence of mechanical loading might have overwhelmed the convective transport. These tracer experiments and our current study suggest that a relatively larger molecular marker be used to track convective interstitial bone fluid flow. In fact, a recent study by Knothe Tate et al. (2001) successfully demonstrated a greater enhancement of transport using a larger Dextran tracer (molecular weight: 10,000 Daltons) compared to procion red (molecular weight: 300-400 Daltons).

In summary, this study yields important information on the interstitial fluid pathway in bone. This perfusion study with reactive red (~1 nm), microperoxidase (~2 nm), horseradish peroxidase (~6 nm), and ferritin (~10 nm) in the rat bone provides indirect evidence of the pore size inside the lacunar-canalicular fluid channels is 6-10 nm because all four tracers except ferritin passed through the canaliculi and labeled osteocytes. Tracers with a molecular size between 6 nm and 10 nm, e.g., albumin (7 nm), could be used to further delineate the pore size of the lacunar-canalicular porosity. This study also shows that reactive red (1 nm), the smallest tracer we used, is excluded from the mineralized matrix. Tracers with a smaller size should be used to explore the pore size of the collagen hydroxyapatite porosity in the mineralized matrix. In addition, tracer diffusion, in terms of the density of labeled osteocytes in the mid-diaphysial cross-section, was found to decrease with increasing molecular weight and size. This result suggests that tracers with relatively large molecular weight are more suitable to track convective interstitial fluid flow and to demonstrate the mechanical load-enhanced mass transport in bone.

Reproduced with permission of the copyright owner. Further reproduction prohibited without permission.

Acknowledgments

The authors thank Drs. Roberts Majeska and Mitchell Schaffler for the suggestion that the lining cells on the canal wall take up ferritin. We also thank Ms. Orla O'Shea, Ms. Janane N. Diouri and Mr. Anthony Labissiere for their technical support. This study was supported by the NIH (NIAMS grant AR46429).

Reproduced with permission of the copyright owner. Further reproduction prohibited without permission.

Table 4-1. Four Tracers Injected Into The Rat

	Reactive red	MP	HRP	Ferritin
Molecular Weight (Daltons)	1470	1862	40,000	440,000
Approximate Molecular Diameter (nm)	1	2	6	10
Dosage (mg/100 g body weight)	8	25	25	70

Reproduced with permission of the copyright owner. Further reproduction prohibited without permission.

Reproduced with permission of the copyright owner. Further reproduction prohibited without permission.

Table 4-2. Histological Processing Protocols

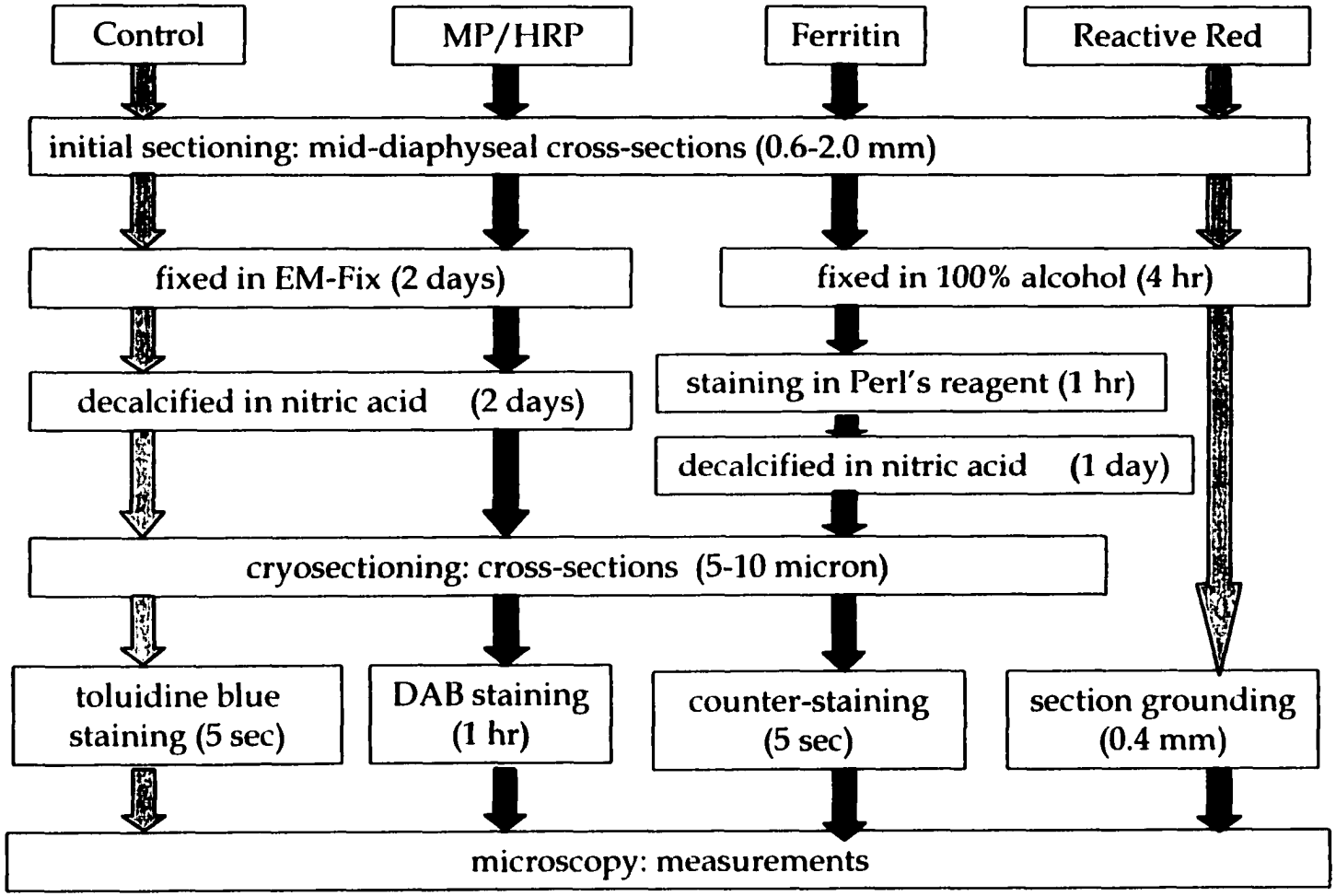

Table 4-3. Tracer Movement in the Absence of Mechanical Loading

	control	reactive red	MP	HRP	ferritin
d_c (#/mm^2)					
A	1209 ± 74	1175 ± 238	662 ± 97	830 ± 88	0 ± 0
L	1260 ± 97	926 ± 243	764 ± 220	506 ± 108	0 ± 0
M	1275 ± 30	1202 ± 315	1097 ± 86	799 ± 50	0 ± 0
Pooled	1390 ± 106	1101 ± 266	838 ± 226	712 ± 247	0 ± 0
Percentage	100%	88%	67%	57%	0%
d_v (#/mm^2)					
A	91 ± 14	N/A	83 ± 38	16 ± 9	52 ± 12
L	143 ± 9	N/A	89 ± 16	93 ± 16	53 ± 24
M	112 ± 26	N/A	95 ± 13	95 ± 11	54 ± 30
Pooled	115 ± 28	N/A	90 ± 22	101 ± 15	53 ± 20
Percentage	100%	N/A	78%	87%	46%

Note: The density of the labeled cells (d_c) and the density of the labeled vessels (d_c) were measured in the anterior (A), posterior lateral (L), and posterior medial (M) regions. Data were reported as mean ± std. Pooled data were calculated using measurements from the three regions. The percentage was calculated by dividing the mean value of each tracer group with that of the control group, which served as a reference of 100%.

Reproduced with permission of the copyright owner. Further reproduction prohibited without permission.

Table 4-4. Summary of Tracer Studies in Bone

Tracer	Studies	Animal	Circulation Time	Tracer Labeling Patterns	Histological Processing
Procion Red	Knothe Tate et al. (1998b)	rat tibia & metacarpi	20 min	Appeared in VP, LCP, not in MM	Fresh-prepared, ~hrs.
	Knothe Tate & Knothe (2000)	sheep forelimb	2 – 18 min	Appeared in VP, LCP, not in MM, enhanced transport in loaded limb	Fresh-prepared, ~hrs
	Knothe Tate et al. (2000)	rat tibia	7 sec – 3 min	Appeared in VP, LCP, not in MM, enhanced transport in loaded limb	Fresh-prepared, ~hrs
	Knothe Tate et al. (2001)	rat ulna	9 sec	Appeared in VP, LCP, and MM, enhanced transport in loaded limb	PMMA-embedding
Reactive red	This study	rat tibia	5 min	Appeared in VP, LCP, not in MM	Fresh-prepared, hrs
MP	Tanaka and Sakano (1985)	rat alveolar bone	2 hrs	Appeared in VP, LCP, not in MM	Frozen sections, ~3 days
	Knothe Tate et al. (1998b)	rat tibia, metacarpi	2 hrs	Found two bands of labeling in MM near bone surfaces	Frozen decalcified sections, ~2 weeks
	This study	rat tibia	5 min	Appeared in VP, LCP, not in MM	Frozen sections, 5 days
HRP	Doty and Schofield (1972)	rat femur	15, 30 min	Appeared in VP, LCP, not in MM	- not specified
	Dillaman et al. (1991)	rat femur	5 min –1 d	Appeared in VP, LCP, & endosteal MM	- not specified
	Knothe Tate et al. (1998b)	rat tibia and metacarpi	2 hrs	Appeared in VP, LCP of the inner half of the cortex	Frozen sections, ~2 weeks
	This study	rat tibia	5 min	Appeared in VP, LCP of the cortex	Frozen sections, 5 days
Ferritin	Dillaman (1984)	chick femur	5-60 min	Halo-shaped labeling within MM	plastic embedding
	Montgomery et al. (1988)	dog tibia	1 - 60 min	Fuzzy halo-liked labeling within MM	MMA embedding
	Qin et al. (1999)	goat tibia	0 min	Halos observed in the MM	MMA embedding
	Mak et al. (2000)	adult goat tibia	~ 10 min	Halos observed in the MM and enhanced transport in loaded bone	MMA embedding
	This study	rat tibia	5 min	Halo-shaped labeling along canal wall, not within MM	2 days

Note: Circulation time is defined as the time period between the finishing of tracer injection and the stopping of blood circulation. VP represents vascular pores (osteonal canals in cortical bone); LCP represents lacunar-canalicular pores housing osteocytes and cell processes; MM represents the extracellular mineralized matrix, excluding the vascular and lacunar-canalicular pores.

Reproduced with permission of the copyright owner. Further reproduction prohibited without permission.

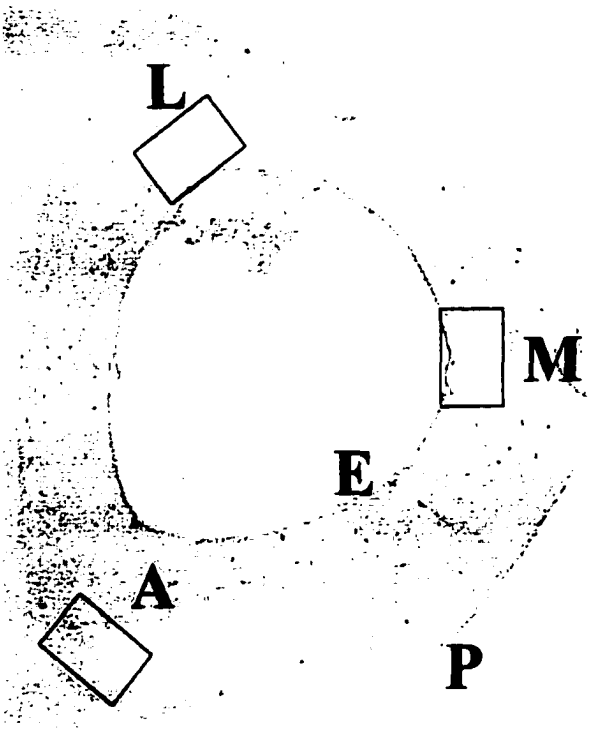

Fig. 4-1. A cross section of the mid-diaphysis of the rat tibia (magnification: 35x). Measurements were performed on three local regions: anterior (A), posterior lateral (L), and posterior medial (M) regions in the cortex between endosteum (E) and periosteum (P).

Reproduced with permission of the copyright owner. Further reproduction prohibited without permission.

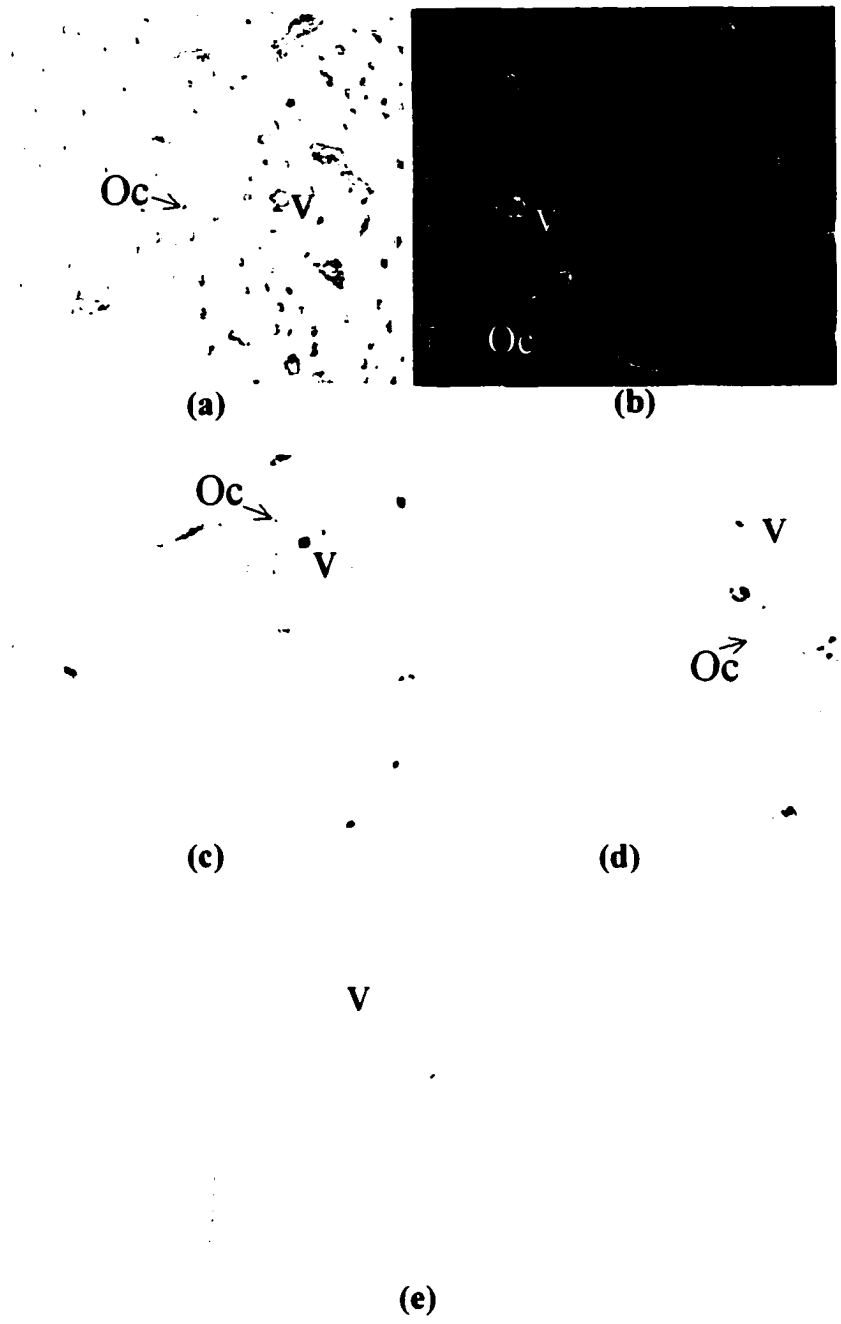

Fig. 4-2. Different tracer labeling patterns at the posterior medial region of the rat tibia (magnification: 700x). (a) Toluidine blue stains all the osteocytes (Oc), blood vessels (v), and bone matrix. (b) Reactive red appears in most blood vessels (v) and osteocytic lacunae (Oc) but not in the bone matrix. (c) MP labels some blood vessels (v) and osteocytes (Oc). (d) HRP shows similar labeling as MP. (e) Ferritin only labels some blood vessels (v) but no osteocytes.

Reproduced with permission of the copyright owner. Further reproduction prohibited without permission.

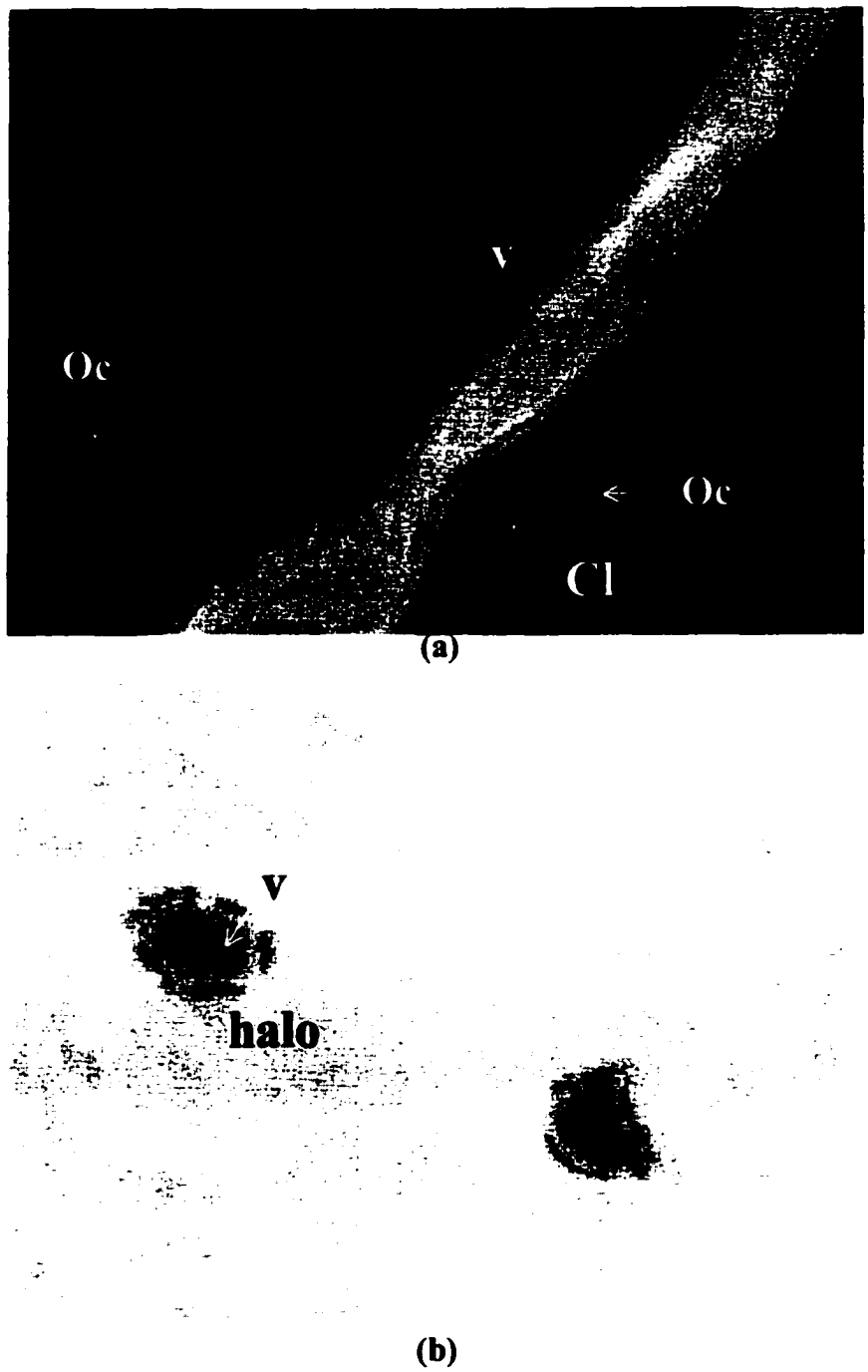

Fig. 4-3. Detailed tracer labeling at higher magnification (magnification: 1400x). (a) Reactive red appears in blood vessels (v), osteocytic lacunae (Oc), and canaliculi (Cl). (b) In the ferritin-labeled section counterstained with acid fuchsin, ferritin halos surround the blood vessel walls with a small gap. The counterstained shade in the gap between the halos and the vessels appears to be much stronger than other areas, suggesting the halos outline the canal surface and do not label the mineralized matrix.

Reproduced with permission of the copyright owner. Further reproduction prohibited without permission.

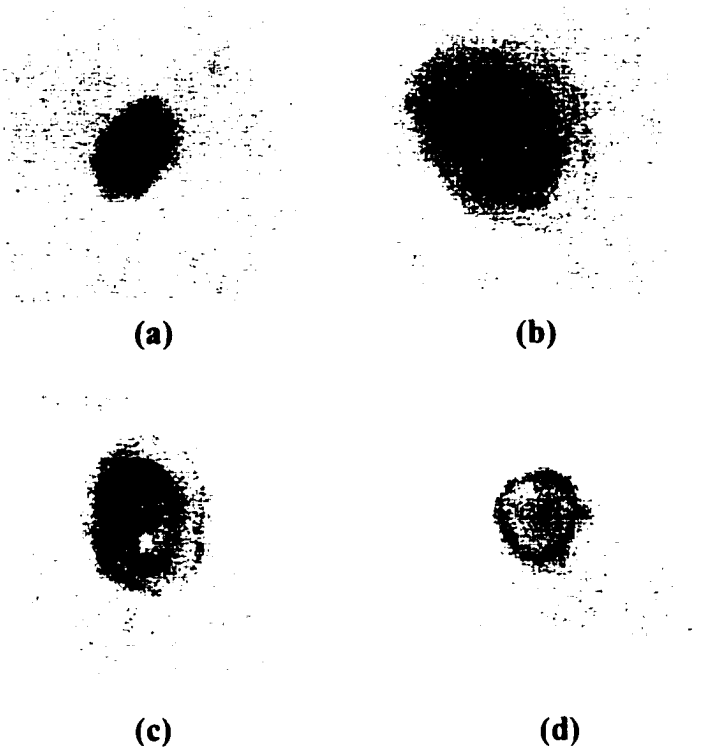

Fig. 4-4. Variations of ferritin labeling (magnification: 1400x). (a) A ferritin halo surrounds a labeled blood vessel with a strong solid intensity. (b) Discrete labeling spots along the vessel wall have a stronger labeling than that inside the vessel. Note a stronger background shade exists between the vessel wall and the halo compared to the overall background color in this and the next panel. (c) Stronger labeling is shown along the vessel wall and the halo. (d) A ferritin halo is found surrounding a vessel that shows nearly no labeling.

Reproduced with permission of the copyright owner. Further reproduction prohibited without permission.

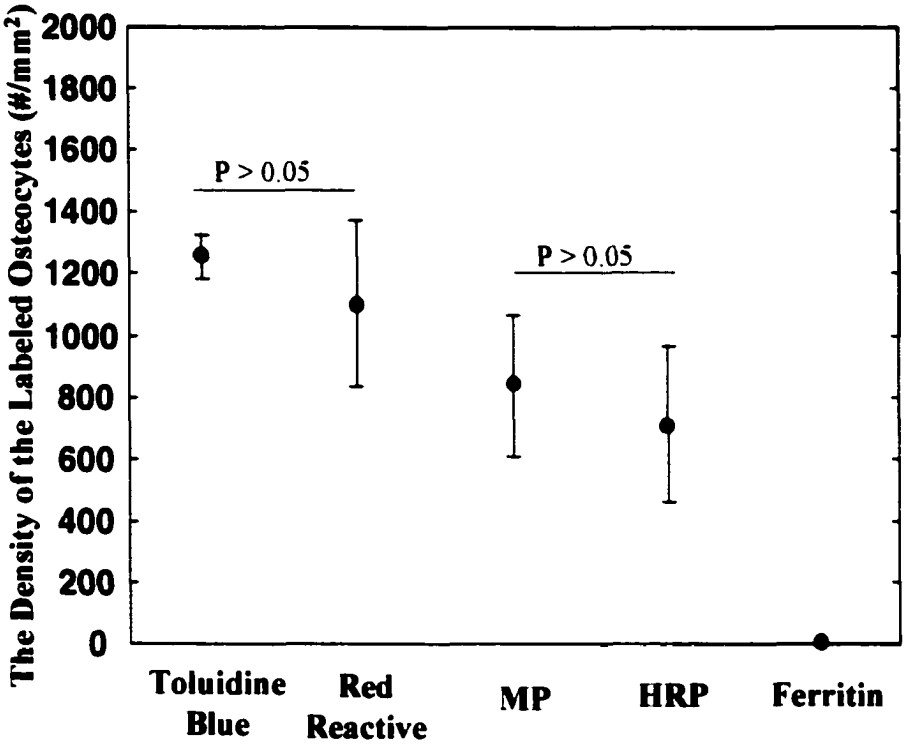

Fig. 4-5. The density of the osteocytes (#/mm^2) labeled with toluidine blue, reactive red, MP, HRP and ferritin. The density of the labeled osteocytes decreases with increasing tracer molecular weight, in the order of toluidine blue, reactive red, MP, HRP, and ferritin. An analysis of variance showed that the difference between the group means was significant ($P < 0.05$). Pairwise comparison tests showed that all pairs of group means were significantly different ($P < 0.05$), except for the two pairs: reactive red and MP; and MP and HRP, which were found not significant ($P > 0.05$). These results also suggest that the pore size of the fluid flow pathway is larger than 6 nm (the size of the HRP) and smaller than 10 nm (the size of the ferritin).

Reproduced with permission of the copyright owner. Further reproduction prohibited without permission.

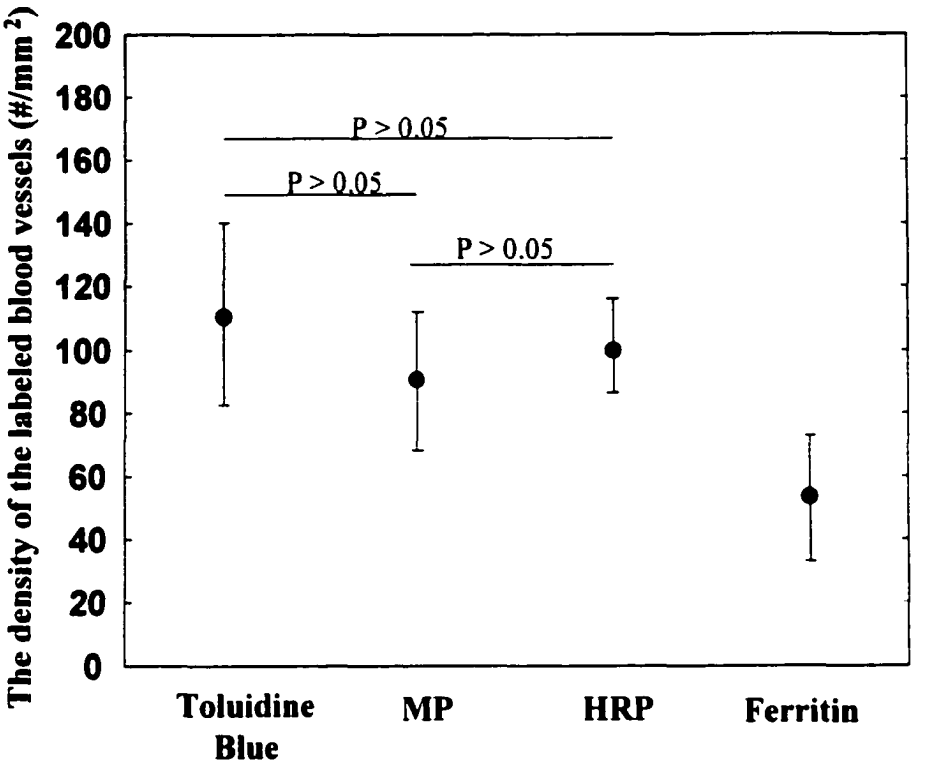

Fig. 4-6. The density of blood vessels (#/mm^2) labeled with toluidine blue, MP, HRP and ferritin. Post-ANOVA pairwise tests showed that the difference between toluidine blue, MP, and HRP was not significant ($P > 0.05$), and the difference between ferritin and all other groups was significant ($P < 0.05$), probably due to losing of ferritin during the histological process.

Reproduced with permission of the copyright owner. Further reproduction prohibited without permission.

Chapter 5 Blood Pressure-Driven Interstitial Fluid Flow in Bone

Abstract

Several experimental results have linked increased periosteal bone growth to compromised venous return (venous stasis). Increased interstitial fluid flow induced by the increased intramedullary pressure caused by the venous stasis has been proposed to account for the periosteal response. To investigate the osteogenic effect of blood pressure-driven fluid flow, a poroelastic model for interstitial bone fluid flow is extended to the situation in which the bone fluid flow in an osteon is driven by the pulsatile blood flow in the bone microvasculature as well as by the applied cyclic mechanical loading. The amplitudes of the fluid responses (i.e., pore fluid pressure, radial pressure gradient, and shear stress acting on the osteocytic cell process) due to the mechanical loading and pulsatile blood pressure are analyzed as a function of frequency and amplitude of the two driving forces. Our results show that, under normal conditions, the pulsatile blood pressure due to cardiac contraction (10 mm Hg at 2 Hz) and muscle contraction (30 mm Hg at 1 Hz) induce dynamic shear stresses on the osteocytic processes that are two orders of magnitude lower than those induced by physiological mechanical loading (1 MPa at 1 Hz). In venous stasis the induced dynamic shear stress is reduced further because, although the mean blood pressure is increased, the amplitude of the pulsatile component of the blood pressure is decreased. These results do not support the hypothesis that increased interstitial fluid flow causes the periosteal bone growth in venous stasis. We put forward this new hypothesis: in venous stasis the increased mean hydraulic pressure acting on the periosteum can trigger cell proliferation, enhance transport of nutrient or/and signaling molecules, and stimulate periosteal bone growth.

Reproduced with permission of the copyright owner. Further reproduction prohibited without permission.

Introduction

The ability of blood flow to influence bone growth and remodeling has been recognized for a long time (Trueta, 1963; Kiaer, 1994). Altered circulation such as stasis in the venous system of an extremity caused by applying tourniquets or vein ligation has been shown to stimulate bone formation or increase bone mass in the young dog (Kelly and Bronk, 1990), the young goat (Welch et al., 1993), and in a disuse rat model (hindlimb suspended) (Bergula et al., 1999). There are many other studies demonstrating similar effects (e.g., Lilly and Kelly, 1970; Arnoldi et al., 1972; Green and Griffin, 1982; Liu and Ho, 1991). The blocking or compromised venous drainage in animal experiments has been found to be associated with increased intramedullary pressure, decreased artery inflow, and decreased pulse of the intramedullary pressure. The underlying mechanism of the periosteal bone growth induced by venous stasis, however, remains unclear. Several factors associated with bone vasculature have been proposed, including changes in oxygen tension, CO_2 tension, local pH (reviewed in Kiaer, 1994), increased interstitial fluid flow (shear stress or streaming potentials) (Kelly and Bronk, 1990; Hillsley and Frangos, 1994; Welch et al., 1993; Bergula et al., 1999), and increased transcapillary filtration (Kelly et al., 1990; Bronk et al., 1993).

To test the hypothesis that increased interstitial fluid flow causes the periosteal bone growth in venous stasis, an osteon model is developed to theoretically connect interstitial fluid flow with pulsatile blood pressure in the bone microcirculation. An analytical model for bone fluid flow in an osteon due to mechanical loading alone (Zeng et al., 1994) is extended to include bone fluid flow due to the pulsatile blood pressure in addition to the axial cyclic loading applied to the osteon. In order to compare the two driving forces, the

Reproduced with permission of the copyright owner. Further reproduction prohibited without permission.

total bone fluid flow is decomposed into two separate components contributed by each loading mechanism alone. The amplitudes of the fluid responses (i.e., pore fluid pressure, radial pressure gradient, and fluid shear stress acting on the osteocytic cell process membrane) due to the two different driving forces are given and compared.

Unlike previous theoretical models that focus on tracer distribution under blood pressure (Dillaman et al., 1991; Keanini et al., 1995), the new model developed here aims to quantitatively investigate the osteogenic effect of blood flow and mechanical loading in terms of shear stress of bone fluid flow. Our results show that the blood pressure in either physiological or pathological conditions induces much smaller (two orders of magnitude lower) shear stress than does the physiological mechanical loading. Therefore, this study does not support the hypothesis that blood pressure-induced interstitial fluid flow causes periosteal bone growth in the condition of venous stasis. Other factors associated with the experimentally imposed vascular changes are necessary to understand the increased periosteal bone growth found in venous stasis. Alternative stimulating mechanisms are examined in the context of venous stasis and periosteal bone growth. We make a new hypothesis that, for the first time, links the periosteal bone changes due to venous stasis with the hydraulic pressure acting on the periosteum.

Methods

As fluid shear stress has been proposed to be the stimulating signal for bone cells (Weinbaum et al., 1991; 1994; Hillsley and Frangos, 1994), the osteogenic effect (capacity) of mechanical loading and blood flow is examined in terms of peak shear stresses on the osteocytic process. Although a recent study (You et al., 2001) suggests another mechanism for osteocyte excitation via deformation of cell cytoskeleton due to

Reproduced with permission of the copyright owner. Further reproduction prohibited without permission.

the fluid drag force, we will show later that the relative osteogenic capacity between mechanical loading and blood flow remains the same order for both stimulating mechanisms, secondary to interstitial bone fluid flow.

Theoretical model for bone fluid flow

Although the effect of the venous stasis on interstitial fluid flow is on the whole bone level, we are going to focus on a single osteon, because one of our early studies (Wang et al., 1999) showed that osteonal canals influence the local patterns of the interstitial fluid flow in bone. In addition, since the vascular porosity has a much higher permeability compared to the lacunar-canalicular porosity through which the interstitial bone fluid flows (Zhang et al., 1998; Wang et al., 1999), the extravascular fluid pressure within the osteonal canals in the cortex is spatially uniform and equals the intramedullary pressure in the marrow cavity. Therefore, in osteonal bone, the interstitial fluid flow in a whole bone can be studied using an osteon model.

The problem considered here is that of determining the bone interstitial fluid pressure field $p(r, t)$ in the lacunar-canalicular porosity of an osteon. The osteon is modeled as a right circular cylinder of radius r_o containing an osteonal canal and the osteonal canal is modeled as a smaller concentric, right circular cylinder of radius r_i. The annular region of the osteon contains the lacunar-canalicular porosity (Fig. 5-1a). The interstitial fluid is assumed to flow through the lacunar-canalicular channel surrounding the osteocytic process as in earlier models (Fig. 5-1b, Weinbaum et al., 1994), with the channel assumed to be filled with a pericellular gel-like matrix. A recent electron microscopic study has provided strong evidence of the existence of such a fiber matrix (You et al., 2002). The mineralized matrix surrounding the lacunar-canalicular porosity has a Young's modulus

Reproduced with permission of the copyright owner. Further reproduction prohibited without permission.

E, and bone permeability at the lacunar-canalicular porosity level is theoretically determined by the detailed structures of the pericellular fiber matrix and the canalicular channels, since there are no experimental measurements to date (Weinbaum et al., 1994; Cowin et al., 1995). The characteristic relaxation time for pore fluid pressure τ_r is roughly inversely proportional to bone permeability, but it is a structural property and not a material property (Weinbaum et al., 1994; Cowin et al., 1995).

The osteon is subjected to two types of oscillatory loading. The first oscillatory loading is a cyclic applied axial stress with an amplitude σ_o and an applied circular frequency ω ($\sigma = -\sigma_o \sin \omega t$). The second oscillatory loading is due to the local blood pressure and is implemented by a boundary condition at the osteonal canal surface ($r = r_i$) that requires that extravascular fluid pressure be equal to the intramedullary pressure. The local extravascular fluid pressure is represented by $p = p_b \sin(\Omega t + \psi) + p_0$ where p_0 is the mean pressure (DC component); the sinusoidal term is the fluctuation of the fluid pressure due to pulsatile blood pressure or pulse pressure caused by cardiac contraction (Brookes and Revell, 1998; Ficat and Arlet, 1980). The interstitial fluid flow driven by this pulse hydraulic pressure is called the blood pressure-driven fluid flow in the following text, because the driving force is produced due to the blood circulation. The amplitude of the pulsatile fluid pressure is denoted by p_b, its angular frequency by Ω (i.e., the heart rate), and its phase angle ψ with respect to the applied axial loading. Due to the relative impermeability of the outer boundary (cement line) of the osteon, a non-leakage boundary condition is assumed as in our previous models (Zeng et al., 1994; Wang et al., 2000).

Reproduced with permission of the copyright owner. Further reproduction prohibited without permission.

The fluid pore pressure, radial fluid pressure gradient, and shear stress are derived in the next three sections using poroelasticity theory. To facilitate the comparison of the relative contribution of mechanical loading and pulsatile blood pressure to the interstitial fluid flow, we decompose the fluid pore pressure, radial fluid pressure gradient, and shear stress into the mechanical load- and blood pressure-induced components. The parameters associated with the load-induced component are notated with a subscript *l* and those associated with blood pressure-induced component are notated with a subscript *b*.

Bone Fluid Pressure

A closely related problem was solved by Zeng et al. (1994) where an osteon was subjected to an axial cyclic stress alone. Zeng et al. (1994) employed a boundary condition that requires the fluid pore pressure to vanish at the canal surface ($p = 0$ at $r = r_i$). The problem considered here replaces that boundary condition with one that requires that the bone fluid pore pressure equals the blood pressure, $p = p_b \sin(\Omega t + \psi) + p_0$, at the canal surface ($r = r_i$). The partial differential equation in cylindrical coordinates for the dimensionless bone fluid pressure P is

$$\frac{\partial^2 P}{\partial R^2} + \frac{1}{R}\frac{\partial P}{\partial R} + \frac{1}{R^2}\frac{\partial^2 P}{\partial \theta^2} - \frac{\partial P}{\partial \tau} = -\cos T\tau . \tag{1}$$

where R is a dimensionless radial coordinate, θ is the cylindrical coordinate and τ is a dimensionless time given by $\tau = t/\tau_r$ where τ_r is the characteristic relaxation time of the pore fluid pressure via the lacunar-canalicular porosity in the osteon (Zeng et al., 1994). The non-dimensional variables R, R_i, T, W and P are defined as

$$R = \frac{r}{ro}, R_i = \frac{r_i}{ro}, T = \omega\tau_r, W = \frac{\Omega}{\omega}, P = \frac{3p}{\sigma_0 BT}, \tag{2}$$

Reproduced with permission of the copyright owner. Further reproduction prohibited without permission.

where r is the radial coordinate, r_o is the radius of the cement line, r_i is the radius of the osteonal canal, W is the ratio of the frequency of the pulsatile blood pressure and the mechanical loading, and B is the Skempton pore pressure coefficient that represents the relative compressibility of the fluid and solid phases of the porous bone matrix (Cowin, 1999; Zhang et al., 1998). The boundary conditions due to the blood pressure, expressed in terms of the dimensionless pressure field P, are

$$P = \frac{3}{\sigma_0 BT}(p_b \sin(WT\tau + \psi) + p_0) \text{ at } R = R_i, \text{ and } \partial P/\partial R = 0 \text{ at } R = 1. \tag{3}$$

When $p_b = 0$ these boundary conditions reduce to those of Zeng et al. (1994). The solution to Eq. 1 subject to the above boundary conditions is obtained as follows (the detailed derivation is given in the Appendix):

$$P(R,\tau) = \frac{1}{T}\mathrm{Re}\{ie^{iT\tau}\frac{J(R,T)}{J(R_i,T)}\} + \frac{1}{T}\sin(T\tau) + \frac{3p_b}{\sigma_0 B}\cdot\frac{1}{T}\mathrm{Re}\{ie^{i(WT\tau-\psi)}\frac{J(R,WT)}{J(R_i,WT)}\} + \frac{3p_0}{\sigma_0 B}\cdot\frac{1}{T}, \tag{4}$$

where Re is the real part, $J(R,T)$ is given by

$$J(R,T) = I_0(\sqrt{iT}R)K_1(\sqrt{iT}) + I_1(\sqrt{iT})K_0(\sqrt{iT}R), \tag{5}$$

and I_o, K_o, I_1, and K_1 are modified Bessel functions of the first and second kind. In order to obtain the fluid pore pressure from the dimensionless fluid pressure, we multiply a factor of $\sigma_0 BT/3$ to both sides of Eq. 4, substitute ωt for $T\tau$ and Ωt for $WT\tau$ and then rewrite the complex functions using real-valued functions. The fluid pore pressure p is then as follows:

$$p = \frac{B\sigma_0}{3}(U_1\cos\omega t - (V_1 - 1)\sin\omega t) + p_b(U_b\cos\Omega t - V_b\sin\Omega t) + p_0 \tag{6}$$

where U_1, V_1, U_b, V_b are real-valued functions defined as follows:

Reproduced with permission of the copyright owner. Further reproduction prohibited without permission.

$$U_l + iV_l = \frac{iJ(R,T)}{J(R_i,T)}; U_b + iV_b = \frac{iJ(R,WT)}{J(R_i,WT)} \quad . \tag{7}$$

Combining the sinusoidal terms with the same frequency, the fluid pore pressure is the summation of three terms:

$$p = A_l \sigma_0 \sin(\omega t + \phi_1) + A_b p_b \sin(\Omega t + \phi_2) + p_0 \tag{8}$$

where the coefficients and phases (A_l ϕ_l, A_b, ϕ_2) associated with the two sinusoidal components are

$$A_l = \frac{B}{3}\sqrt{U_l^2 + (V_l - 1)^2}, \phi_1 = -\tan^{-1}(\frac{U_l}{V_l - 1}), A_b = \sqrt{U_b^2 + V_b^2}, \phi_2 = -\tan^{-1}(\frac{U_b}{V_b}). \tag{9}$$

The first sinusoidal term with the frequency of the mechanical loading ω is caused by mechanical loading; the second sinusoidal term with the frequency of blood pressure Ω and the constant term are caused by the blood pressure. We will show next that the mean blood pressure p_0 makes no contribution to the fluid pressure gradient or shear stress. Therefore, we are going to neglect this DC component and, instead, focus on the time-varying (AC) component (pulsatile blood pressure) only. The amplitudes of the load and blood-induced fluid pressure components are

$$p_l^{amp} = A_l \sigma_0, \; p_b^{amp} = A_b p_b \tag{10}$$

where A_l and A_b are functions of spatial position (R) and frequency of the driving forces (see Eqs. 7, 9).

Fluid Pressure Gradient

The dimensionless fluid pressure gradient (i.e., the rate of pressure change in the radial direction) is readily derived from Eq. 4. The fluid pressure gradient is obtained from the dimensionless expression as

Reproduced with permission of the copyright owner. Further reproduction prohibited without permission.

$$\frac{\partial p}{\partial r} = \frac{B\sigma_0}{3r_0}(U_l' \cos\omega t - V_l' \sin\omega t) + \frac{p_b}{r_0}(U_b' \cos\Omega t - V_b' \sin\Omega t), \quad (11)$$

where U_l', V_l', U_b', V_b' are real-valued functions defined as follows:

$$U_l' + iV_l' = \frac{iJ'(R,T)}{J(R_i,T)}; U_b' + iV_b' = \frac{iJ'(R,WT)}{J(R_i,WT)}$$

(12)

and

$$J'(R,T) = \sqrt{iT}[I_1(\sqrt{iT}R)K_1(\sqrt{iT}) - I_1(\sqrt{iT})K_1(\sqrt{iT}R)]. \quad (13)$$

Combining the sinusoidal terms with the same frequency, the fluid pressure gradient consists of two sinusoidal components caused by the mechanical loading and pulsatile blood pressure, respectively:

$$\frac{\partial p}{\partial r} = A_l' \sigma_0 \sin(\omega t + \phi_3) + A_b' p_b \sin(\Omega t + \phi_4), \quad (14)$$

where the coefficients and phases (A_l', ϕ_3, A_b', ϕ_4) associated with the two sinusoidal components are

$$A_l' = \frac{B}{3r_0}\sqrt{U_l'^2 + V_l'^2}, \phi_3 = -\tan^{-1}(\frac{U_l'}{V_l'}), A_b' = \frac{1}{r_0}\sqrt{U_b'^2 + V_b'^2}, \phi_4 = -\tan^{-1}(\frac{U_b'}{V_b'}). \quad (15)$$

The first sinusoidal term is the load-induced component with the loading frequency ω; the second term is the blood pressure-induced pressure gradient component with the frequency of Ω. Their amplitudes are

$$\left(\frac{\partial p}{\partial r}\right)_l^{amp} = A_l'\sigma_0, \left(\frac{\partial p}{\partial r}\right)_b^{amp} = A_b' p_b \quad (16)$$

where A_l' and A_b' are functions of spatial position (R) and frequencies of the driving forces (see Eqs. 12, 13, 15).

Reproduced with permission of the copyright owner. Further reproduction prohibited without permission.

Shear Stress

Previous models have shown that the shear stress s(a) experienced by an osteocytic cell process of radius a in a canaliculus is directly proportional to the bone fluid pressure gradient and is also related to the detailed structure of the canalicular channel and the pericellular matrix (Weinbaum et al., 1994; Zeng et al., 1994), as shown below:

$$s(a) = \frac{\partial p}{\partial r}\frac{b}{\gamma}(A_1 I_1(\gamma/q) - B_1 K_1(\gamma/q)) \tag{17}$$

$$A_1 = \frac{k_0(\gamma) - k_0(\gamma/q)}{I_0(\gamma/q)k_0(\gamma) - I_0(\gamma)k_0(\gamma/q)}, B_1 = \frac{I_0(\gamma/q) - I_0(\gamma)}{I_0(\gamma/q)k_0(\gamma) - I_0(\gamma)k_0(\gamma/q)}, \tag{18}$$

where b is the canalicular wall radius, Δ is the fiber spacing, q is the ratio of the canalicular wall radius to the radius of the cell process ($q = b/a$), and γ is the non-dimensional ratio $\gamma = b/\Delta$ (Weinbaum et al., 1994; Zeng et al., 1994).

Since the load- and blood-induced radial fluid pressure gradients are sinusoidal (Eq. 14), their induced fluid shear stresses on the osteocytic process are also sinusoidal with the following amplitudes:

$$s(a)_l^{amp} = \frac{A_l' \sigma_0 b}{\gamma}(A_1 I_1(\gamma/q) - B_1 K_1(\gamma/q)), \tag{19a}$$

$$s(a)_b^{amp} = \frac{A_b' p_b b}{\gamma}(A_1 I_1(\gamma/q) - B_1 K_1(\gamma/q)). \tag{19b}$$

Parameter values

The osteon we model here has a canal radius $r_i = 20$ μm and a cement line radius $r_o =$ 100 μm (Zeng et al., 1994; Cooper et al., 1966), giving a dimensionless $R_i = 0.20$. The

Reproduced with permission of the copyright owner. Further reproduction prohibited without permission.

dimensionless coordinate $R = 0.2 \rightarrow 1$ thus represents the bone annulus of the osteon. The relative compressibility between the fluid and solid phases B is taken to be 0.43 (Zhang et al., 1998). Most venous stasis experiments used young animals, thus we employ a Young's modulus for young bone, $E = 10$ GPa (Torzilli et al., 1982). Unless indicated otherwise, the following geometric data will be employed: the canaliculus has an outer radius $b = 0.2$ μm, an osteocytic cell process radius $a = 0.1$ μm, giving $q = b/a = 2$. The fiber spacing Δ is chosen to be 7 nm as used in Zeng et al. (1994).

The spatial distribution profiles of the pore fluid pressure, pressure gradients, and resultant fluid shear stress on the osteocytic process membrane induced by the mechanical loading and pulsatile blood pressure are calculated using Eqs. 10, 16, and 19. For mechanical loading two fundamental strains are considered: one strain has a magnitude of 100 microstrain and a frequency of 1 Hz and is associated with slow locomotion and the other has a smaller magnitude (10 microstrain) and a higher frequency (20 Hz) and is associated with maintaining posture (Rubin et al., 2001). For pulsatile extravascular pressure that equals the intramedullary pressure, two cases are considered: one is associated with normal cardiac contractions and has a magnitude of 10 mm Hg (1.33 kPa) (Brookes and Revell, 1998) and a frequency of 2 Hz (2 Hz is the heart rate for big laboratory animals such as the dog and goat (Lawson, 2000); and the other is associated with muscle contraction with an increased amplitude of 30 mmHg (3.99 kPa) and a lower frequency of 1 Hz (Shim et al., 1972; Ficat and Arlet, 1980).

Since loading frequency has been found to affect the resultant shear stress significantly (Zeng et al., 1994), the peak shear stress induced by either the mechanical loading or the pulsatile blood pressure is evaluated as a function of loading or pulse

Reproduced with permission of the copyright owner. Further reproduction prohibited without permission.

frequency. The amplitudes of the mechanical loading and the pulsatile blood pressure are assumed to remain the same, 100 microstrain and 10 mm Hg, respectively, while their frequencies are varied from 1 to 20 Hz. These numerical values are chosen parametrically in order to study the frequency response of the shear stress. We understand that the in vivo pulsatile blood pressure is unlikely to have a frequency higher than 10 Hz (Lawson, 2000) and the high-frequency mechanical strains usually have decreased amplitudes (Fritton et al., 2000).

To evaluate the osteogenic effect for different loading or blood pressure conditions, we define an index called the relative osteogenic capacity, which is calculated using the peak shear stress induced by the individual loading and dividing it by the peak shear stress produced by the locomotion strain (100 microstrain and 1 Hz), which we (arbitrarily) consider here to be 100% osteogenic capacity.

Since the magnitude of the peak shear stress induced by the mechanical loading and pulsatile blood pressure varies with the numerical values of the input parameters used in the model, a parametric study is performed to show the sensitivity of the output (shear stress) to the inputs of the model. Among the many input parameters we used, bone permeability has the most significant effect on the shear stress (Zhang et al., 1998; Wang et al., 1999). Since the bone permeability is estimated from the fiber spacing of the pericellular matrix and the fluid space the canalicular channels (Weinbaum et al., 1994; Cowin et al., 1995), shear stress is evaluated for a fiber spacing ranging from 4 to 10 nm and a fluid annular spacing ranging from 50 to 150 nm.

Results

Reproduced with permission of the copyright owner. Further reproduction prohibited without permission.

The total fluid flow is a linear summation of the load- and blood pressure-induced components. Since both the mechanical loading and the pulsatile blood pressure are modeled as temporal sinusoidal signals, the fluid flow induced by the two driving forces is also sinusoidal in the time domain. The amplitudes of the sinusoidal interstitial fluid pressure and shear stress applied on the cell membrane vary with location and depend on the frequency of the driving force (Figs. 5-2 and 5-3).

The amplitude of load-induced fluid pore pressure increases radially from the canal to the cement line and increases with increased loading frequency (Fig. 5-2a). For a mechanical loading with a given magnitude, the induced fluid pressure is much higher at 20 Hz than at 1 Hz (Fig. 5-2a). At lower loading frequencies the load-induced fluid flow has enough time to relax across the osteon and thus it is difficult for the fluid pressure to build up. At higher loading frequencies the time period available for fluid relaxation is shorter and an excess fluid pressure can therefore be produced. This result is consistent with our previous studies (Weinbaum et al., 1994; Cowin et al., 1995; Wang et al., 1999).

On the other hand, the amplitude of blood pressure-induced fluid pore pressure decreases both across the osteon radius and with increasing frequency of the pulsatile blood pressure (Fig. 5-2b). At 1 Hz, the pulsatile pressure within the osteonal canal can propagate to the whole osteon nearly uniformly with less than 5% decay in magnitude. At 20 Hz, the pulsatile pressure decreases rapidly at locations further away from the osteonal canal. In fact the amplitude of pulsatile fluid pressure at the cement line is only 50% of that in the canal. This model also predicts that a mean blood pressure in the central canal will cause a uniform pore pressure distribution across the osteon (Eq. 6).

Both the load- and blood-induced fluid flows have the same spatial distribution pattern of the fluid pressure gradients (and resulting shear stress) (Fig. 5-3) despite the

Reproduced with permission of the copyright owner. Further reproduction prohibited without permission.

apparent different appearance of the fluid pressure profiles (Fig. 5-2). The largest pressure gradients (and peak shear stresses) are found at the osteonal canal wall surface ($R = R_l$) and the pressure gradients (shear stresses) diminish at the cement line ($R = 1$) (Fig. 5-3). Two typical mechanical loading conditions, 100 microstrain at 1 Hz associated with locomotion and 10 microstrain at 20 Hz associated with posture, produce shear stress of the same approximate magnitude (Fig. 5-3). If the magnitude of the mechanical loading or blood pressure is held constant, the peak shear stress at the canal wall surface exhibits a 15-fold increase as the frequency increases from 1 to 20 Hz (Table 5-1).

In general, the peak shear stress acting on the osteocyte process induced by pulsatile blood pressure is at least two orders of magnitude smaller than that induced by physiological mechanical loading (Tables 5-1 and 5-2). The normal pulse pressure (10 mm Hg at 2 Hz) and the raised blood pressure due to muscle contraction (30 mm Hg at 1 Hz) have only 2% and 3% relative osteogenic capacity, respectively, if a 100% relative osteogenic capacity is assigned for a mechanical loading due to locomotion (100 microstrain at 1 Hz).

The peak shear stress induced by the normal pulse blood pressure is predicted to vary with bone permeability (Table 5-3). When the fiber spacing is varied from 4 to 20 nm and the fluid annulus is changed by a factor of 3, bone permeability varies over 2 orders of magnitude and the peak shear stress calculated from this model varies by a factor of ten. The peak shear stress induced by mechanical loading has the same sensitivity to the model parameters as that induced by pulsatile blood pressure shown in Table 5-3.

Discussion

Reproduced with permission of the copyright owner. Further reproduction prohibited without permission.

We have expanded the poroelastic model for bone interstitial fluid flow (Zeng et al., 1994) to the situation in which fluid flow in an osteon is driven by the pulsatile blood flow in the bone microvasculature as well as by the applied cyclic mechanical loading. This is the first model to provide a quantitative tool to investigate the relative osteogenic effect of blood flow and mechanical loading in terms of shear stress induced by the bone fluid flowing over the osteocytic cell process membrane.

Shear stresses induced by the pulsatile blood pressure do not seem to be osteogenic. If the cement line is assumed to be impermeable, the mean blood pressure cannot produce any fluid flow in the mineralized matrix (Eq.11) in the present model. The driving force for the shear stress, and thus osteocyte excitation, is the amplitude of the pulsatile blood pressure (pulse pressure, the AC component), not the mean blood pressure (the DC component). The induced shear stress is 0.3 dyn/cm^{2}under "normal conditions" consisting of a pulse pressure of about 10 mm Hg (Ficat and Arlet, 1980) and a heart rate of 1-2 Hz for human and big laboratory animals such as the dog and goat (Lawson, 2000). For a smaller animal, such as a rat, the shear stress is ~0.75 dyn/cm^2 if we assume a pulse pressure of about 10 mm Hg and a heart rate of about 5-6 Hz (Lawson, 2000) (Table 5-1). Numerous studies have shown that bone cells only respond to shear stress larger than 5 dyn/cm^2 (Reich et al., 1990; Hung et al., 1995; Klein-Nulend et al., 1995; Ajubi et al., 1996; Johnson et al., 1996; Cheng et al., 2001). The magnitudes of the shear stresses induced by the blood circulation are less than the magnitude of the shear stress necessary for osteocytic cell excitation.

Results from this idealized osteon model, using the parameters employed, do not support the hypothesis that an increased interstitial fluid flow or streaming potential would account for the increased periosteal bone growth due to venous stasis. Although

Reproduced with permission of the copyright owner. Further reproduction prohibited without permission.

the mean intramedullary pressure is increased several-fold compared to controls (Kelly and Bronk, 1990; Bergula et al., 1999; Welch et al., 1993), the amplitude of the pulsatile blood pressure decreases in the condition of venous congestion (Stein et al., 1957; Shim et al., 1972; Ficat and Arlet, 1980). Although there are multiple vessels draining a long bone (Brookes and Revell, 1998), once one big vein (e.g., femoral vein or nutrient vein) is ligated, or the muscle veins draining bone are compressed using tourniquets, the ability of the system to drain the blood is compromised. More blood is kept in the organ and is rerouted to the rest functioning vessels. Those vessels have to expand their size to accommodate the increasing volume of blood and raise the vascular pressure as a result. Due to the leakage of the vessel wall, the increased infiltration flux will raise the extravascular pressure because bone is a relatively tight compartment. This raised extravascular pressure counteracts with the vascular pressure and a new equilibrating steady state is achieved quickly within a minute (Welch et al., 1993). Since now the vessel wall is stretched and becomes stiffer, the pulsatile vascular pressure induced by cardiac contraction drops or disappears. The pulse pressure of the intramedullary pressure was found to be dramatically decreased in venous stasis (Ficat and Arlet, 1980). According to this model, an even smaller shear stress can be produced on the osteocytic membrane due to the blood circulation in venous stasis compared to normal conditions, suggesting it is even more unlikely to be osteogenic.

In addition to the increased interstitial fluid flow, increased filtration across the capillary wall is also proposed to induce interstitial fluid flow or streaming potentials, which could account for periosteal bone growth (Kelly and Bronk, 1990; Bronk et al., 1993). This transcapillary flux is not included in the present model. The transcapillary fluid movement follows Starling's law, $J_A = L_A\{(P_c - P_i) - \sigma(\Pi_c - \Pi_i)\}$, which says that

Reproduced with permission of the copyright owner. Further reproduction prohibited without permission.

the filtration rate J_A is determined by the hydraulic pressure difference between the capillary P_c and the surrounding tissue P_i as well as the osmotic pressure difference between the tissue Π_i and the capillary Π_c. The two coefficients L_A and σ represent the fluid conductivity and reflection of the capillary wall, respectively. From Starling's law, an increased hydraulic pressure in the capillary P_c does not necessarily increase the transcapillary flux as suggested in Kelly et al. (1990). The sustained time of this flux has been shown to be very short (within a minute, Welch et al., 1993), because bone is such an incompliant compartment and there are no lymphatic pathways in bone (Anderson, 1960; Bazantova, 1989). Therefore, transcapillary flux in venous stasis is unlikely to produce interstitial fluid flows or streaming potentials in the lacunar-canalicular porosity for osteocyte excitation..

One may ask then which signal triggers the periosteal response to venous congestion? If we look at all the factors secondary to venous stasis, one pronounced phenomenon is the sustained high intramedullary pressure compared to controls (40 vs. 12 mm Hg in the dog, Kelly and Bronk, 1990; 29 vs. 16 mm Hg in the goat, Welch et al., 1993; 28 vs. 16 mm Hg in the rat, Bergula et al., 1999). We also note that the periosteum, a dense fibrous layer containing fibroblasts and precursor cells of chondrocytes, covers the external surface of a whole bone as an impermeable seal due to its relatively low permeability compared to the mineralized matrix (Rouhana et al., 1981; Li et al., 1987; Grimm and Williams, 1997). Therefore, in venous stasis the increased intramedullary pressure is applied directly to the interior face of the periosteum and stretches the periosteum in a way similar to the way high-pressured air inside a balloon stretches the skin of the balloon. The pressurization and stretching of the periosteum due to the raised intramedullary pressure may be the signal to trigger the cellular activity that results in

Reproduced with permission of the copyright owner. Further reproduction prohibited without permission.

periosteal bone growth. The periosteum has been shown to produce woven bone under direct pressurization in four-point bending experiments in vivo (Turner et al., 1991). Rapid increase of periosteal gene expression (protooncogene c-fos, insulin-like growth factor I (IGF-I), transforming growth factor-beta (TGF-beta), and collagen type I) under mechanical forces has been found experimentally, suggesting that the acute periosteal response to external mechanical loading is a change in the pattern of gene expression, which may signal cell proliferation (Zaman et al., 1992; Raab-Cullen et al., 1994). In addition, periosteal explants have been shown to respond to immersion in a low fluid pressure (100 mm Hg) bath, but not a high-pressure (800 mm Hg) bath by proliferating in vitro both short-term (3 days, Saris et al., 1999) and long-term (28 days, Mukherjee et al., 2001).

Based on the above analysis and experimental evidence, we postulate that the high intramedullary pressure applied to the periosteum due to the sustained increased blood pressure in venous stasis may cause the increased periosteal new bone growth. In venous stasis, the intramedullary pressure is increased up to 40 mm Hg, which is not far away from the pressure level (100 mm Hg) that has been shown to cause periosteal response in vitro (Saris et al., 1999; Mukherjee et al., 2001). Compared to transcapillary influx that may be short-lived, the high intramedullary pressure can be sustained up to 42 days (Kelly and Bronk, 1990). The elevated pressure on the periosteum may regulate related gene expression (Raab-Cullen et al., 1994), or change mass transport of these genes or other metabolic factors within the periosteum.

The present model provides useful insights into the periosteal bone growth in venous stasis. However, as an idealized model, it has several limitations. The first is that, since bone permeability is usually measured at the vascular porosity level and not at the

Reproduced with permission of the copyright owner. Further reproduction prohibited without permission.

lacunar-canalicular porosity level (Rouhana et al., 1981; Li et al., 1987; Grimm and Williams, 1997), we have calculated the lacunar-canalicular porosity permeability based on an assumed pericellular matrix in an idealized canalicular channel. We have shown that the parameters associated with the fiber matrix and the canalicular geometry would change the numerical value of the induced shear stress accordingly. However, the conclusion that the blood pressure produces much smaller shear stress is valid for the whole range of the parameter changes. The second limitation is that the cement line is assumed to be impermeable, which may not be the case in vivo. Results from one of our previous studies (Wang et al., 1999) shows that the permeability of the cement line has little effect on the local fluid pressure profile around the osteonal canal, suggesting the peak shear stress at the canal wall surface in vivo would not be significantly different from the current analysis. The third limitation is that the mechanical loading and pulsatile blood pressure are simplified as sinusoidal signals while in vivo they have much more complicated waveforms. As the model is a linear system, the fluid flow induced by mechanical loading or blood pressure of any arbitrary waveform can be decomposed into the summation of the fluid flows induced by a series of sinusoidal signals. We also only consider two typical mechanical strains, one associated with locomotion (100 microstrain at 1 Hz) and one associated with posture (10 microstrain at 20 Hz). We appreciate that the mechanical strains that a bone experiences in vivo have varied frequencies and magnitudes, depending on the species and age of the animal and locations of the strain recording (Fritton et al., 2000; Fritton and Rubin, 2001). In the present model we chose a relatively low locomotion strain (100 microstrain) to represent walking and a higher strain (e.g., 1000 microstrain) would have shown an even lower contribution of blood pressure to shear stress.

Reproduced with permission of the copyright owner. Further reproduction prohibited without permission.

The fourth limitation is that we assume the osteocytes sense the external loading via shearing stress on the osteocytic process membrane and the relative osteogenic capacity is calculated using the peak shear stress induced by the mechanical loading and the blood pressure. However multiple signaling pathways may be involved in osteogenesis. In a recent study, You et al. (2001) propose that the drag force induced by mechanical loading deforms the transverse fibrils of the pericellular matrix and then induces a hoop strain on the intracellular actin cytoskeleton. Since the hoop strain of the cytoskeleton and the shear stress on the osteocytic process are both secondary to the interstitial fluid flow, we should get a similar estimation of the relative osteogenic capacity for a given mechanical strain or blood pressure, no matter whether the shear stress or hoop strain is used for the calculation, because the shear stress is proportional to the drag force and the relationship between the drag force and hoop strain is not strictly linear but can be reasonably approximated to be linear (You et al., 2001).

In the present model, the extravascular fluid pressure inside the osteonal canal is assumed to be equal to the intramedullary pressure reported in the literature (i.e., mean value that is less than 100 mm Hg, pulsatile ~10 mmHg, frequency 1-6 Hz (Ficat and Arlet, 1980)). We argue above that, due to the high permeability of the vascular porosity in bone, the steady extravascular fluid pressure in an osteon will equal the intramedullary pressure. However, because of the intrusive recording methods of intramedullary pressure (Stein et al., 1957; Azuma, 1964; Arnoldi et al., 1971; Shim et al., 1972; Wilkes and Visscher, 1975; Tondevold, 1983; Bergula et al., 1999; Zachos et al., 2001) and the heterogeneity of the intramedullary tissue including minute and numerous venous sinuses, arterioles, and venules, the intramedullary pressure recording may not be the tissue pressure, but the pressure of an artificial blood pool surrounding the recording tip instead.

Reproduced with permission of the copyright owner. Further reproduction prohibited without permission.

Therefore, it is not surprising that the intramedullary pressure recording shows very large variations depending on the local vasculature and the degree of the damage (Ficat and Arlet, 1980). Despite the big variation, most of the recordings of the pulsatile and mean intramedullary pressure fall in the range of 4-30 mm Hg and 10-100 mm Hg, respectively, in long bones for human and larger laboratory animals such as the dog, goat, cat, and rabbit in normal conditions (Ficat and Arlet, 1980).

In summary, in order to evaluate the osteogenic effect of blood pressure, we have expanded our previous poroelastic models to assess quantitatively the relative contribution of two driving forces (mechanical loading and blood pressure) to interstitial fluid flow. Our results suggest that mechanical loading is the major contributor to shear stress that acts on the osteocytic process membrane. We conclude that the dynamic component of the blood pressure has a very limited effect on bone cells in terms of shear stress excitation. As to the periosteal bone growth in venous stasis, the present model suggests that the dynamic component of the blood pressure-induced interstitial fluid flow and transcapillary flux are unlikely to be osteogenic. The metabolic changes due to venous congestion, such as oxygen tension, carbon dioxide tension, and local pH value, may cause the periosteal response. Finally, we suggest that the extravascular fluid pressure, due to the mean blood pressure rather than its dynamic component, may account for the periosteal new bone growth.

Acknowledgments

We are indebted to Dr. Howard Winet for discussions on the subject of this paper and for bringing the work of Ficat and Arlet, (1980) to our attention. This work was supported by NIH grant AR46429

Reproduced with permission of the copyright owner. Further reproduction prohibited without permission.

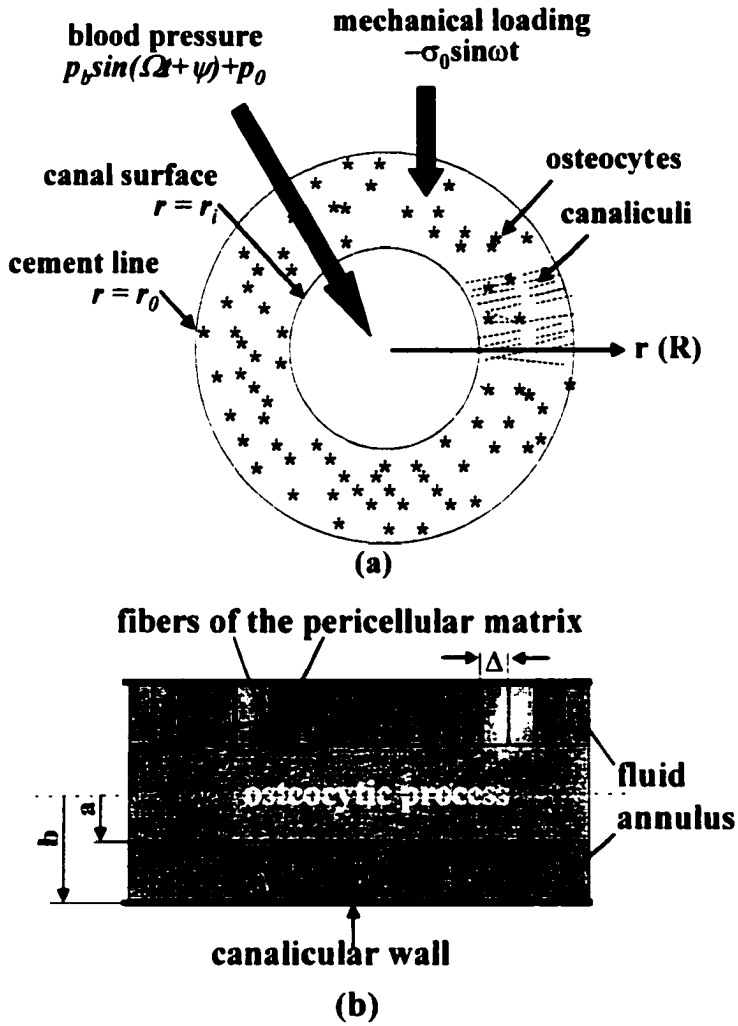

Fig. 5-1. (a) A cross-section of an osteon with an outer radius r_i and an inner radius r_o. A cyclic mechanical loading with a uniform stress $\sigma = -\sigma_0 \sin\omega t$ is applied axially to the osteon. At the interior surface, the fluid pressure is assumed to be the blood pressure ($p = p_b \sin(\Omega t + \psi) + p_0$), while the boundary condition at the cement line (the outer surface) is that of no leakage of bone fluid ($\partial p/\partial r = 0$). Osteocytes encased in the mineralized matrix are linked together with each other and with the central canal via the canalicular channels. (b) A schematic model of a longitudinal cross-section of a canaliculus. The osteocytic process is located in the center of the canaliculus. A pericellular fiber matrix fills the fluid space between the cell process (radius a) and the canalicular wall (radius b). The spacing between the fibers is Δ. The lacunar-canalicular porosity permeability is calculated from these structural parameters and the interstitial fluid pressure within the osteon is calculated using poroelasticity theory.

Reproduced with permission of the copyright owner. Further reproduction prohibited without permission.

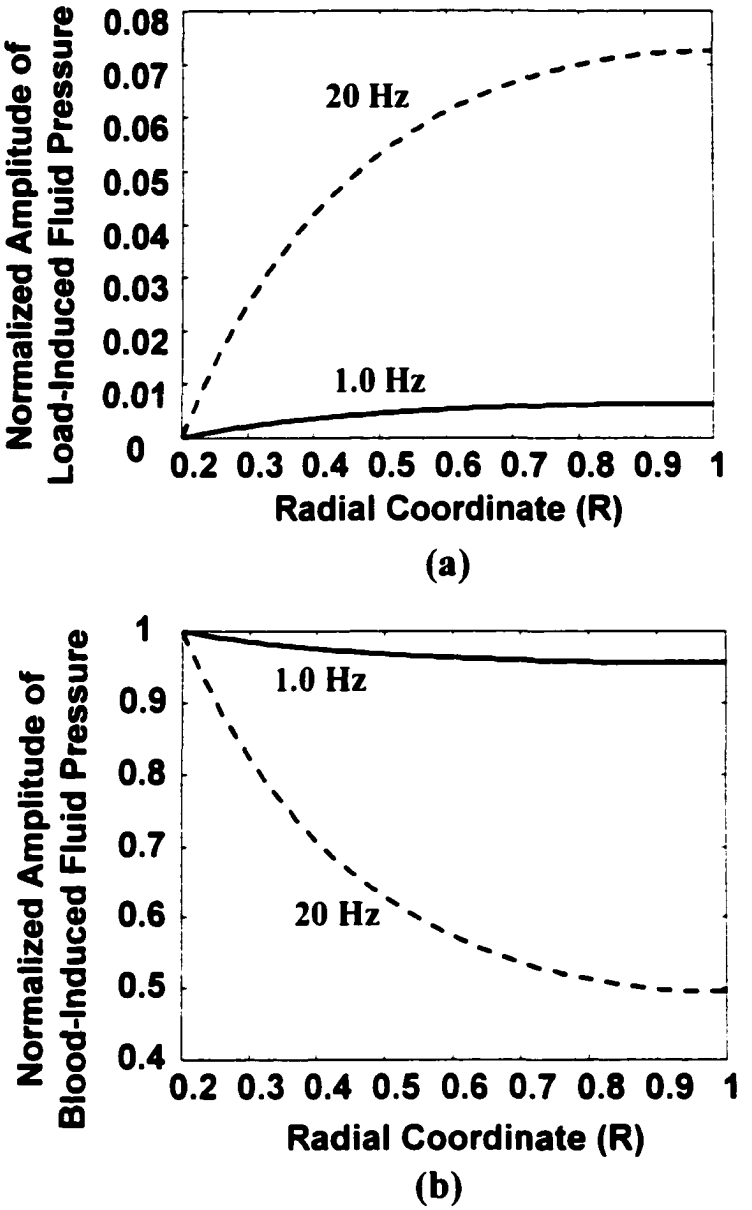

Fig. 5-2. The spatial distribution profiles of the interstitial fluid pressure in the radial coordinate from the canal surface (R = 0.2) to the cement line (R = 1) depend on the type of the loading (mechanical or blood pressure) and the loading frequency. (a) The normalized amplitude of the fluid pressure induced by mechanical loading (p_l^{amp}/σ_0) increases radially from the canal to the cement line. The induced fluid pressure is much higher at 20 Hz than at 1 Hz across the osteon. (b) The normalized amplitude of the blood pressure-induced fluid pressure (p_b^{amp}/p_b) decreases both across the osteon radius and with increasing frequency of the pulsatile blood pressure. At 1 Hz, the pulsatile pressure within the osteonal canal can propagate to the whole osteon nearly uniformly with less than 5% decay in magnitude. At 20 Hz, the pulsatile pressure decreased rapidly as the location is further away from the canal. The amplitude of the pulsatile pressure at the cement line is only 50% of that in the canal.

Reproduced with permission of the copyright owner. Further reproduction prohibited without permission.

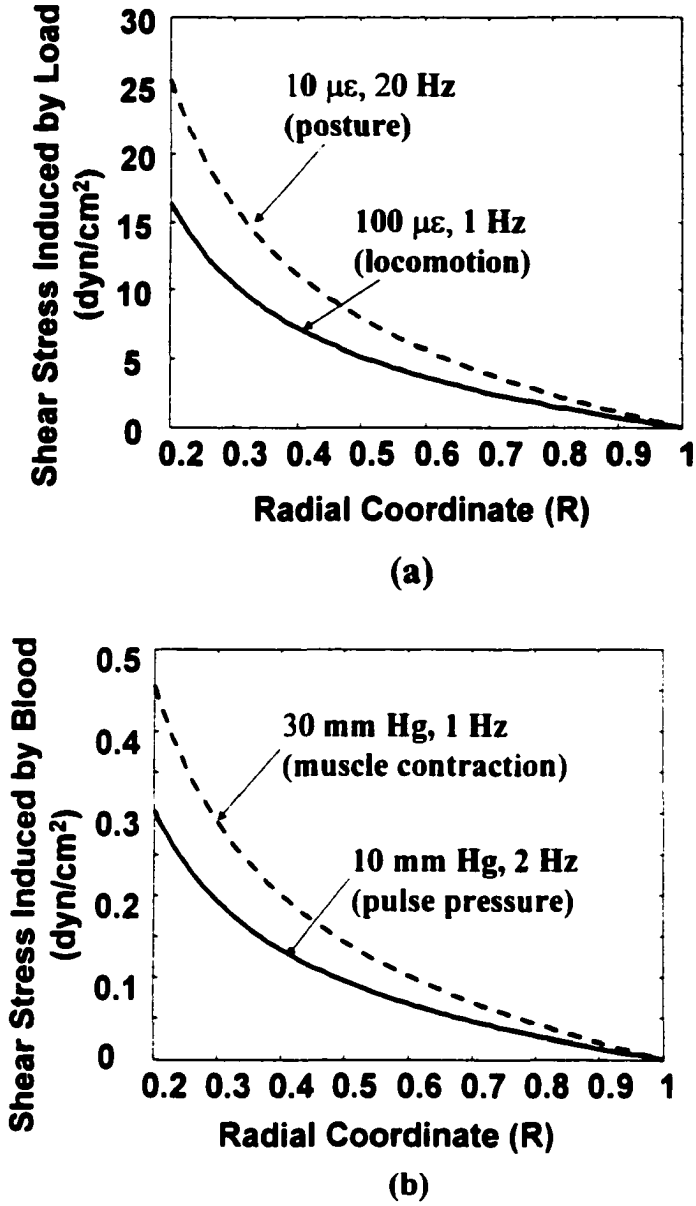

Fig. 5-3. The spatial distribution of the shear stress on the osteocytic process membrane induced by (a) mechanical loading and (b) pulsatile blood pressure. Since the fluid pressure gradients are proportional to shear stress, the spatial distribution of the fluid pressure gradients has the same pattern (profile) as shown here. Two typical mechanical strains are considered; one is related to locomotion (100 microstrain at 1 Hz) and the other is associated with posture (10 microstrain at 20 Hz). The two blood pressures considered are a normal pulse pressure due to the heart beat (10 mm Hg at 2 Hz), and an increased blood pressure induced by repeated muscle contraction and release (30 mm Hg at 1 Hz). The peak shear stresses and the fluid pressure gradients induced by both mechanical loading and blood pressure are located at the inner canal surface of the osteon.

Reproduced with permission of the copyright owner. Further reproduction prohibited without permission.

Table 5-1: Peak shear stress induced by cyclic mechanical loading and blood pressure[a]

Frequency	1 Hz	2 Hz	5 Hz	10 Hz	20 Hz
load: 100 με	16.	32.	80.	150	250
blood: 10 mm Hg	0.15	0.30	0.75	1.4	2.4

[a]The peak value of shear stress (in dyn/cm^2) occurs at the osteonal canal surface at different frequencies. The ratio between the shear stress induced by the mechanical loading (100 microstrain (με)) and the pulsatile blood pressure (10 mm Hg) is ~109 for all the frequencies.

Table 5-2: Relative osteogenic capacity for different loading conditions[a]

Loading conditions	Locomotion (100 με,1 Hz)	Posture (10 με, 20Hz)	Pulse blood pressure (10 mmHg, 2 Hz)	Raised blood pressure by muscle contraction (30 mm Hg, 1 Hz)
Shear stress (dyn/cm^2)	16.4	25.4	0.30	0.45
Relative osteogenic capacity	100%	155%	2%	3%

[a]The relative osteogenic capacity in terms of peak shear stress at the osteonal canal surface that the individual loading condition can produce. The osteogenic capacity of locomotion is assumed to be 100% as a reference and other loading conditions are compared to this loading. (με represents microstrain).

Reproduced with permission of the copyright owner. Further reproduction prohibited without permission.

Table 5-3: Sensitivity of shear stress to model parameters[a]

Frequency	1 Hz	2 Hz	5 Hz	10 Hz	20 Hz
Δ = 4 nm	0.24	0.48	1.1	1.6	2.00
Δ = 7 nm	0.15	0.30	0.75	1.4	2.4
Δ = 20 nm	0.08	0.16	0.39	0.79	1.6
b-a = 50 nm	0.74	1.4	2.7	3.5	3.9
b-a = 100 nm	0.15	0.30	0.75	1.4	2.4
b-a = 150 nm	0.06	0.12	0.32	0.63	1.2

[a]Table of the predicted peak shear stress (dyn/cm^2) on the osteocytic process membrane obtained for different cases, where the fiber spacing Δ is taken to be 4, 7, and 20 nm while the width of the fluid annulus keeps constant (b-a = 100 nm), or the width of the fluid annulus b-a is taken to be 50, 100, 150 nm while the fiber spacing remains to be 7 nm. The magnitude of the pulsatile blood pressure is assumed to be 10 mm Hg and there is no mechanical loading applied to the osteon.

Reproduced with permission of the copyright owner. Further reproduction prohibited without permission.

Appendix

The partial differential equation of interest is

$$\frac{\partial^2 P}{\partial R^2}+\frac{1}{R}\frac{\partial P}{\partial R}+\frac{1}{R^2}\frac{\partial^2 P}{\partial \theta^2}-\frac{\partial P}{\partial \tau}=-\cos T\tau \qquad \text{(A1)}$$

with the following boundary conditions:

$$P=\frac{3}{\sigma_0 BT}(p_b \sin(WT\tau+\psi)+p_0) \text{ at } R=R_t$$

$$\partial P/\partial R=0 \text{ at } R=1.$$

Assuming $P = P_1 + N^*P_2 + P_0$, where $N=\frac{3p_b}{\sigma_0 BT}$ and $P_0=\frac{3p_0}{\sigma_0 BT}$, P_1 and P_2 should satisfy the following equations and boundary conditions:

$$\frac{\partial^2 P_1}{\partial R^2}+\frac{1}{R}\frac{\partial P_1}{\partial R}-\frac{\partial P_1}{\partial \tau}=-\cos T\tau \qquad \text{(A2)}$$

$$P_1=0 \text{ at } R=R_t$$

$$\partial P_1/\partial R=0 \text{ at } R=1$$

and

$$\frac{\partial^2 P_2}{\partial R^2}+\frac{1}{R}\frac{\partial P_2}{\partial R}-\frac{\partial P_2}{\partial \tau}=0 \qquad \text{(A3)}$$

$$P_2=\sin(WT\tau+\psi) \text{ at } R=R_t$$

$$\partial P_2/\partial R=0 \text{ at } R=1.$$

Using the complex method and separation of variables, the solution to Eq. (A2) is given as:

$$P_1(R,\tau)=\frac{1}{T}\mathrm{Re}\{ie^{iT\tau}\frac{J(R,T)}{J(R_t,T)}\}+\frac{1}{T}\sin(T\tau) \qquad \text{(A4)}$$

where Re is the real part and $J(R,T)=I_0(\sqrt{iT}R)K_1(\sqrt{iT})+I_1(\sqrt{iT})K_0(\sqrt{iT}R)$.

To solve Eq. (A3), we assume $P_2'=P_2+\sin(WT\tau+\psi)$, substitute into Eq. (A3), and then we get:

$$\frac{\partial^2 P_2'}{\partial R^2}+\frac{1}{R}\frac{\partial P_2'}{\partial R}-\frac{\partial P_2'}{\partial \tau}=-WT\cos(WT\tau+\psi) \qquad \text{(A5)}$$

$$P_2'=0 \text{ at } R=R_t$$

Reproduced with permission of the copyright owner. Further reproduction prohibited without permission.

$$\partial P_2'/\partial R = 0 \text{ at } R = 1.$$

Similar to Eq. (A2), the solution of Eq. (A5) is

$$P_2'(R,\tau) = \mathrm{Re}\{ie^{i(WT\tau+\psi)}\frac{J(R,WT)}{J(R_i,WT)}\} + \sin(WT\tau+\psi). \qquad \text{(A6)}$$

Thus, the solution to Eq. (A3) is

$$P_2(R,\tau) = \mathrm{Re}\{ie^{i(WT\tau+\psi)}\frac{J(R,WT)}{J(R_i,WT)}\}. \qquad \text{(A7)}$$

Therefore, the solution to Eq. (A1) is:

$$P(R,\tau) = \frac{1}{T}\mathrm{Re}\{ie^{iT\tau}\frac{J(R,T)}{J(R_i,T)}\} + \frac{1}{T}\sin(T\tau) + \frac{3p_b}{\sigma_0 BT}\mathrm{Re}\{ie^{i(WT\tau+\psi)}\frac{J(R,WT)}{J(R_i,WT)}\} + \frac{3p_0}{\sigma_0 BT}. \qquad \text{(A8)}$$

Reproduced with permission of the copyright owner. Further reproduction prohibited without permission.

Chapter 6 Conclusions and Future Work

Conclusions

Both theoretical and experimental approaches have been presented here to better understand the behavior of bone interstitial fluid flow and how it may play a role in bone's mechanosensory system and bone metabolism. The three theoretical models presented in this dissertation, the six array-osteon model in Chapter 2, the lacunar mixing model in Chapter 3, and the blood-pressure driven fluid flow model in Chapter 5, are all based on a previous model of a canaliculus where the fluid annulus in the canalicular channel is filled with a pericellular matrix, a structure that behaves as a molecular sieve and determines the hydraulic resistance of the lacunar-canalicular pores (Weinbaum et al., 1994; Cowin et al., 1995). The experimental work of tracer perfusion presented in Chapter 4 is designed to validate the predictions of the lacunar-mixing model as well as to provide indirect evidence of the existence and pore size of such a pericellular matrix.

The macroscopic model of a piece of osteonal bone specimen developed in Chapter 2 successfully explained the non-linear cusp-like fluid pressure profiles near the osteonal canals in bone matrix, which had been found experimentally but previously unexplained. This model showed that the microstructure of the bone matrix, especially the vascular pores, determines the local fluid flow patterns, and that the peak fluid pressure gradients and shearing stresses are located on the canal surface. Compared to lacunar-canalicular pores, the osteonal canals in osteonal bone are the primary relaxation pathways for fluid flow. Therefore, each osteon behaves as an independent unit.

The lacunar-mixing model presented in Chapter 3 focused on the convective transport of nutrient and signaling molecules, an important component of bone adaptation and

Reproduced with permission of the copyright owner. Further reproduction prohibited without permission.

metabolism. In this model, the interstitial fluid flow induced by mechanical loading was shown to carry more solute molecules into the lacunae compared to those out of the lacunae due to the proposed fluid mixing in the lacunae. This model predicted that convective mass transport increases with loading magnitude and decreases with increasing loading frequency.

To begin to validate the above model, I performed in vivo experiments to quantify interstitial fluid movement in bone (Chapter 4). I quantified tracer diffusion in unloaded rat bone using four tracers of various sizes (reactive red, microperoxidase, horseradish peroxidase, and ferritin with a molecular diameter of 1, 2, 6, and 10 nm, respectively). After circulating for 5 minutes, reactive red saturated both the vascular and lacunar-canalicular pores, ferritin filled the vascular pores only, and microperoxidase and horseradish peroxidase labeled the vascular pores and some of the lacunae. This study suggested that if there exists a gel-like pericellular fiber matrix surrounding the osteocyte process in the fluid channels (canaliculi), the pore size (fiber spacing) of the pericellular matrix is between 6-10 nm. The results also suggested that microperoxidase and horseradish peroxidase be used in future studies for tracking fluid flow in mechanically loaded bone because they are small enough to pass the lacunar-canalicular fluid pathway and big enough to have limited diffusion.

Besides mechanical loading, blood circulation has been found to influence bone growth and adaptation. Chapter 5 presented a model that links blood pressure induced interstitial fluid flow with venous stasis induced periosteal bone growth. The relative osteogenic capacity in terms of shear stress was examined for different cases of blood pressures and mechanical strains. This model showed that the shear stress due to blood

Reproduced with permission of the copyright owner. Further reproduction prohibited without permission.

flow is usually two orders of magnitude lower than that due to mechanical loading, which suggests that the blood pressure in venous stasis is unlikely to produce sufficient shear stress stimuli for osteocyte excitation. Therefore, other factors besides the interstitial fluid flow may account for the periosteal bone growth under venous stasis. I postulate that the relative high pressures and pressure gradients acting on the periosteum may trigger the periosteal response in venous stasis.

Future Work

There is much work that can be done in the future to continue these investigations. In the three theoretical models presented here, the interstitial fluid flow is believed to flow in the canaliculi with a pericellular fiber matrix surrounding the osteocytic process filling the fluid annulus with a fiber spacing of 7 nm. Although electron microscopy studies have suggested the existence of such a pericellular structure (Wassermann and Yaeger, 1965; Sauren et al., 1992; Shapiro et al., 1995; Aarden et al., 1996), there are no direct data on the fine structure of the pericellular matrix. Our perfusion studies yield indirect evidence that the fiber spacing is in the range of 6-10 nm based on the passing or exclusion of tracers with certain sizes in the canaliculi. It would be more convincing if an ultrastructure electron microscopic study could show the fibers and the fiber spacing were measured directly.

Besides the ultrastructure of the canaliculi, the pore size of the collagen-hydroxyapatite porosity needs careful examination. Whether this microporosity is a continuous fluid pathway is still debated since tracer studies yield conflicting results. Although our tracer study (Chapter 4) showed that reactive red appears to not be present in the collagen-hydroxyapatite porosity, studies using a smaller tracer (procion red)

Reproduced with permission of the copyright owner. Further reproduction prohibited without permission.

indicated that this tracer could not penetrate into the collagen-hydroxyapatite pores in one study (Knothe Tate et al., 1998b) while the same tracer was found in the mineralized matrix in another study provided conflicting results (Knothe Tate et al., 2001). Future studies can utilize smaller fluorescent tracers and more powerful visualizing tools such as confocal laser microscopy to examine the tracer perfusion in the collagen-hydroxyapatite porosity.

Although bone permeability of the vascular porosity has been measured (Rouhana et al., 1981; Li et al., 1987; Grimm and Williams, 1997), there is no measurement of the permeability of the lacunar-canalicular porosity in the literature, which is essential to calculate the fluid pressures and shear stresses in mechanically loaded bone. In this dissertation, the permeability of the lacunar-canalicular porosity was estimated from the structural data of the pericellular matrix and canalicular channels, such as the fiber radius, fiber spacing, the number of canaliculi per unit area, the canalicular wall radius, and the osteocyte process radius (Chapters 2, 3, 5). The permeability estimation may vary several orders using different parameters (Chapter 2). Therefore, experimental measurement of the permeability of the lacunar-canalicular porosity is needed to confirm the theoretical estimations. If a piece of mineralized bone tissue without any vascular canals, say a trabecula, or a piece of bone with the vascular pores sealed, say an osteon, can be obtained and used to measure the fluid flow under a pressure gradient, the permeability at the lacunar-canalicular porosity can be measured. Of course, this would be a very difficult experiment because of the small size of the sample and the difficulty of preventing leakage in the system. Care also should be taken to preserve the cells and the pericellular matrix during the sample preparation and measurement.

Reproduced with permission of the copyright owner. Further reproduction prohibited without permission.

Loaded-induced fluid flow can be tracked using the protocol developed in the perfusion study (Chapter 4). The goal is to demonstrate and quantify the convective transport due to mechanical loading. Results from the current study indicate that microperoxidase and horseradish peroxidase can be used for this purpose. Since the processing time for both tracers is several days, care should be taken to reduce any diffusion artifacts in case the artifacts overwhelm the effect of mechanical loading. Another possibility is to use larger fluorescent dyes that have a molecular size in the range of 6 nm (HRP) to 10 nm (ferritin). Besides molecular weight, other properties of the dye should be considered, such as its electrical charge, molecular shape, and whether it can be fixed chemically.

Although the contribution of mechanical loading and blood pressure to interstitial fluid flow was examined in Chapter 5, how the load-induced interstitial fluid flow affects blood pressure is not well understood at the present time. In the model developed in Chapter 5, the blood pressure is assumed to remain the same regardless of the applied mechanical loading. However, an experimental study has shown that a much higher intramedullary pressure was recorded in an axially compressed isolated turkey ulna (Qin, 1997). This high intramedullary pressure will definitely affect blood circulation. To further address this issue, I have developed a model in a whole bone with coupled fluid flows in both the vascular and lacunar-canalicular pores in the cortex (Fritton et al., 2001). The preliminary results show that the fluid influx into the marrow cavity is not large enough to cause the intramedullary pressure to increase as shown in the experiments. For future work, it would be interesting to include the effect of direct deformation of the

Reproduced with permission of the copyright owner. Further reproduction prohibited without permission.

marrow cavity induced by the mechanical compression as well as the collapsibility of the blood vessels.

In conclusion, bone interstitial fluid flow is an important signal pathway to transfer mechanical stimuli from the tissue level to the cellular level. It can also enhance transport of nutrient and signaling molecules from the bone blood vessels to bone cells. This dissertation used a combined theoretical and experimental approach to better understand the behavior of bone interstitial fluid flow under mechanical and vascular influences. These studies yield valuable insights into the cellular mechanisms of bone adaptation and bone growth, which are helpful to investigate the pathologies of many bone diseases associated with abnormal bone growth and adaptation.

Reproduced with permission of the copyright owner. Further reproduction prohibited without permission.

Bibliography

Chapter 1

Adachi, T., Tsubota, K., Tomita, Y., and Hollister, S. J., 2001. Trabecular surface remodeling simulation for cancellous bone using microstructural voxel finite element models. J Biomech Eng 123, 403-9.

Arnoldi, C. C., Linderholm, H., and Mussbichler, H., 1972. Venous engorgement and intraosseous hypertension in osteoarthritis of the hip. J Bone Joint Surg Br 54, 409-21.

Bentolila, V., Boyce, T. M., Fyhrie, D. P., Drumb, R., Skerry, T. M., and Schaffler, M. B., 1998. Intracortical remodeling in adult rat long bones after fatigue loading. Bone 23, 275-81.

Bergula, A. P., Huang, W., and Frangos, J. A., 1999. Femoral vein ligation increases bone mass in the hindlimb suspended rat. Bone 24, 171-7.

Black, J., Mattson, R., and Korostoff, E., 1974. Haversian osteons: size, distribution, internal structure, and orientation. J Biomed Mater Res 8, 299-319.

Bronk, J. T., Meadows, T. H., and Kelly, P. J., 1993. The relationship of increased capillary filtration and bone formation. Clin Orthop, 338-45.

Brown, T. D., Pedersen, D. R., Gray, M. L., Brand, R. A., and Rubin, C. T., 1990. Toward an identification of mechanical parameters initiating periosteal remodeling: a combined experimental and analytic approach. J Biomech 23, 893-905.

Buckley, M. J., Banes, A. J., and Jordan, R. D., 1990. The effects of mechanical strain on osteoblasts in vitro. J Oral Maxillofac Surg 48, 276-82.

Burger, E. H., and Klein-Nulend, J., 1999. Mechanotransduction in bone--role of the lacuno-canalicular network. Faseb J 13, S101-12.

Burger, E. H., Klein-Nulend, J., van der Plas, A., and Nijweide, P. J., 1995. Function of osteocytes in bone--their role in mechanotransduction. J Nutr 125, 2020S-2023S.

Burger, E. H., Klein-Nulend, J., and Veldhuijzen, J. P., 1991. Modulation of osteogenesis in fetal bone rudiments by mechanical stress in vitro. J Biomech 24, 101-9.

Burr, D. B., 1993. Remodeling and the repair of fatigue damage. Calcif Tissue Int 53, S75-80; discussion S80-1.

Burr, D. B., Martin, R. B., Schaffler, M. B., and Radin, E. L., 1985. Bone remodeling in response to in vivo fatigue microdamage. J Biomech 18, 189-200.

Reproduced with permission of the copyright owner. Further reproduction prohibited without permission.

Burr, D. B., Milgrom, C., Fyhrie, D., Forwood, M., Nyska, M., Finestone, A., Hoshaw, S., Saiag, E., and Simkin, A., 1996. In vivo measurement of human tibial strains during vigorous activity. Bone 18, 405-10.

Carter, D. R., Fyhrie, D. P., and Whalen, R. T., 1987. Trabecular bone density and loading history: regulation of connective tissue biology by mechanical energy. J Biomech 20, 785-94.

Carter, D. R., and Hayes, W. C., 1977. Compact bone fatigue damage: a microscopic examination. Clin Orthop 127, 265-74.

Chambers, T. J., Evans, M., Gardner, T. N., Turner-Smith, A., and Chow, J. W., 1993. Induction of bone formation in rat tail vertebrae by mechanical loading. Bone Miner 20, 167-78.

Chen, N. X., Ryder, K. D., Pavalko, F. M., Turner, C. H., Burr, D. B., Qiu, J., and Duncan, R. L., 2000. Ca(2+) regulates fluid shear-induced cytoskeletal reorganization and gene expression in osteoblasts. Am J Physiol Cell Physiol 278, C989-97.

Cheng, B., Zhao, S., Luo, J., Sprague, E., Bonewald, L. F., and Jiang, J. X., 2001. Expression of functional gap junctions and regulation by fluid flow in osteocyte-like MLO-Y4 cells. J Bone Miner Res 16, 249-59.

Chiquet, M., 1999. Regulation of extracellular matrix gene expression by mechanical stress. Matrix Biol 18, 417-26.

Cooper, R. R., Milgram, J. W., and Robinson, R. A., 1966. Morphology of the osteon. An electron microscopic study. J Bone Joint Surg Am 48, 1239-71.

Cowin, S. C., 1983. The mechanical and stress adaptive properties of bone. Ann Biomed Eng 11, 263-95.

Cowin, S. C., Moss-Salentijn, L., and Moss, M. L., 1991. Candidates for the mechanosensory system in bone. J Biomech Eng 113, 191-7.

Cowin, S. C., and Weinbaum, S., 1998. Strain amplification in the bone mechanosensory system. Am J Med Sci 316, 184-8.

Cowin, S. C., Weinbaum, S., and Zeng, Y., 1995. A case for bone canaliculi as the anatomical site of strain generated potentials. J Biomech 28, 1281-97.

Cullen, D. M., Smith, R. T., and Akhter, M. P., 2001. Bone-loading response varies with strain magnitude and cycle number. J Appl Physiol 91, 1971-6.

Reproduced with permission of the copyright owner. Further reproduction prohibited without permission.

Curtis, T.A., Ashrafi, S.H., and Weber, D., 1985. Canalicular communication in the cortices of human long bones. Anatomical Record 212, 336-344.

Dillaman, R. M., 1984. Movement of ferritin in the 2-day-old chick femur. Anat Rec 209, 445-53.

Dillaman, R. M., Roer, R. D., and Gay, D. M., 1991. Fluid movement in bone: theoretical and empirical. J Biomech 24, 163-77.

Donahue, S. W., Jacobs, C. R., and Donahue, H. J., 2001. Flow-induced calcium oscillations in rat osteoblasts are age, loading frequency, and shear stress dependent. Am J Physiol Cell Physiol 281, C1635-41.

Doty, S. B., and Schofield, B. H., 1972. Methabolic and structural changes within osteocytes of rat bone. In Calcium, Parathyroid Hormone and the Calcitonins, R. V. Talmage and P. L. Munson, eds. (Amsterdam: Elsevier), pp. 353-64.

Duncan, R., and Misler, S., 1989. Voltage-activated and stretch-activated Ba2+ conducting channels in an osteoblast-like cell line (UMR 106). FEBS Lett 251, 17-21.

Duncan, R. L., and Turner, C. H., 1995. Mechanotransduction and the functional response of bone to mechanical strain. Calcif Tissue Int 57, 344-58.

Eriksson, C., 1974. Streaming potentials and other water-dependent effects in mineralized tissues. Ann N Y Acad Sci 238, 321-38.

Fernandes, P., Rodrigues, H., and Jacobs, C., 1999. A model of bone adaptation using a global optimisation criterion based on the trajectorial theory of Wolff. Comput Methods Biomech Biomed Engin 2, 125-138.

Ficat, P. R., and Arlet, J., 1980. Ischemia and necroses of bone. D. S. Hungerford (Ed). Williams & Wilkins, Baltimore.

Fritton, S. P., and Rubin, C. T., 2001. In vivo measurement of bone deformations using strain gauges. In: S. C. Cowin (Ed), Bone Mechanics Handbook. CRC Press, Boca Raton, Florida. pp 8-1-8-41.

Green, N. E., and Griffin, P. P., 1982. Intra-osseous venous pressure in Legg-Perthes disease. J Bone Joint Surg Am 64, 666-71.

Gross, D., and Williams, W. S., 1982. Streaming potential and the electromechanical response of physiologically-moist bone. J Biomech 15, 277-95.

Gross, T. S., Edwards, J. L., McLeod, K. J., and Rubin, C. T., 1997. Strain gradients correlate with sites of periosteal bone formation. J Bone Miner Res 12, 982-8.

Reproduced with permission of the copyright owner. Further reproduction prohibited without permission.

Hart, R. T., Davy, D. T., and Heiple, K. G., 1984. Mathematical modeling and numerical solutions for functionally dependent bone remodeling. Calcif Tissue Int 36, S104-9.

Hillsley, M. V., and Frangos, J. A., 1994. Bone tissue engineering: the role of interstitial fluid flow. Biotechnol Bioeng 43, 573-81.

Huiskes, R., Weinans, H., Grootenboer, H. J., Dalstra, M., Fudala, B., and Slooff, T. J., 1987. Adaptive bone-remodeling theory applied to prosthetic-design analysis. J Biomech 20, 1135-50.

Hung, C. T., Pollack, S. R., Reilly, T. M., and Brighton, C. T., 1995. Real-time calcium response of cultured bone cells to fluid flow. Clin Orthop, 256-69.

Jacobs, C. R., Yellowley, C. E., Davis, B. R., Zhou, Z., Cimbala, J. M., and Donahue, H. J., 1998. Differential effect of steady versus oscillating flow on bone cells. J Biomech 31, 969-76.

Johnson, D. L., McAllister, T. N., and Frangos, J. A., 1996. Fluid flow stimulates rapid and continuous release of nitric oxide in osteoblasts. Am J Physiol 271, E205-8.

Judex, S., Gross, T. S., and Zernicke, R. F., 1997. Strain gradients correlate with sites of exercise-induced bone-forming surfaces in the adult skeleton. J Bone Miner Res 12, 1737-45.

Judex, S., and Zernicke, R. F., 2000. Does the mechanical milieu associated with high-speed running lead to adaptive changes in diaphyseal growing bone? Bone 26, 153-9.

Keanini, R. G., Roer, R. D., and Dillaman, R. M., 1995. A theoretical model of circulatory interstitial fluid flow and species transport within porous cortical bone. J Biomech 28, 901-14.

Kelly, P. J., and Bronk, J. T., 1990. Venous pressure and bone formation. Microvasc Res 39, 364-75.

Kelly, P. J., Montgomery, R. J., and Bronk, J. T., 1990. Reaction of the circulatory system to injury and regeneration. Clin Orthop, 275-88.

Kiaer, T., 1994. Bone perfusion and oxygenation. Animal experiments and clinical observations. Acta Orthop Scand Suppl 257, 1-41.

Klein-Nulend, J., Semeins, C. M., Ajubi, N. E., Nijweide, P. J., and Burger, E. H., 1995. Pulsating fluid flow increases nitric oxide (NO) synthesis by osteocytes but not periosteal fibroblasts--correlation with prostaglandin upregulation. Biochem Biophys Res Commun 217, 640-8.

Reproduced with permission of the copyright owner. Further reproduction prohibited without permission.

Knothe Tate, M. L., Tami, A., Nasser, P. R., Steck, R., and Schaffler, M. B., 2001. Permeability characteristics of different molecular tracers in loaded and unloaded bone. In Transactions of the 47th Meeting of the Orthopaedic Society 26: 138.

Knothe Tate, M. L., and Knothe, U., 2000. An ex vivo model to study transport processes and fluid flow in loaded bone. J Biomech 33, 247-54.

Knothe Tate, M. L., Knothe, U., and Niederer, P., 1998a. Experimental elucidation of mechanical load-induced fluid flow and its potential role in bone metabolism and functional adaptation. Am J Med Sci 316, 189-95.

Knothe Tate, M. L., Steck, R., Forwood, M. R., and Niederer, P., 2000. In vivo demonstration of load-induced fluid flow in the rat tibia and its potential implications for processes associated with functional adaptation. J Exp Biol 203 Pt 18, 2737-45.

Knothe Tate, M. L., Niederer, P., and Knothe, U., 1998b. In vivo tracer transport through the lacunocanalicular system of rat bone in an environment devoid of mechanical loading. Bone 22, 107-17.

Knothe Tate, M. L., and Niederer, P., 1998c. A theoretical FE-based model developed to predict the relative contribution of convective and diffusive transport mechanisms for the maintenance of local equilibria within cortical bone. ASME HTD-Vol. 362/BED-Vol. 40, 133-142.

Kufahl, R. H., and Saha, S., 1990. A theoretical model for stress-generated fluid flow in the canaliculi- lacunae network in bone tissue. J Biomech 23, 171-80.

Kurata, K., Uemura, T., Nemoto, A., Tateishi, T., Murakami, T., Higaki, H., Miura, H., and Iwamoto, Y., 2001. Mechanical strain effect on bone-resorbing activity and messenger RNA expressions of marker enzymes in isolated osteoclast culture. J Bone Miner Res 16, 722-30.

Lanyon, L. E., Goodship, A. E., Pye, C. J., and MacFie, J. H., 1982. Mechanically adaptive bone remodelling. J Biomech 15, 141-54.

Levenston, M. E., and Carter, D. R., 1998. An energy dissipation-based model for damage stimulated bone adaptation. J Biomech 31, 579-86.

Lilly, A. D., and Kelly, P. J., 1970. Effects of venous ligation on bone remodeling in the canine tibia. J Bone Joint Surg Am 52, 515-20.

Liu, S. L., and Ho, T. C., 1991. The role of venous hypertension in the pathogenesis of Legg-Perthes disease. A clinical and experimental study. J Bone Joint Surg Am 73, 194-200.

Reproduced with permission of the copyright owner. Further reproduction prohibited without permission.

MacGinitie, L. A., Stanely, G. D., Bieber, W. A., and Wu, D. D., 1997. Bone streaming potentials and currents depend on anatomical structure and loading orientation. J Biomech 30, 1133-9.

Mak, A. F., Qin, L., Hung, L. K., Cheng, C. W., and Tin, C. F., 2000. A histomorphometric observation of flows in cortical bone under dynamic loading. Microvasc Res 59, 290-300.

Martin, B., 1992. A theory of fatigue damage accumulation and repair in cortical bone. J Orthop Res 10, 818-25.

Mikuni-Takagaki, Y., 1999. Mechanical responses and signal transduction pathways in stretched osteocytes. J Bone Miner Metab 17, 57-60.

Milgrom, C., Finestone, A., Levi, Y., Simkin, A., Ekenman, I., Mendelson, S., Millgram, M., Nyska, M., Benjuya, N., and Burr, D., 2000. Do high impact exercises produce higher tibial strains than running? Br J Sports Med 34, 195-9.

Montgomery, R. J., Sutker, B. D., Bronk, J. T., Smith, S. R., and Kelly, P. J., 1988. Interstitial fluid flow in cortical bone. Microvasc Res 35, 295-307.

Mori, S., and Burr, D. B., 1993. Increased intracortical remodeling following fatigue damage. Bone 14, 103-9.

Mosley, J. R., and Lanyon, L. E., 1998. Strain rate as a controlling influence on adaptive modeling in response to dynamic loading of the ulna in growing male rats. Bone 23, 313-8.

Moss, M. L., 1997. The functional matrix hypothesis revisited. 2. The role of an osseous connected cellular network. Am J Orthod Dentofacial Orthop 112, 221-6.

Neuman, W. F., and Neuman, M. W., 1958. The Chemical Dynamics of Bone. University of Chicago Press, Chicago.

Ogasawara, A., Arakawa, T., Kaneda, T., Takuma, T., Sato, T., Kaneko, H., Kumegawa, M., and Hakeda, Y., 2001. Fluid shear stress-induced cyclooxygenase-2 expression is mediated by C/EBP beta, cAMP-response element-binding protein, and AP-1 in osteoblastic MC3T3-E1 cells. J Biol Chem 276, 7048-54.

O'Connor, J. A., Lanyon, L. E., and MacFie, H., 1982. The influence of strain rate on adaptive bone remodelling. J Biomech 15, 767-81.

Otter, M. W., MacGinitie, L. A., Seiz, K. G., Johnson, M. W., Dell, R. B., and Cochran, G. V. B., 1994. Dependence of streaming potential frequency response on sample thickness: implications for fluid flow through bone microstructure. Biomemetics 2, 57-75.

Reproduced with permission of the copyright owner. Further reproduction prohibited without permission.

Otter, M. W., Palmieri, V. R., and Cochran, G. V., 1990. Transcortical streaming potentials are generated by circulatory pressure gradients in living canine tibia. J Orthop Res 8, 119-26.

Petrov, N., Pollack, S., and Blagoeva, R., 1989. A discrete model for streaming potentials in a single osteon. J Biomech 22, 517-21.

Piekarski, K., and Munro, M., 1977. Transport mechanism operating between blood supply and osteocytes in long bones. Nature 269, 80-2.

Pienkowski, D., and Pollack, S. R., 1983. The origin of stress-generated potentials in fluid-saturated bone. J Orthop Res 1, 30-41.

Qin, L., Mak, A. T., Cheng, C. W., Hung, L. K., and Chan, K. M., 1999. Histomorphological study on pattern of fluid movement in cortical bone in goats. Anat Rec 255, 380-7.

Qin, Y. X., Rubin, C. T., and McLeod, K. J., 1998. Nonlinear dependence of loading intensity and cycle number in the maintenance of bone mass and morphology. J Orthop Res 16, 482-9.

Ramtani, S., and Zidi, M., 2001. A theoretical model of the effect of continuum damage on a bone adaptation model. J Biomech 34, 471-9.

Rawlinson, S. C., Pitsillides, A. A., and Lanyon, L. E., 1996. Involvement of different ion channels in osteoblasts' and osteocytes' early responses to mechanical strain. Bone 19, 609-14.

Reich, K. M., Gay, C. V., and Frangos, J. A., 1990. Fluid shear stress as a mediator of osteoblast cyclic adenosine monophosphate production. J Cell Physiol 143, 100-4.

Rubin, C. T., and Lanyon, L. E., 1987. Kappa Delta Award paper. Osteoregulatory nature of mechanical stimuli: function as a determinant for adaptive remodeling in bone. J Orthop Res 5, 300-10.

Salzstein, R. A., Pollack, S. R., Mak, A. F., and Petrov, N., 1987. Electromechanical potentials in cortical bone--I. A continuum approach. J Biomech 20, 261-70.

Scott, G. C., and Korostoff, E., 1990. Oscillatory and step response electromechanical phenomena in human and bovine bone. J Biomech 23, 127-43.

Siffert, R. S., Luo, G. M., Cowin, S. C., and Kaufman, J. J., 1996. Dynamic relationships of trabecular bone density, architecture, and strength in a computational model of osteopenia. Bone 18, 197-206.

Reproduced with permission of the copyright owner. Further reproduction prohibited without permission.

Smalt, R., Mitchell, F. T., Howard, R. L., and Chambers, T. J., 1997. Mechanotransduction in bone cells: induction of nitric oxide and prostaglandin synthesis by fluid shear stress, but not by mechanical strain. Adv Exp Med Biol 433, 311-4.

Starkebaum, W., Pollack, S. R., and Korostoff, E., 1979. Microelectrode studies of stress-generated potentials in four-point bending of bone. J Biomed Mater Res 13, 729-51.

Tanaka, T., and Sakano, A., 1985. Differences in permeability of microperoxidase and horseradish peroxidase into the alveolar bone of developing rats. J Dent Res 64, 870-6.

Taylor, D., and Prendergast, P. J., 1997. A model for fatigue crack propagation and remodelling in compact bone. Proc Inst Mech Eng [H] 211, 369-75.

Toma, C. D., Ashkar, S., Gray, M. L., Schaffer, J. L., and Gerstenfeld, L. C., 1997. Signal transduction of mechanical stimuli is dependent on microfilament integrity: identification of osteopontin as a mechanically induced gene in osteoblasts. J Bone Miner Res 12, 1626-36.

Torrance, A. G., Mosley, J. R., Suswillo, R. F., and Lanyon, L. E., 1994. Noninvasive loading of the rat ulna in vivo induces a strain-related modeling response uncomplicated by trauma or periostal pressure. Calcif Tissue Int 54, 241-7.

Trueta, J., 1963. The role of the vessels in osteogenesis. Journal of Bone and Joint Surgery 45 B, 402-418.

Turner, C. H., Forwood, M. R., and Otter, M. W., 1994. Mechanotransduction in bone: do bone cells act as sensors of fluid flow? Faseb J 8, 875-8.

Turner, C. H., Owan, I., and Takano, Y., 1995. Mechanotransduction in bone: role of strain rate. Am J Physiol 269, E438-42.

Verborgt, O., Gibson, G. J., and Schaffler, M. B., 2000. Loss of osteocyte integrity in association with microdamage and bone remodeling after fatigue in vivo. J Bone Miner Res 15, 60-7.

Walker, L. M., Publicover, S. J., Preston, M. R., Said Ahmed, M. A., and El Haj, A. J., 2000. Calcium-channel activation and matrix protein upregulation in bone cells in response to mechanical strain. J Cell Biochem 79, 648-61.

Wang, L., Cowin, S. C., Weinbaum, S., and Fritton, S. P., 2000. Modeling tracer transport in an osteon under cyclic loading. Ann Biomed Eng 28, 1200-9.

Wang, L., Fritton, S. P., Cowin, S. C., and Weinbaum, S., 1999. Fluid pressure relaxation depends upon osteonal microstructure: modeling an oscillatory bending experiment. J Biomech 32, 663-72.

Reproduced with permission of the copyright owner. Further reproduction prohibited without permission.

Weinbaum, S., Cowin, S. C., and Zeng, Y., 1991. A model for the fluid shear stress excitation of membrane ion channels in osteocytic process due to bone strain. In Advances in Bioengineering, J. R. Vanderby, ed., New York: American Society of Mechanical Engineers, pp. 317-320.

Weinbaum, S., Cowin, S. C., and Zeng, Y., 1994. A model for the excitation of osteocytes by mechanical loading-induced bone fluid shear stresses. J Biomech 27, 339-60.

Welch, R. D., Johnston, C. E., 2nd, Waldron, M. J., and Poteet, B., 1993. Bone changes associated with intraosseous hypertension in the caprine tibia. J Bone Joint Surg Am 75, 53-60.

Williams, J. L., Iannotti, J. P., Ham, A., Bleuit, J., and Chen, J. H., 1994. Effects of fluid shear stress on bone cells. Biorheology 31, 163-70.

Yoshikawa, T., Mori, S., Santiesteban, A. J., Sun, T. C., Hafstad, E., Chen, J., and Burr, D. B., 1994. The effects of muscle fatigue on bone strain. J Exp Biol 188, 217-33.

You, L., Cowin, S. C., Schaffler, M. B., and Weinbaum, S., 2001. A model for strain amplification in the actin cytoskeleton of osteocytes due to fluid drag on pericellular matrix. J Biomech 34, 1375-86.

You, L., Weinbaum, S., Cowin, S. C., and Schaffler, M. B., 2002. Ultrastructure of the osteocyte process. Anatomical Record, in submission.

Zeng, Y., Cowin, S. C., and Weinbaum, S., 1994. A fiber matrix model for fluid flow and streaming potentials in the canaliculi of an osteon. Ann Biomed Eng 22, 280-92.

Zhang, D., Cowin, S. C., and Weinbaum, S., 1997. Electrical signal transmission and gap junction regulation in a bone cell network: a cable model for an osteon. Ann Biomed Eng 25, 357-74.

Ziambaras, K., Lecanda, F., Steinberg, T. H., and Civitelli, R., 1998. Cyclic stretch enhances gap junctional communication between osteoblastic cells. J Bone Miner Res 13, 218-28.

Chapter 2

Ayasaka, N., Kondo, T., Goto, T., Kido, M.A., Nagata, E., and Tanaka, T., 1992. Differences in the transport systems between cementocytes and osteocytes in rats using microperoxidase as a tracer. Archives of Oral Biology 37, 363-368.

Cowin, S.C., Weinbaum, S., and Zeng, Y., 1995. A case for bone canaliculi as the anatomical site of strain generated potentials. Journal of Biomechanics 28, 1281-1296.

Reproduced with permission of the copyright owner. Further reproduction prohibited without permission.

Cowin, S.C., 1999. Bone poroelasticity. Journal of Biomechanics 32, 217-238.

Curtis, T.A., Ashrafi, S.H., and Weber, D., 1985. Canalicular communication in the cortices of human long bones. Anatomical Record 212, 336-344.

Hung C.T., Pollack S.R., Reilly T.M., and Brighton C.T., 1995. Real-time calcium response of cultured bone cells to fluid flow. Clinical Orthopaedics 313, 256-69.

Klein-Nulend, J., van der Plas, A., Semeins, C.M., Ajubi. N.E., Frangos, J.A., Nijweide, P.J. and Burger. E.H., 1995. Sensitivity of osteocytes to biomechanical stress in vitro. FASEB Journal 9, 441-445.

Knothe Tate, M.L., Niederer, P., and knothe, U., 1998. In vivo tracer transport through the lacunocanalicular system of rat bone in an environment devoid of mechanical loading. Bone, 22, 107-117.

Kufahl, R.H. and Saha, S., 1990. A theoretical model for stress-generated fluid flow in the canaliculi-lacunae network in bone tissue. Journal of Biomechanics 23, 171-180.

Li, G., Bronk, J.T., An, K. and Kelly, P.J., 1987. Permeability of cortical bone of canine tibiae. Microvascular Research 34, 302-310.

Mak, A.T., Huang, D.T., Zhang, J.D. and Tong, P., 1997. Deformation-induced hierarchical flows and drag forces in bone canaliculi and matrix microporosity. Journal of Biomechanics 30, 11-18.

Otter, M.W., MacGinitie, L.A., Seiz, K.G., Johnson, M.W., Dell, R.B. and Cochran, G.V.B., 1994. Dependence of streaming potential frequency response on sample thickness: implications for fluid flow through bone microstructure. Biomemetics 2, 57-75.

Petrov, N., Pollack, S.R. and Blagoeva, R., 1989. A discrete model for streaming potentials in a single osteon. Journal of Biomechanics 22, 517-521.

Piekarski, K. and Munro, M., 1977. Transport mechanism operating between blood supply and osteocytes in long bones. Nature 269, 80-82.

Pollack, S.R., Petrov, N., Salzstein, R., Brankov, G. and Blagoeva, R., 1984. An anatomical model for streaming potentials in osteons. Journal of Biomechanics 17, 627-636.

Reich, K.M., Gay, C.V. and Frangos, J.A., 1990. Fluid shear stress as a mediator of osteoblast cyclic adenosine monophosphate production. Journal of Cellular Physiology 143, 100-104.

Reproduced with permission of the copyright owner. Further reproduction prohibited without permission.

Rouhana, S.W., Johnson, M.W., Chakkalakal, D.R., Harper, R.A., and Katz, J.L., 1981. Permeability of compact bone. Joint ASME-ASCE Conference Biomechanics Symposium AMD 43, 169-172.

Rubin, C.T. and McLeod, K.J., 1994. Promotion of bony ingrowth by frequency specific, low amplitude mechanical strain. Clinical Orthopedics and Related Research 298, 165-174.

Rubin, C.T. and McLeod, K.J., 1996. Inhibition of osteopenia by biophysical intervention. In: Marcus, R., Eldman, D., Kelsey, J. (Eds), Osteoporosis. Academic Press, pp.351-371.

Salzstein, R.A., Pollack, S.R., Mak, A.F.T., and Petrov, N., 1987. Electromechanical potentials in cortical bone – I. A continuum approach. Journal of Biomechanics 20, 261-270.

Salzstein, R.A. and Pollack, S.R., 1987 Electromechanical potentials in cortical bone – II. Experimental analysis. Journal of Biomechanics 20, 271-280.

Scott, G.C. and Korostoff, E., 1990. Oscillatory and step response of electromechanical phenomena in human and bovine bone. Journal of Biomechanics 23, 127-143.

Starkebaum, W., Pollack, S.R. and Korostoff, E., 1979. Microelectrode studies of stress-generated potentials in four-point bending of bone. Journal of Biomedical Materials Research 13, 729-751.

Tanaka, T. and Sakano, A., 1985. Differences in permeability of microperoxidase and horseradish peroxidase into the alveolar bone of developing rats. Journal of Dental Research 64, 870-876.

Turner, C.H., Forwood, M.R. and Otter, M.W., 1994. Mechanotransduction in bone: Do bone cells act as sensors of fluid flow? FASEB Journal 8, 875-878.

Weinbaum, S., Cowin, S.C., and Zeng, Y., 1994. A model for the excitation of osteocytes by mechanical loading-induced bone fluid shear stresses. Journal of Biomechanics 27, 339-360.

Wilkes, C.H. and Visscher, M.B., 1975. Some physiological aspects of bone marrow pressure. Journal of Bone Joint Surgery [A]57, 49-57.

Williams, J.L., Iannotti, J.P., Ham, A., Bleuit, J. and Chen, J.H., 1994. Effects of fluid shear stress on bone cells. Biorheology 31, 163-170.

Zeng, Y., Cowin, S.C. and Weinbaum, S., 1994. A fiber matrix model for fluid flow and streaming potentials in the canaliculi of an osteon. Annals Biomedical Engineering 22, 280-292.

Reproduced with permission of the copyright owner. Further reproduction prohibited without permission.

Zhang, D., Weinbaum, S., and Cowin, S.C., 1998. Estimates of the peak pressure in the bone pore water. Journal of Biomechanical Engineering 120, 697-703.

Chapter 3

[1]Cane, V., G. Marotti, G. Volpi, D. Zaffe, S. Palazzini, F. Remaggi, and M.A. Muglia. Size and density of osteocyte lacunae in different regions of long bones. *Calcif. Tissue Int.* 34:558-563, 1982.

[2]Cooper, R.R., J.W. Milgram, and R.A. Robinson. Morphology of the osteon. *J. Bone Joint Surg.* 48A:1239-1271, 1966.

[3]Cowin, S.C., S. Weinbaum, and Y. Zeng. A case for bone canaliculi as the anatomical site of strain generated potentials. *J. Biomech.* 28:1281-1296, 1995.

[4]Cowin, S.C. Bone poroelasticity. *J. Biomech.* 32:218-238, 1999.

[5]Curtis, T.A., S.H. Ashrafi, and D.F. Weber. Canalicular communication in the cortices of human long bones. *Anat. Rec.* 212:336-344, 1985.

[6]Dilliman, R.M. Movement of ferritin in the 2-day-old chick femur. *Anat. Rec.* 209:445-453, 1984.

[7]Fritton, S.P., K.J. McLeod, and C.T. Rubin. Quantifying the strain history of bone: spatial uniformity and self-similarity of low magnitude strains. *J. Biomech.* 33:317-325, 2000.

[8]Fyhrie, D.P. and J.H. Kimura. Cancellous bone biomechanics. *J. Biomech.* 32:1139-1148, 1999.

[9]Ham, W. Some histophysiological problems peculiar to calcified tissues. *J. Bone Joint Surg.* 34A:706-728, 1952.

[10]Haines, R.W., L. Mehta, and A. Mohiuddin. Nutrition of interstitial lamellae of bone. *Anat. Anz. Jena.* 154:233-236, 1983.

[11]Hillsley, M.V. and J.A. Frangos. Osteoblast hydraulic conductivity is regulated by calcitonin and parathyroid hormone. *J. Bone Miner. Res.* 11:114-124, 1996.

[12]Hughes, S.P.F. and P.J. Kelly. "The mechanism of ion transfer in bone". In *Bone Circulation*, edited by Arlet, J, R.P. Ficat, and D.S. Hungerford. Baltimore: Williams and Wilkins, 1984, pp. 207-212.

[13]Jande, S.S. and L.F. Belanger. Electron microscopy of osteocytes and the pericellular matrix in rat trabecular bone. *Calcif. Tissue Int.* 6:280-289, 1971.

Reproduced with permission of the copyright owner. Further reproduction prohibited without permission.

[14]Ker, R.F., Bennett, M.B., Alexander, R.M., and Kester R.C. Foot strike and the properties of the human heel pad. Proc. Inst. Mech. Eng. [H] 203(4), 191-196, 1989.

[15]Knothe Tate, M.L. and U. Knothe. An ex vivo model to study transport processes and fluid flow in loaded bone. *J. Biomech.* 33, 247-254, 2000.

[16]Knothe Tate, M.L. and P. Niederer. A theoretical FE-based model developed to predict the relative contribution of convective and diffusive transport mechanisms for the maintenance of local equilibria within cortical bone. *Advances in Heat and Mass Transfer in Biotechnology (ASME) HTD-Vol. 362/BED-Vol.* 40, 133-142, 1998.

[17]Knothe Tate, M.L., P. Niederer, and U. Knothe. In vivo tracer transport through the lacunocanalicular system of rat bone in an environment devoid of mechanical loading. *Bone* 22:107-117, 1998.

[18]Kufahl, R.H. and S. Saha. A theoretical model for stress-generated fluid flow in the canaliculi-lacunae network in bone tissue. *J. Biomech.* 23:171-180, 1990.

[19]Li, G., J.T. Bronk, K. An, and P.J. Kelly. Permeability of cortical bone of canine tibiae. *Microvasc. Res.* 34:302-310, 1987.

[20]Marotti, G., M.A. Muglia, and D. Zaffe. A SEM study of osteocyte orientation in alternately structured osteons. *Bone* 6:331-334, 1985.

[21]Marotti, G., M. Ferretti, F. Remaggi, and C. Palumbo. Quantitative evaluation on osteocyte canalicular density in human secondary osteons. *Bone* 16:125-128, 1995.

[22]Marotti, G., D. Farneti, F. Remaggi, and F. Tartari. Morphometric investigation on osteocytes in human auditory ossicles. *Anat. Anz.* 180:449-453, 1998.

[23]Maroudas, A., R.A. Stockwell, A. Nachemson, and J. Urban. Factors involved in the nutrition of human lumbar intervertebral disc: cellularity and diffusion of glucose in vitro. *J. Anat.* 120:113-130, 1975.

[24]McCarthy, I.D. and S.P.F Hughes. "Is there a blood-bone barrier?" In *Bone Circulation and Bone Necrosis*, edited by Arlet, J. and B. Mazieres. New York: Springer-Verlag, 1987, pp. 30-34.

[25]McCarthy, I.D. and S.P.F Hughes. "Transport of small molecules across capillaries in bone". In *Blood Flow: Theory and Practice*, edited by Taylor, D.E.M., and A.L. Stevens. New York: Academic Press, 1983, pp. 313-329.

[26]Montgomery, R.J., B.D. Sutker, J.T. Bronk, S.R. Smith, and P.J. Kelly. Interstitial fluid flow in cortical bone. *Microvasc. Res.* 35:295-307, 1988.

Reproduced with permission of the copyright owner. Further reproduction prohibited without permission.

[27]Neuman, W.F. and M.W. Newman. *The Chemical Dynamics of Bone Mineral. Chicago.* Chicago: University Press, 1958.

[28]Neuman, W.F. and W.K. Ramp. "The concept of a bone membrane: some implications". In: *Cellular Mechanisms for Calcium Transfer and Homeostasis*, edited by Nichols, G. Jr. and R.H. Wasserman. New York: Academic Press, 1971, pp. 197-209.

[29]Piekarski, K. and M. Munro. Transport mechanism operating between blood supply and osteocytes in long bones. *Nature* 269:80-82, 1977.

[30]Rouhana, S.W., M.W. Johnson, D.R. Chakkalakal, R.A. Harper, and J.L. Katz. Permeability of compact bone. *Joint ASME-ASCE Conference Biomechanics Symposium AMD* 43:169-172, 1981.

[31]Rubin, C.T., K.J. McLeod, and S.D. Bain. Functional strains and cortical bone adaptation: epigenetic assurance of skeletal integrity. *J. Biomech.* 23:43-54, 1990.

[32]Sauren, Y.M.H.F., R.H.P. Mieremet, and C.G. Groot. An electron microscopic study on the presence of proteoglycans in the mineralized matrix of rat and human compact lamellar bone. *Anat. Rec.* 232:36-44, 1992.

[33]Skerry, T.M., R. Suswillo, A.J. el. Hai, N.N. Ali, R.A. Dodds, and L.E. Lanyon. Load-induced proteoglycan orientation in bone tissue in vivo and in vitro. *Calcif. Tissue Int.* 46:318-326, 1990.

[34]Weinbaum, S., S.C. Cowin, and Y. Zeng. A model of the excitation of osteocytes by mechanical loading-induced bone fluid shear stresses. *J. Biomech.* 27:339-360, 1994.
[35]Wilkes, C.H. and M.B. Visscher. Some physiological aspects of bone marrow pressure. *J. Bone Joint Surg.* 57A:49-57, 1975.

[36]Zeng, Y., S.C. Cowin, and S. Weinbaum. A fiber matrix for fluid flow and streaming potentials in the canaliculi of an osteon. *Ann. Biomed. Eng.* 22:280-292, 1994.

[37]Zhang, D., S. Weinbaum, and S.C. Cowin. Estimates of the peak pressure in the bone pore water. *J. Biomech. Eng.* 120:697-703, 1998.

Chapter 4

Aarden, E. M., Wassenaar, A. M., Alblas, M. J., and Nijweide, P. J., 1996. Immunocytochemical demonstration of extracellular matrix proteins in isolated osteocytes. Histochem Cell Biol 106, 495-501.

Adachi, T., Tsubota, K., Tomita, Y., and Hollister, S. J., 2001. Trabecular surface remodeling simulation for cancellous bone using microstructural voxel finite element models. J Biomech Eng 123, 403-9.

Reproduced with permission of the copyright owner. Further reproduction prohibited without permission.

Bagge, M., 2000. A model of bone adaptation as an optimization process. J Biomech 33, 1349-57.

Burger, E. H., and Klein-Nulend, J., 1999. Mechanotransduction in bone--role of the lacuno-canalicular network. Faseb J 13, S101-12.

Carter, D. R., Fyhrie, D. P., and Whalen, R. T., 1987. Trabecular bone density and loading history: regulation of connective tissue biology by mechanical energy. J Biomech 20, 785-94.

Chambers, T. J., Evans, M., Gardner, T. N., Turner-Smith, A., and Chow, J. W., 1993. Induction of bone formation in rat tail vertebrae by mechanical loading. Bone Miner 20, 167-78.

Chen, N. X., Ryder, K. D., Pavalko, F. M., Turner, C. H., Burr, D. B., Qiu, J., and Duncan, R. L., 2000. Ca(2+) regulates fluid shear-induced cytoskeletal reorganization and gene expression in osteoblasts. Am J Physiol Cell Physiol 278, C989-97.

Cowin, S. C., 1983. The mechanical and stress adaptive properties of bone. Ann Biomed Eng 11, 263-95.

Cowin, S. C., Weinbaum, S., and Zeng, Y., 1995. A case for bone canaliculi as the anatomical site of strain generated potentials. J Biomech 28, 1281-97.

Dillaman, R. M., 1984. Movement of ferritin in the 2-day-old chick femur. Anat Rec 209, 445-53.

Dillaman, R. M., Roer, R. D., and Gay, D. M., 1991. Fluid movement in bone: theoretical and empirical. J Biomech 24, 163-77.

Doty, S. B., and Schofield, B. H., 1972. Methabolic and structural changes within osteocytes of rat bone. In Calcium, Parathyroid Hormone and the Calcitonins, R. V. Talmage and P. L. Munson, eds. (Amsterdam: Elsevier), pp. 353-64.

Hart, R. T., Davy, D. T., and Heiple, K. G., 1984. Mathematical modeling and numerical solutions for functionally dependent bone remodeling. Calcif Tissue Int 36, S104-9.

Hillsley, M. V., and Frangos, J. A., 1994. Bone tissue engineering: the role of interstitial fluid flow. Biotechnol Bioeng 43, 573-81.

Huiskes, R., 2000. If bone is the answer, then what is the question? J Anat 197, 145-56.

Huiskes, R., Weinans, H., Grootenboer, H. J., Dalstra, M., Fudala, B., and Slooff, T. J., 1987. Adaptive bone-remodeling theory applied to prosthetic-design analysis. J Biomech 20, 1135-50.

Reproduced with permission of the copyright owner. Further reproduction prohibited without permission.

Jacobs, C. R., Yellowley, C. E., Davis, B. R., Zhou, Z., Cimbala, J. M., and Donahue, H. J., 1998. Differential effect of steady versus oscillating flow on bone cells. J Biomech 31, 969-76.

Jee, W. S., Li, X. J., and Schaffler, M. B., 1991. Adaptation of diaphyseal structure with aging and increased mechanical usage in the adult rat: a histomorphometrical and biomechanical study. Anat Rec 230, 332-8.

Klein-Nulend, J., Semeins, C. M., and Burger, E. H., 1996. Prostaglandin mediated modulation of transforming growth factor-beta metabolism in primary mouse osteoblastic cells in vitro. J Cell Physiol 168, 1-7.

Knothe Tate, M. L., and Knothe, U., 2000. An ex vivo model to study transport processes and fluid flow in loaded bone. J Biomech 33, 247-54.

Knothe Tate, M. L., Knothe, U., and Niederer, P., 1998a. Experimental elucidation of mechanical load-induced fluid flow and its potential role in bone metabolism and functional adaptation. Am J Med Sci 316, 189-95.

Knothe Tate, M. L., Steck, R., Forwood, M. R., and Niederer, P., 2000. In vivo demonstration of load-induced fluid flow in the rat tibia and its potential implications for processes associated with functional adaptation. J Exp Biol 203 Pt 18, 2737-45.

Knothe Tate, M. L., Tami, A., Nasser, P. R., Steck, R., and Schaffler, M. B., 2001. Permeability characteristics of different molecular tracers in loaded and unloaded bone. In Transactions of the 47th Meeting of the Orthopaedic Society (San Fransisco), pp. 138.

KnotheTate, M. L., Niederer, P., and Knothe, U., 1998b. In vivo tracer transport through the lacunocanalicular system of rat bone in an environment devoid of mechanical loading. Bone 22, 107-17.

Kufahl, R. H., and Saha, S., 1990. A theoretical model for stress-generated fluid flow in the canaliculi- lacunae network in bone tissue. J Biomech 23, 171-80.

Lanyon, L. E., Goodship, A. E., Pye, C. J., and MacFie, J. H., 1982. Mechanically adaptive bone remodelling. J Biomech 15, 141-54.

Li, G. P., Bronk, J. T., An, K. N., and Kelly, P. J., 1987. Permeability of cortical bone of canine tibiae. Microvasc Res 34, 302-10.

Mak, A. F., Qin, L., Hung, L. K., Cheng, C. W., and Tin, C. F., 2000. A histomorphometric observation of flows in cortical bone under dynamic loading. Microvasc Res 59, 290-300.

Miles, R. R., Turner, C. H., Santerre, R., Tu, Y., McClelland, P., Argot, J., DeHoff, B. S., Mundy, C. W., Rosteck, P. R., Jr., Bidwell, J., Sluka, J. P., Hock, J., and Onyia, J. E.,

Reproduced with permission of the copyright owner. Further reproduction prohibited without permission.

1998. Analysis of differential gene expression in rat tibia after an osteogenic stimulus in vivo: mechanical loading regulates osteopontin and myeloperoxidase. J Cell Biochem 68. 355-65.

Moalli, M. R., Caldwell, N. J., Patil, P. V., and Goldstein, S. A., 2000. An in vivo model for investigations of mechanical signal transduction in trabecular bone. J Bone Miner Res 15, 1346-53.

Montgomery, R. J., Sutker, B. D., Bronk, J. T., Smith, S. R., and Kelly, P. J., 1988. Interstitial fluid flow in cortical bone. Microvasc Res 35, 295-307.

Mosley, J. R., 2000. Osteoporosis and bone functional adaptation: mechanobiological regulation of bone architecture in growing and adult bone, a review. J Rehabil Res Dev 37, 189-99.

Mosley, J. R., and Lanyon, L. E., 1998. Strain rate as a controlling influence on adaptive modeling in response to dynamic loading of the ulna in growing male rats. Bone 23, 313-8.

Piekarski, K., and Munro, M., 1977. Transport mechanism operating between blood supply and osteocytes in long bones. Nature 269, 80-2.

Prendergast, P. J., and Taylor, D., 1994. Prediction of bone adaptation using damage accumulation. J Biomech 27, 1067-76.

Qin, L., Mak, A. T., Cheng, C. W., Hung, L. K., and Chan, K. M., 1999. Histomorphological study on pattern of fluid movement in cortical bone in goats. Anat Rec 255, 380-7.

Raab-Cullen, D. M., Thiede, M. A., Petersen, D. N., Kimmel, D. B., and Recker, R. R., 1994. Mechanical loading stimulates rapid changes in periosteal gene expression. Calcif Tissue Int 55, 473-8.

Rubin, C., Turner, A. S., Bain, S., Mallinckrodt, C., and McLeod, K., 2001. Anabolism. Low mechanical signals strengthen long bones. Nature 412, 603-4.

Rubin, C. T., and Lanyon, L. E., 1987. Kappa Delta Award paper. Osteoregulatory nature of mechanical stimuli: function as a determinant for adaptive remodeling in bone. J Orthop Res 5, 300-10.

Sauren, Y. M., Mieremet, R. H., Groot, C. G., and Scherft, J. P., 1992. An electron microscopic study on the presence of proteoglycans in the mineralized matrix of rat and human compact lamellar bone. Anat Rec 232, 36-44.

Reproduced with permission of the copyright owner. Further reproduction prohibited without permission.

Shapiro, F., Cahill, C., Malatantis, G., and Nayak, R. C., 1995. Transmission electron microscopic demonstration of vimentin in rat osteoblast and osteocyte cell bodies and processes using the immunogold technique. Anat Rec 241, 39-48.

Tanaka, T., and Sakano, A., 1985. Differences in permeability of microperoxidase and horseradish peroxidase into the alveolar bone of developing rats. J Dent Res 64, 870-6.

Torrance, A. G., Mosley, J. R., Suswillo, R. F., and Lanyon, L. E., 1994. Noninvasive loading of the rat ulna in vivo induces a strain-related modeling response uncomplicated by trauma or periostal pressure. Calcif Tissue Int 54, 241-7.

Turner, C. H., Akhter, M. P., Raab, D. M., Kimmel, D. B., and Recker, R. R., 1991. A noninvasive, in vivo model for studying strain adaptive bone modeling. Bone 12, 73-9.

Turner, C. H., Forwood, M. R., and Otter, M. W., 1994. Mechanotransduction in bone: do bone cells act as sensors of fluid flow? Faseb J 8, 875-8.

Wang, L., Cowin, S. C., Weinbaum, S., and Fritton, S. P., 2000. Modeling tracer transport in an osteon under cyclic loading. Ann Biomed Eng 28, 1200-9.

Wang, L., Fritton, S. P., Cowin, S. C., and Weinbaum, S., 1999. Fluid pressure relaxation depends upon osteonal microstructure: modeling an oscillatory bending experiment. J Biomech 32, 663-72.

Wassermann, F., and Yaeger, J. A., 1965. Fine structure of the osteocyte capsule and of the wall of the lacunae in bone. Zeitschrift fur Zellforschung 67, 636-652.

Weinbaum, S., Cowin, S. C., and Zeng, Y., 1991. A model for the fluid shear stress excitation of membrane ion channels in osteocytic process due to bone strain. In Advances in Bioengineering, J. R. Vanderby, ed., New York: American Society of Mechanical Engineers, pp. 317-320.

Weinbaum, S., Cowin, S. C., and Zeng, Y., 1994. A model for the excitation of osteocytes by mechanical loading-induced bone fluid shear stresses. J Biomech 27, 339-60.

Weinbaum, S., Guo, P., and You, L., 2001. A new view of mechanotransduction and strain amplification in cells with microvilli and cell processes. Biorheology 38, 119-42.

You, J., Reilly, G. C., Zhen, X., Yellowley, C. E., Chen, Q., Donahue, H. J., and Jacobs, C. R., 2001a. Osteopontin gene regulation by oscillatory fluid flow via intracellular calcium mobilization and activation of mitogen-activated protein kinase in MC3T3-E1 osteoblasts. J Biol Chem 276, 13365-71.

Reproduced with permission of the copyright owner. Further reproduction prohibited without permission.

You, L., Cowin, S. C., Schaffler, M. B., and Weinbaum, S., 2001b. A model for strain amplification in the actin cytoskeleton of osteocytes due to fluid drag on pericellular matrix. J Biomech 34, 1375-86.

Chapter 5

Ajubi, N. E., Klein-Nulend, J., Nijweide, P. J., Vrijheid-Lammers, T., Alblas, M. J., and Burger, E. H., 1996. Pulsating fluid flow increases prostaglandin production by cultured chicken osteocytes--a cytoskeleton-dependent process. Biochem Biophys Res Commun 225, 62-8.

Anderson, W., 1960. Studies of the lymphatic pathways of bone and bone marrow. Journal of Bone and Joint Surgery 42-A, 716.

Arnoldi, C. C., Lemperg, R., and Linderholm, H., 1971. Immediate effect of osteotomy on the intramedullary pressure in the femoral head and neck in patients with degenerative osteoarthritis. Acta Orthop Scand 42, 454-5.

Arnoldi, C. C., Linderholm, H., and Mussbichler, H., 1972. Venous engorgement and intraosseous hypertension in osteoarthritis of the hip. J Bone Joint Surg 54-B, 409-21.

Azuma, H., 1964. Intraosseous pressure as a measure of hemodynamic changes in bone marrow. Angiology 15, 396-406.

Bazantova, I., 1989. The blood and lymph bed in Haversian bone. Folia Morphol 37, 213-5.

Bergula, A. P., Huang, W., and Frangos, J. A., 1999. Femoral vein ligation increases bone mass in the hindlimb suspended rat. Bone 24, 171-7.

Bronk, J. T., Meadows, T. H., and Kelly, P. J., 1993. The relationship of increased capillary filtration and bone formation. Clin Orthop 293, 338-45.

Brookes, M., and Revell, W. J., 1998. Blood Supply to Bone, 2nd Edition, London, Springer-Verlag.

Cheng, B., Zhao, S., Luo, J., Sprague, E., Bonewald, L. F., and Jiang, J. X., 2001. Expression of functional gap junctions and regulation by fluid flow in osteocyte-like MLO-Y4 cells. J Bone Miner Res 16, 249-59.

Cooper, R. R., Milgram, J. W., and Robinson, R. A., 1966. Morphology of the osteon. An electron microscopic study. J Bone Joint Surg 48-A, 1239-71.

Cowin, S. C., 1999. Bone poroelasticity. J Biomech 32, 217-38.

Reproduced with permission of the copyright owner. Further reproduction prohibited without permission.

Cowin, S. C., Weinbaum, S., and Zeng, Y., 1995. A case for bone canaliculi as the anatomical site of strain generated potentials. J Biomech 28, 1281-97.

Dillaman, R. M., Roer, R. D., and Gay, D. M., 1991. Fluid movement in bone: theoretical and empirical. J Biomech 24, 163-77.

Ficat, P. R., and Arlet, J., 1980. Ischemia and necroses of bone. D. S. Hungerford, ed. Baltimore, Williams & Wilkins.

Fritton, S. P., McLeod, K. J., and Rubin, C. T., 2000. Quantifying the strain history of bone: spatial uniformity and self- similarity of low-magnitude strains. J Biomech 33, 317-25.

Fritton, S. P., and Rubin, C. T., 2001. In vivo measurement of bone deformations using strain gauges. In: S. C. Cowin (Ed). Bone Mechanics Handbook. CRC Press, Boca Raton, Florida, pp 8-1-8-41.

Green, N. E., and Griffin, P. P., 1982. Intra-osseous venous pressure in Legg-Perthes disease. J Bone Joint Surg 64-A, 666-71.

Grimm, M., and Williams, J., 1997. Measurement of permeability in human calcaneal trabecular bone. Journal of Biomechanics 30, 743-745.

Hillsley, M. V., and Frangos, J. A., 1994. Bone tissue engineering: the role of interstitial fluid flow. Biotechnol Bioeng 43, 573-81.

Hung, C. T., Pollack, S. R., Reilly, T. M., and Brighton, C. T., 1995. Real-time calcium response of cultured bone cells to fluid flow. Clin Orthop 313, 256-69.

Johnson, D. L., McAllister, T. N., and Frangos, J. A., 1996. Fluid flow stimulates rapid and continuous release of nitric oxide in osteoblasts. Am J Physiol 271, E205-8.

Keanini, R. G., Roer, R. D., and Dillaman, R. M., 1995. A theoretical model of circulatory interstitial fluid flow and species transport within porous cortical bone. J Biomech 28, 901-14.

Kelly, P. J., and Bronk, J. T., 1990. Venous pressure and bone formation. Microvasc Res 39, 364-75.

Kelly, P. J., Montgomery, R. J., and Bronk, J. T., 1990. Reaction of the circulatory system to injury and regeneration. Clin Orthop 254, 275-88.

Kiaer, T., 1994. Bone perfusion and oxygenation. Animal experiments and clinical observations. Acta Orthop Scand Suppl 257, 1-41.

Reproduced with permission of the copyright owner. Further reproduction prohibited without permission.

Klein-Nulend, J., Semeins, C. M., Ajubi, N. E., Nijweide, P. J., and Burger, E. H., 1995. Pulsating fluid flow increases nitric oxide (NO) synthesis by osteocytes but not periosteal fibroblasts--correlation with prostaglandin upregulation. Biochem Biophys Res Commun 217, 640-8.

Lawson, P. T., 2000. Assistant laboratory animal technician training manual. American Association for Laboratory Animal Science, Memphis.

Li, G. P., Bronk, J. T., An, K. N., and Kelly, P. J., 1987. Permeability of cortical bone of canine tibiae. Microvasc Res 34, 302-10.

Lilly, A. D., and Kelly, P. J., 1970. Effects of venous ligation on bone remodeling in the canine tibia. J Bone Joint Surg 52-A, 515-20.

Liu, S. L., and Ho, T. C., 1991. The role of venous hypertension in the pathogenesis of Legg-Perthes disease. A clinical and experimental study. J Bone Joint Surg 73-A, 194-200.

Michelsen, K., 1967. Pressure relationships in the bone marrow vascular bed. Acta Physiol Scand 71, 16-29.

Mukherjee, N., Saris, D. B., Schultz, F. M., Berglund, L. J., An, K. N., and O'Driscoll, S. W., 2001. The enhancement of periosteal chondrogenesis in organ culture by dynamic fluid pressure. J Orthop Res 19, 524-30.

Raab-Cullen, D. M., Thiede, M. A., Petersen, D. N., Kimmel, D. B., and Recker, R. R., 1994. Mechanical loading stimulates rapid changes in periosteal gene expression. Calcif Tissue Int 55, 473-8.

Reich, K. M., Gay, C. V., and Frangos, J. A., 1990. Fluid shear stress as a mediator of osteoblast cyclic adenosine monophosphate production. J Cell Physiol 143, 100-4.

Rouhana, S., Johnson, M., Chakkalakal, D., and Harper, R., 1981. Permeability of compact bone. In Joint ASME-ASCE Conference, pp. 169-172.

Rubin, C., Turner, A. S., Bain, S., Mallinckrodt, C., and McLeod, K., 2001. Anabolism. Low mechanical signals strengthen long bones. Nature 412, 603-4.

Saris, D. B., Sanyal, A., An, K. N., Fitzsimmons, J. S., and O'Driscoll, S. W., 1999. Periosteum responds to dynamic fluid pressure by proliferating in vitro. J Orthop Res 17, 668-77.

Shim, S. S., Hawk, H. E., and Yu, W. Y., 1972. The relationship between blood flow and marrow cavity pressure of bone. Surg Gynecol Obstet 135, 353-60.

Reproduced with permission of the copyright owner. Further reproduction prohibited without permission.

Stein, A. J., Morgan HC, and Reynolds FC. 1957. Variations in normal bone-marrow pressures. Journal of Bone and Joint Surgery 39-A, 1129-1134.

Tondevold, E., 1983. Haemodynamics of long bones. An experimental study on dogs. Acta Orthop Scand Suppl 205, 9-48.

Torzilli, P. A., Takebe, K., Burstein, A. H., Zika, J. M., and Heiple, K. G., 1982. The material properties of immature bone. J Biomech Eng 104, 12-20.

Turner, C. H., Akhter, M. P., Raab, D. M., Kimmel, D. B., and Recker, R. R., 1991. A noninvasive, in vivo model for studying strain adaptive bone modeling. Bone 12, 73-9.

Trueta, J., 1963. The role of the vessels in osteogenesis. Journal of Bone and Joint Surgery 45-B, 402-418.

Wang, L., Cowin, S. C., Weinbaum, S., and Fritton, S. P., 2000. Modeling tracer transport in an osteon under cyclic loading. Ann Biomed Eng 28, 1200-9.

Wang, L., Fritton, S. P., Cowin, S. C., and Weinbaum, S., 1999. Fluid pressure relaxation depends upon osteonal microstructure: modeling an oscillatory bending experiment. J Biomech 32, 663-72.

Weinbaum, S., Cowin, S. C., and Zeng, Y., 1991. A model for the fluid shear stress excitation of membrane ion channels in osteocytic process due to bone strain. In Advances in Bioengineering, J. R. Vanderby, ed., New York: American Society of Mechanical Engineers, pp. 317-320.

Weinbaum, S., Cowin, S. C., and Zeng, Y., 1994. A model for the excitation of osteocytes by mechanical loading-induced bone fluid shear stresses. J Biomech 27, 339-60.

Welch, R. D., Johnston, C. E., Waldron, M. J., and Poteet, B., 1993. Bone changes associated with intraosseous hypertension in the caprine tibia. J Bone Joint Surg 75-A, 53-60.

Wilkes, C. H., and Visscher, M. B., 1975. Some physiological aspects of bone marrow pressure. J Bone Joint Surg 57-A, 49-57.

Yoffey, J. M., 1965. Structural peculiarities of the blood vessels of the bone marrow. Bibl Anat 7, 298-303.

You, L., Cowin, S. C., Schaffler, M. B., and Weinbaum, S., 2001. A model for strain amplification in the actin cytoskeleton of osteocytes due to fluid drag on pericellular matrix. J Biomech 34, 1375-86.

Reproduced with permission of the copyright owner. Further reproduction prohibited without permission.

You, L., Weinbaum, S., Cowin, S. C., and Schaffler, M. B., 2002. Ultrastructure of the osteocyte process. Anatomical Record, in submission.

Zachos, T. A., Aiken, S. W., DiResta, G. R., and Healey, J. H., 2001. Interstitial fluid pressure and blood flow in canine osteosarcoma and other tumors. Clin Orthop. 230-6.

Zaman, G., Dallas, S. L., and Lanyon, L. E., 1992. Cultured embryonic bone shafts show osteogenic responses to mechanical loading. Calcif Tissue Int 51, 132-6.

Zeng, Y., Cowin, S. C., and Weinbaum, S., 1994. A fiber matrix model for fluid flow and streaming potentials in the canaliculi of an osteon. Ann Biomed Eng 22, 280-92.

Zhang, D., Weinbaum, S., and Cowin, S. C., 1998. Estimates of the peak pressures in bone pore water. J Biomech Eng 120, 697-703.

Chapter 6

Aarden, E. M., Wassenaar, A. M., Alblas, M. J., and Nijweide, P. J., 1996. Immunocytochemical demonstration of extracellular matrix proteins in isolated osteocytes. Histochem Cell Biol 106, 495-501.

Cowin, S.C., Weinbaum, S., Zeng, Y., 1995. A case for bone canaliculi as the anatomical site of strain-generated potentials. Journal of Biomechanics 28, 1281-1296.

Fritton, S. P., Wang, L., Weinbaum, S., and Cowin, S. C., 2001. Interaction of Mechanical Loading, Blood Flow, and Interstitial Fluid Flow in Osteonal Bone. In The Proceedings of ASME Bioengineering Conference, Snowbird, Utah.

Grimm, M., and Williams, J., 1997. Measurement of permeability in human calcaneal trabecular bone. Journal of Biomechanics 30, 743-745.

Knothe Tate, M. L., Tami, A., Nasser, P. R., Steck, R., and Schaffler, M. B., 2001. Permeability characteristics of different molecular tracers in loaded and unloaded bone. In Transactions of the 47th Meeting of the Orthopaedic Society (San Fransisco), pp. 138.

KnotheTate, M. L., Niederer, P., and Knothe, U., 1998b. In vivo tracer transport through the lacunocanalicular system of rat bone in an environment devoid of mechanical loading. Bone 22, 107-17.

Li, G. P., Bronk, J. T., An, K. N., and Kelly, P. J., 1987. Permeability of cortical bone of canine tibiae. Microvasc Res 34, 302-10.

Qin, Y., 1997. Fluid flow, matrix strain and loading frequency as interdependent control parameters in skeletal adaptation. Ph.D. thesis, State University of New York at Stony Brook.

Reproduced with permission of the copyright owner. Further reproduction prohibited without permission.

Rouhana, S., Johnson, M., Chakkalakal, D., and Harper, R., 1981. Permeability of compact bone. In Joint ASME-ASCE Conference, pp. 169-172.

Sauren, Y. M., Mieremet, R. H., Groot, C. G., and Scherft, J. P., 1992. An electron microscopic study on the presence of proteoglycans in the mineralized matrix of rat and human compact lamellar bone. Anat Rec 232, 36-44.

Shapiro, F., Cahill, C., Malatantis, G., and Nayak, R. C., 1995. Transmission electron microscopic demonstration of vimentin in rat osteoblast and osteocyte cell bodies and processes using the immunogold technique. Anat Rec 241, 39-48.

Wassermann, F., and Yaeger, J. A., 1965. Fine structure of the osteocyte capsule and of the wall of the lacunae in bone. Zeitschrift fur Zellforschung 67, 636-652.

Weinbaum, S., Cowin, S.C., Zeng, Y., 1994. A model for the excitation of osteocytes by mechanical loading-induced bone fluid shear stresses. Journal of Biomechanics 27, 339-360.

Reproduced with permission of the copyright owner. Further reproduction prohibited without permission.